Synthesis and optical properties of plasmonic fluorescent quantum dots

Botao Ji

THESE DE DOCTORAT DE

L'UNIVERSITE PIERRE ET MARIE CURIE

Spécialité

Physique et Chimie des Matériaux (ED397)

Présentée par

M. **Botao JI**

Pour obtenir le grade de

DOCTEUR de l'UNIVERSITÉ PIERRE ET MARIE CURIE

Titre de la thèse

SYNTHESIS AND OPTICAL PROPERTIES OF PLASMONIC FLUORESCENT QUANTUM DOTS

Soutenance le 11 juillet 2014

Devant la commission d'examen formée de :

M. Stephane	ROUX	Rapporteur
M. Alexandre	BOUHELIER	Rapporteur
M. Zeger	HENS	Examinateur
M^{me} Agnes	MAITRE	Examinateur
M. Benoit	DUBERTRET	Directeur de thèse
M. Nicolas	LEQUEUX	Codirecteur de thèse

Contents

General Introduction **6**

Chapter 1 Surface Plasmons, Fluorescence and Their Coupling **13**

1.1 Surface Plasmon Resonance 13

1.1.1 Introduction to Plasmon resonance 13

1.1.2 Propagating Surface Plasmon Resonance (PSPR) 14

1.1.3 Localized Surface Plasmon Resonance (LSPR) 15

1.1.4 Optical properties of metal nanoshells 17

1.2 Fluorescence 19

1.2.1 Introduction to the fluorescence phenomenon 19

1.2.2 Characteristics of Fluorescence Emission 19

1.2.3 Classification of Fluorescent Substances 20

1.2.4 Colloidal Semiconductors 21

1.2.4.1 Introduction to Colloidal Semiconductors 21

1.2.4.2 Nanocrystal Structure 22

1.2.4.3 Optical properties 24

1.3 The interaction between plasmons and excitons 25

1.3.1 Weak coupling between surface plasmons and excitons 25

1.3.1.1 Enhancement of fluorescent intensity 25

1.3.1.2 New phenomena arising from the coupling between excitons and plasmons 29

1.3.2 Strong coupling between surface plasmons and excitons 32

References 33

Chapter 2 Synthesis of Quantum Dots and Their Incorporation in Silica **40**

2.1 Synthesis of QDs 40

2.1.1 Introduction 40

2.1.2 Precursors preparation 41

2.1.3 Synthesis of 6 nm-in-radius-CdSe/CdS core/shell QDs 41
2.1.3.1 Synthesis of CdSe QDs 41
2.1.3.2 Formation of a CdS shell on CdSe cores 42
2.1.4 Synthesis of 15 nm-in-radius-CdSe/CdS core/shell QDs 43
2.1.4.1 Synthesis of CdSe cores 43
2.1.4.2 Formation of a CdS shell on CdSe cores 43
2.1.5 Synthesis of CdSe/CdS/ZnS 44
2.1.5.1 Synthesis of CdSe/CdS 44
2.1.5.2 ZnS shell growth 45
2.2 Synthesis of QD/SiO_2 46
2.2.1 Introduction 46
2.2.2 Selection of surfactant 47
2.2.2.1 Synthesis of QD/SiO_2 NPs with Igepal CO-520 48
2.2.2.2 Synthesis of QD/SiO_2 NPs with Triton X-100 48
2.2.2.3 The effect of the surfactant on the QD/SiO_2 NPs size 48
2.2.3 Effect of the QDs amount 51
2.2.4 Growth of thicker SiO_2 layer *via* Stöber method 52
2.2.4.1 Regrowth of silica on QD/SiO_2 NPs (radius-62 nm) 52
2.2.4.2 Regrowth of silica on QD/SiO_2 NPs (radius-25 nm) 52
2.2.4.3 The effect of the QD/SiO_2 starting size on the silica regrowth 53
2.2.5 Conclusions 54
References 55
Chapter 3 Generalized Synthesis of QD/SiO_2/Au Core/shell/shell Nanoparticles 59
3.1 Introduction 59
3.2 Functionalization of QD/SiO_2 NPs 62
3.2.1 Synthesis of poly(1-vinylimidazole-co-vinyltrimethoxysilane), PVIS 63

3.2.2 Functionalization of the surface of QD/SiO_2 NPs with PVIS or APTMS 64

3.3 Gold seeds adsorption 64

3.3.1 Preparation of the gold seeds solution 64

3.3.2 Adsorption of the gold seeds onto QD/SiO_2 NPs 66

3.3.3 Determination of the optimal amount of PVIS for the functionalization of QD/SiO_2 NPs 67

3.3.4 Effect of the functionalizing agent on the amount of adsorbed gold seeds 68

3.3.5 Effect of the pH on the amount of adsorbed gold seeds 69

3.3.5.1 PVIS-functionalized QD/SiO_2 NPs 69

3.3.5.2 APTMS-functionalized QD/SiO_2 NPs 71

3.3.6 Fresh gold seeds adsorption 72

3.3.6.1 Effect of the functionalizing agent on the amount of adsorbed fresh gold seeds 72

3.3.6.2 Effect of the gold seeds aging on the amount of PVIS-adsorbed gold seeds 73

3.3.6.3 Effect of the pH on the amount of PVIS-adsorbed fresh gold seeds 75

3.4 Growth of the gold nanoshell from QD/SiO_2/Au_{seeds} NPs 78

3.4.1 Reduction methods tested 78

3.4.2 Results, interpretations and choice of the reduction method 80

3.4.3 PVP-K12-assisted gold nanoshell growth.....82

3.4.4 Effect of the gold seeds coverage density 85

3.4.4.1 Gold seeds coverages obtained with APTMS or PVIS 85

3.4.4.2 Gold seeds coverages obtained with PVIS at different pH values 88

3.4.5 Effect of the monolayer/multilayer adsorption of the freshly-made gold seeds 89

3.4.6 Synthesis of golden QDs with tailored thicknesses of gold and silica 91

3.4.6.1 Adjustment of the gold nanoshell thickness on QD/SiO_2 NPs with a fixed size 91

3.4.6.2 Gold nanoshell formation on QD/SiO_2 with various silica thicknesses 93

3.5 Conclusion 94

References 95

Chapter 4 Optical Properties of Golden QDs 98

4.1 Introduction 98

4.2 Optical study of golden 15 nm-in-radius-QDs 99

4.2.1 Mechanisms of the fluorescence emission for CdSe/CdS QDs and for golden QDs. 101

4.2.2 Ensemble measurements 102

4.2.3 Single nanoparticle measurements 106

4.2.4 Photostability 108

4.3 Conclusion 111

References 112

Chapter 5 Self-assembled Colloidal Superparticles 115

5.1 Introduction 115

5.2 Synthesis of SPs 116

5.2.1 Self-assembly of hydrophobic nanocrystals: the mechanism 116

5.2.2 Synthesis of colloidal SPs via self-assembly of QDs. 117

5.2.3 Adjustment of the size of SPs 119

5.3 The incorporation of SPs in silica 121

5.3.1 The effect of injection solvent on the silica shell growth 121

5.3.2 The effect of PVP molecular weight on the silica shell growth 123

5.3.3 Growth of thick silica shell on SPs/SiO_2 123

5.4 Synthesis of SPs and SPs/SiO_2 from different types of nanocrystals 124

5.5 Synthesis of SPs/SiO_2/Au nanoshells (golden SPs) 126

5.6 Conclusion 128

References 129

General Conclusion and Perspectives 132

Appendices 135

A1-Simulation part: numerical model.....135

A2-List of abbreviations.....142

Abstract.....144

General Introduction

Scientific Context

Fluorescence is a photoluminescence process by which light is emitted after a substance has absorbed light or other form of electromagnetic radiation. In most cases, the emitted light has higher wavelengths than that of the excitation source, therefore lower energy.[1,2] The fluorescent wavelength, intensity and shape are dependent on the structure of the fluorescent molecules/materials and the environment they are located in, such as solvent polarity, pH, temperature and oxygen content of the medium, and so forth. Fluorescence-based techniques with high sensitivity, selectivity, simplicity and good reproducibility have been widely applied in the fields of chemistry, biology and materials.[3-5] Single-molecule fluorescence detection is a sought for challenge, very much in need for the understanding of various biologically-relevant mechanisms. However, the detection of fluorescence at a single molecular level is extremely limited by its low brightness, relatively high background signal from the sample and a low photostability.[6]

Through plasmon resonance effects, noble metals can help tuning the fluorescence.[7] The interaction between plasmons and fluorescence emission has great potential to revolutionize a variety of research fields beyond fluorescence detection.[8] When the fluorescent molecules are located in the proximity of plasmonic metals, the oscillating electrons of the metal plasmons can induce various phenomena, including changes in the absorption and emission rates, energy transfer between the two components, reshape of fluorescence, and strong modifications of the radiative lifetime.[9-12] These interactions are complicated and strongly dependent on the specific hybrid structure. To clarify such a mechanism is one of the most challenging subjects in nanotechnology.

Organic molecules (fluorophores) are the most used fluorescent emitters in fluorescence-plasmon coupling investigations.[7] Fluorophores display emission spectra from ultraviolet to visible and have been widely utilized as bio-markers and in optoelectronic devices.[13,14] The fluorophores' functional groups enable their facile binding to metal surfaces through direct binding or via linkers. However, some fluorophores exhibit low quantum yield and fluorescence intensity and by far they show overlapping absorption and emission spectra, which makes it difficult to separate the emission contribution from the excitation light. The

short working life under successive illumination also limits the systematic investigation of fluorescence-plasmon couplings with organic fluorophores.[15,16]

Colloidal semiconductor nanocrystals, known as quantum dots (QDs), with typical dimensions in the range of 1-100 nm display well-tuned emission spectra from ultraviolet to the infrared region by simply changing the size and the composition of the QDs. The emission spectrum has a small full-width-half-maximum (FWHM) and is well-separated from its absorption region. The photostability of QDs is greatly enhanced compared to fluorophores.[17,18] Besides this, carrier multiplication within QDs is another appealing and valuable attribute. It is a phenomenon that the absorption of one single photon produces multiple excitons, resulting in an internal quantum yield greater than 100%.[19,20] All of these unique characteristics make QDs extremely ideal candidate to explore the coupling between the fluorescence and plasmons and to instrument the so much sought for improvement in bio-imaging and in optoelectronic devices.

Although the fluorescence of QDs is much more stable than that of organic dyes, it still suffers from prolonged illumination (photobleaching).[21] Besides that, fluorescence intermittency, also known as blinking, is observed at the single QD level.[22] This not only substantially limits their use as fluorescent probes for bioimaging (since a continuous monitoring is not guaranteed), but also degrades their photoluminescence properties in optoelectronic devices.[22]

Objectives of this thesis

Significant progress has been made in the understanding of the fundamental interactions between surface plasmons and fluorescence through a number of theoretical and experimental investigations. In numerous studies, for instance, lithographically-made or layered metals are applied as a source of surface plasmon resonance (SPR),[23,24] or alternatively multiple light-emitters are contained in one plasmonic structure.[25] The difficulty in reproducing the fabrication or the plurality of light-emitters may greatly restrict the understanding of mutual interactions.

Colloidal single QD/gold hybrids have rarely been synthesized, although these structures are very promising and can be handled very easily since they remain dispersed in solution.

One example of QD coated in a gold shell has been reported, but no evidence of plasmon coupling between the gold shell and the QD was demonstrated.[26]

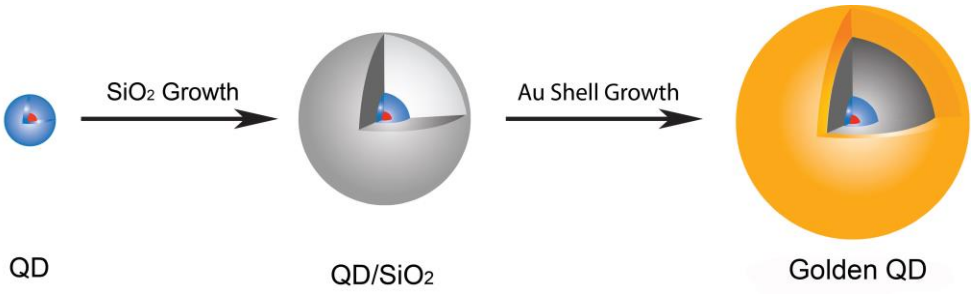

Figure 1. Schematic representation of the synthetic route of QD/SiO_2/Au nanoshell (golden QD).

The aim of this thesis is to elaborate colloidal hybrid nanoparticles by encapsulating single QD at the center of a bead of amorphous silica, followed by the chemical deposition of a gold nanoshell on the silica surface as illustrated in Figure 1. The thickness of the silica and gold layers can be tuned independently. The effect of the plasmonic gold nanoshell to the fluorescence is thus investigated exactly at the single-QD level. The photostability is expected to increase because the gold nanoshell can also prevent the diffusion of oxygen and other species, which could react with the QD. Because the QD is located at the center of the silica bead and the gold nanoshell, the electric field to which the QD is exposed is isotropic, regardless of the direction of the incident light. A spherical model is used to describe numerically the QD/SiO_2/Au core/shell/shell nanostructure (called thereafter "golden QDs").

Organization of the manuscript

The manuscript is organized in five chapters:

Chapter 1 introduces the basics of surface plasmons, of the fluorescence and of the interactions between plasmons and excitons based on recent investigations.

Chapter 2 presents the synthesis of the different types of highly monodispersed QDs with various sizes used in this work. Single CdSe/CdS core/shell QDs of two sizes is encapsulated

in one silica bead through a reverse-microemulsion solution method. The silica thickness can be tuned by the precursor quantity.

Chapter 3 describes the synthetic process of the gold deposition on the surface of silica. A polymer, developed in our lab, is applied to maximize the density of adsorbed Au seeds, which act as nucleation sites for the growth of Au nanoshells on silica. Different Au shell growth methods are also compared.

In chapter 4, the optical properties of the hybrid nanostructures are investigated by ensemble and single golden 15 nm-in-radius-QDs measurements. The plasmonic heterostructure system displays a stable and poissonian emission at room temperature, which results from an enhanced emission decay rate, in very good agreement with the simulations. The gold nanoshell also enhances the resistance of the QD fluorescence to high-power or consecutive photoexcitation.

In chapter 5, colloidal spheres (superparticles, SPs), which contain multiple hydrophobic nanocrystals are synthesized to achieve extremely fluorescent objects by a versatile bottom-up self-assembly approach. A layer of silica is deposited on SPs, followed by the growth of Au nanoshells. This object with high stability, photostability and biocompatibility shows great potential in imaging applications.

References

(1) Kulmala, S.; Suomi, J.: Current status of modern analytical luminescence methods. *Anal. Chim. Acta* **2003**, *500*, 21-69.

(2) Lakowicz, J. R.: Principles of fluorescence spectroscopy. *Anal Chim Acta* **1999**, *500*.

(3) Ow, H.; Larson, D. R.; Srivastava, M.; Baird, B. A.; Webb, W. W.; Wiesner, U.: Bright and stable core−shell fluorescent silica nanoparticles. *Nano Lett* **2004**, *5*, 113-117.

(4) Deng, W.; Jin, D. Y.; Drozdowicz-Tomsia, K.; Yuan, J. L.; Wu, J.; Goldys, E. M.: Ultrabright Eu-doped plasmonic Ag@SiO_2 nanostructures: time-gated bioprobes with single particle sensitivity and negligible background. *Adv Mater* **2011**, *23*, 4649-4654.

(5) Mathew, S.; Yella, A.; Gao, P.; Humphry-Baker, R.; CurchodBasile, F. E.; Ashari-Astani, N.; Tavernelli, I.; Rothlisberger, U.; NazeeruddinMd, K.; Grätzel, M.: Dye-sensitized solar cells with 13% efficiency achieved through the molecular engineering of porphyrin sensitizers. *Nat Chem* **2014**, *6*, 242-247.

(6) Fu, Y.; Lakowicz, J. R.: Modification of single molecule fluorescence near metallic nanostructures. *Laser Photonics Rev* **2009**, *3*, 221-232.

(7) Lakowicz, J. R.: Radiative decay engineering 5: metal-enhanced fluorescence and plasmon emission. *Anal Biochem* **2005**, *337*, 171-194.

(8) Ming, T.; Chen, H. J.; Jiang, R. B.; Li, Q.; Wang, J. F.: Plasmon-controlled fluorescence: beyond the intensity enhancement. *J Phys Chem Lett* **2012**, *3*, 191-202.

(9) Kuhn, S.; Hakanson, U.; Rogobete, L.; Sandoghdar, V.: Enhancement of single-molecule fluorescence using a gold nanoparticle as an optical nanoantenna. *Phys Rev Lett* **2006**, *97*, 017402.

(10) Parak, W. J.; Gerion, D.; Pellegrino, T.; Zanchet, D.; Micheel, C.; Williams, S. C.; Boudreau, R.; Le Gros, M. A.; Larabell, C. A.; Alivisatos, A. P.: Biological applications of colloidal nanocrystals. *Nanotechnology* **2003**, *14*, R15-R27.

(11) Ringler, M.; Schwemer, A.; Wunderlich, M.; Nichtl, A.; Kurzinger, K.; Klar, T. A.; Feldmann, J.: Shaping emission spectra of fluorescent molecules with single plasmonic nanoresonators. *Phys Rev Lett* **2008**, *100*, 203002.

(12) Ma, X. D.; Tan, H.; Kipp, T.; Mews, A.: Fluorescence enhancement, blinking suppression, and gray states of individual semiconductor nanocrystals close to gold nanoparticles. *Nano Lett* **2010**, *10*, 4166-4174.

(13) Burns, A.; Ow, H.; Wiesner, U.: Fluorescent core-shell silica nanoparticles: towards "Lab on a Particle" architectures for nanobiotechnology. *Chemical Society Reviews* **2006**, *35*, 1028-1042.

(14) Oregan, B.; Gratzel, M.: A Low-Cost, High-efficiency solar-cell based on dye-sensitized colloidal TiO_2 films. *Nature* **1991**, *353*, 737-740.

(15) Mehta, A. D.; Rief, M.; Spudich, J. A.: Biomechanics, one molecule at a time. *J Biol Chem* **1999**, *274*, 14517-14520.

(16) Medintz, I. L.; Uyeda, H. T.; Goldman, E. R.; Mattoussi, H.: Quantum dot bioconjugates for imaging, labelling and sensing. *Nat Mater* **2005**, *4*, 435-446.

(17) Peng, X. G.; Schlamp, M. C.; Kadavanich, A. V.; Alivisatos, A. P.: Epitaxial growth of highly luminescent CdSe/CdS core/shell nanocrystals with photostability and electronic accessibility. *J Am Chem Soc* **1997**, *119*, 7019-7029.

(18) Murphy, C. J.: Optical sensing with quantum dots. *Anal Chem* **2002**, *74*, 520a-526a.

(19) Klimov, V. I.: Spectral and dynamical properties of multilexcitons in semiconductor nanocrystals. *Annu Rev Phys Chem* **2007**, *58*, 635-673.

(20) Klimov, V. I.; Mikhailovsky, A. A.; McBranch, D. W.; Leatherdale, C. A.; Bawendi, M. G.: Quantization of multiparticle Auger rates in semiconductor quantum dots. *Science* **2000**, *287*, 1011-1013.

(21) van Sark, W. G. J. H. M.; Frederix, P. L. T. M.; Van den Heuvel, D. J.; Gerritsen, H. C.; Bol, A. A.; van Lingen, J. N. J.; Donega, C. D.; Meijerink, A.: Photooxidation and photobleaching of single CdSe/ZnS quantum dots probed by room-temperature time-resolved spectroscopy. *J Phys Chem B* **2001**, *105*, 8281-8284.

(22) Nirmal, M.; Dabbousi, B. O.; Bawendi, M. G.; Macklin, J. J.; Trautman, J. K.; Harris, T. D.; Brus, L. E.: Fluorescence intermittency in single cadmium selenide nanocrystals. *Nature* **1996**, *383*, 802-804.

(23) Pompa, P. P.; Martiradonna, L.; Della Torre, A.; Della Sala, F.; Manna, L.; De Vittorio, M.; Calabi, F.; Cingolani, R.; Rinaldi, R.: Metal-enhanced fluorescence of colloidal nanocrystals with nanoscale control. *Nat Nanotechnol* **2006**, *1*, 126-130.

(24) Yuan, H.; Khatua, S.; Zijlstra, P.; Yorulmaz, M.; Orrit, M.: Thousand-fold enhancement of single-molecule fluorescence near a single gold nanorod. *Angewandte Chemie International Edition* **2013**, *52*, 1217-1221.

(25) Liu, N. G.; Prall, B. S.; Klimov, V. I.: Hybrid gold/silica/nanocrystal-quantum-dot superstructures: synthesis and analysis of semiconductor-metal interactions. *J Am Chem Soc* **2006**, *128*, 15362-15363.

(26) Jin, Y. D.; Gao, X. H.: Plasmonic fluorescent quantum dots. *Nat Nanotechnol* **2009**, *4*, 571-576.

Chapter 1 Surface Plasmons, Fluorescence and Their Coupling

Hybrid metal-fluorescent emitters heterostructures have attracted much attention over the past decade because the interaction between the metal plasmons and the fluorescence excitons provides an opportunity to tailor fluorescence. So far, different metal-fluorescence emitters heterostructures have been investigated especially at the single fluorescent emitters level to fully understand the interaction between plasmons and excitonic fluorescence. In this chapter, the basic principles of surface plasmon resonance and fluorescence are introduced. Furthermore, and based on the state of the art, the interactions between plasmons and excitons are discussed.

1.1 Surface Plasmon Resonance

1.1.1 Introduction to Plasmon resonance

Plasmon resonance is an optical phenomenon. In metals, free electrons are not bound to a specific metal ion but circulating in the whole metal crystal; they migrate freely on the surface of the metal. Oscillating electric fields originating from incident light can delocalize the electrons and force them to move away from the metal framework. This situation is short lived: the free electrons will be pulled back because of the Coulombic attraction coming from the positively charged cations within the crystal. The resonance condition is established when the frequency of the incident light is coupled to the natural frequency of the electron oscillation in the metal.[1] The natural frequency of the electronic oscillation for a bulk metal of infinite size only depends on the free electron density; most metals have ultraviolet plasmonic frequencies, except the plasmons of Au, Ag and Cu being located in the visible region.[2] Two types of surface plasmons can be generated: Propagating Surface Plasmon Resonance (PSPR) and Localized Surface Plasmon Resonance (LSPR) (which occurs in small size metal particles).

1.1.2 Propagating Surface Plasmon Resonance (PSPR)

PSPR occurs on extended smooth metal surfaces. Positive and negative charges are generated as the electron density waves propagate along the metal surface under the excitation of incident light as shown in Figure 1.1 (a).[3] The resulting plasmons decay evanescently in the direction perpendicular to the metal surface with 1/e decay lengths in the range of 200 nm. However, simple illumination with light on a smooth metal surface in air is not sufficient to induce plasmon resonance because the momentum of the light in the interfacial plane is always smaller than that of the SPs.

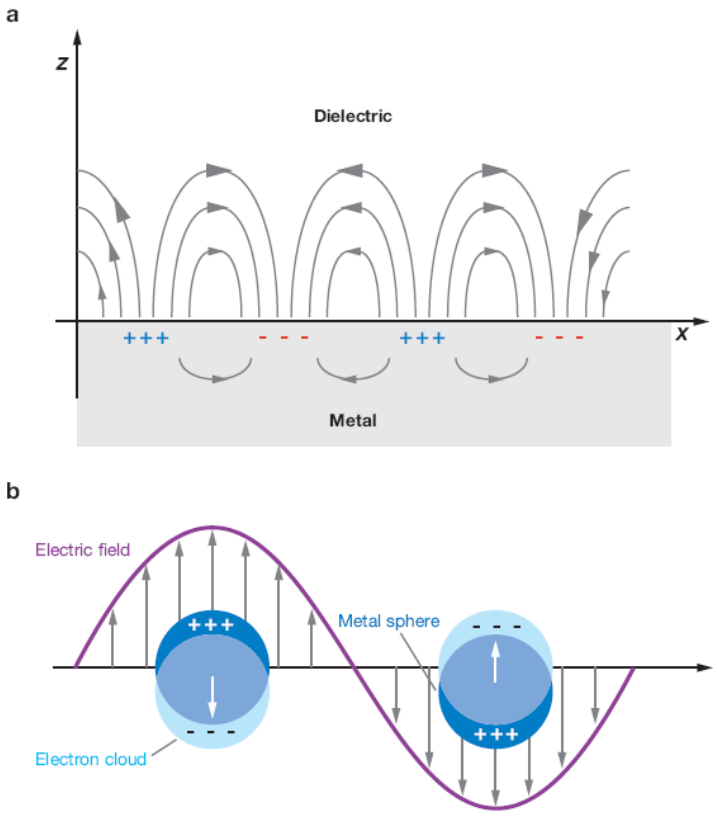

Figure 1.1. Schematic description of (a) propagating surface plasmon resonance (PSPR) and (b) localized surface plasmon resonance (LSPR) of a metal nanosphere. Reprinted from Ref [3].

Auxiliary optical devices, such as a glass prism with higher refractive index than the metal and optical grating are usually employed to generate PSPR.[4] In the case of a glass prism, the light passes from the prism to the metal. Total internal reflectance will appear when the angle of the incident light is equivalent or beyond a critical angle. New evanescent light waves

propagate from the interface into the metal in a very short distance and will couple to metal plasmons at a particular angle. The interaction between a molecular layer and the metalwill cause the change of refractive index of the media near the metal film and therefore the plasmon-coupled condition. This technique has been widely used in bio-analysis. When the incident light illuminates a metal grating, the wave vector will be enlarged as a result of light diffraction.[5] The wave vector of diffracted light in a specific order parallel to the interface is in accordance with the surface plasmons; PSPR is then produced along the grating surface. It should be emphasized that PSPR can be excited by simple illumination with light on randomly roughened metal surfaces because diffraction effects derived from the roughness of the metal film provide the desired wave vector compensation for plasmon resonance.

1.1.3 Localized Surface Plasmon Resonance (LSPR)

LSPR occurs in metal particles with the size smaller than the wavelength of the incident light. Different from the previous PSPR, the oscillation of the free electrons induced by the incident electromagnetic field is strongly confined to the volume of the metal particles. The separation of the charges creates a dipole, whose direction can be switched with a change in the electric field, as displayed in Figure 1.1 (b).[3] When the frequency of the natural dipole oscillation is matched to the incident light, a strong light absorption appears, which is referred as LSPR. Direct illumination of light on metal particles can produce a strong LSPR. The electromagnetic field resides very close to the particle surface due to the localization of the plasmon to the surface of the small metal particles, generating much higher local field enhancements than those of PSPR.[1]

LSPR strongly depends on the components, size and shape of the metal particles, and the dielectric constant of the local environment. For instance, dipole plasmons of Au nanospheres are excited when the size is smaller than 30 nm, thus displaying one single absorption peak, while higher order resonances can be obtained with increasing the size of Au nanospheres, displaying multiple absorption peaks.[1] Thanks to the remarkable development of nanometer-scale fabrication technologies, a variety of metals (mainly Ag and Au because of their chemical stability and strong LSPR adsorption in the visible region) with various shapes and sizes have been successfully synthesized. Figure 1.2 shows TEM images of Au nanorods with various aspect ratios and corresponding absorption spectra (h).[6] The plasmon absorption of

Au nanorods splits into two bonds corresponding to the oscillation of the free electrons parallel and perpendicular to the long axis of the Au nanorods. The transverse mode has a similar resonance than the Au nanosphere at around 520 nm; while the resonance of the longitudinal mode can be tuned by changing the nanorods' aspect ratio (length/diameter).[7] Nowadays, metal nanoparticles with different morphologies including nanospheres,[8-11] nanorods,[12,13] nanoprisms,[14] bowtie nanoantennas,[15] nanoshells,[16,17] thin films,[18,19] nanovoids,[20] hole arrays,[21] nanopatterns[22] *et al.* have been used to investigate the interaction between plasmon and fluorescence.

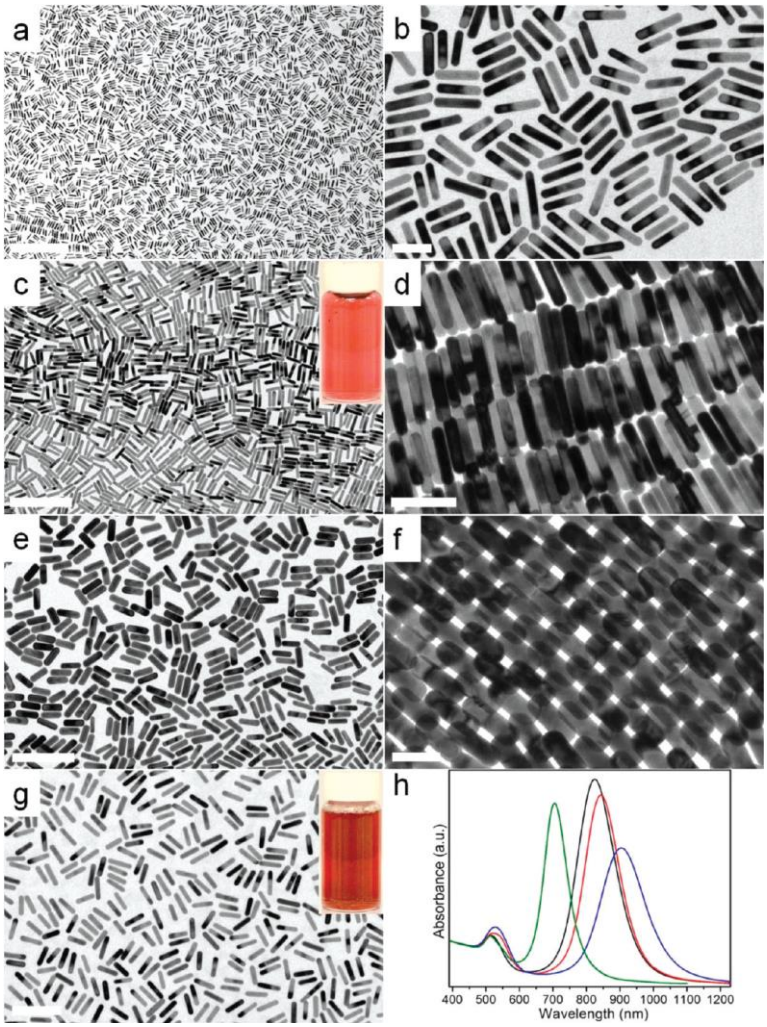

Figure 1.2. (a-g) TEM images of Au nanorods with various aspect ratio and (h) corresponding absorption spectra. The insets of (c) and (g) show the photograph of the corresponding aqueous dispersion of gold nanorods. (h) UV-vis-NIR spectra of gold NRs shown in a and b (red curve), c and d (blue curve), e and f (green curve), and g (black curve), respectively. Each spectrum is normalized by its absorption at 400 nm. Scale bars: (a) 500 nm, (b) 50 nm, (c) 200 nm, (d) 50 nm, (e) 200 nm, (f) 50 nm, (g) 100 nm. Reprinted from Ref [6].

1.1.4 Optical properties of metal nanoshells

Metal nanoshells are a new class of nanoparticles composed of a single dielectric core nanoparticle (such as silica) coated with a metallic shell.[23] The plasmon resonance of metal nanoshells can be tuned across the visible or infrared regions by varying the size of the core and the shell thickness. The capacity to tune plasmons resonance opens up opportunities for applications in the biomedical and surface-enhanced Raman scattering fields. Zhou *et al.* synthesized the first metal nanoshell which consisted of an Au_2S core and an Au shell by mixing chloroauric acid and sodium sulfide in one step.[24] The nanoshells plasmon resonance could be adjusted from 520 to 900 nm through variations in the ratio between the two precursors. However, this synthetic approach lacks a precise control over the core and shell dimensions.

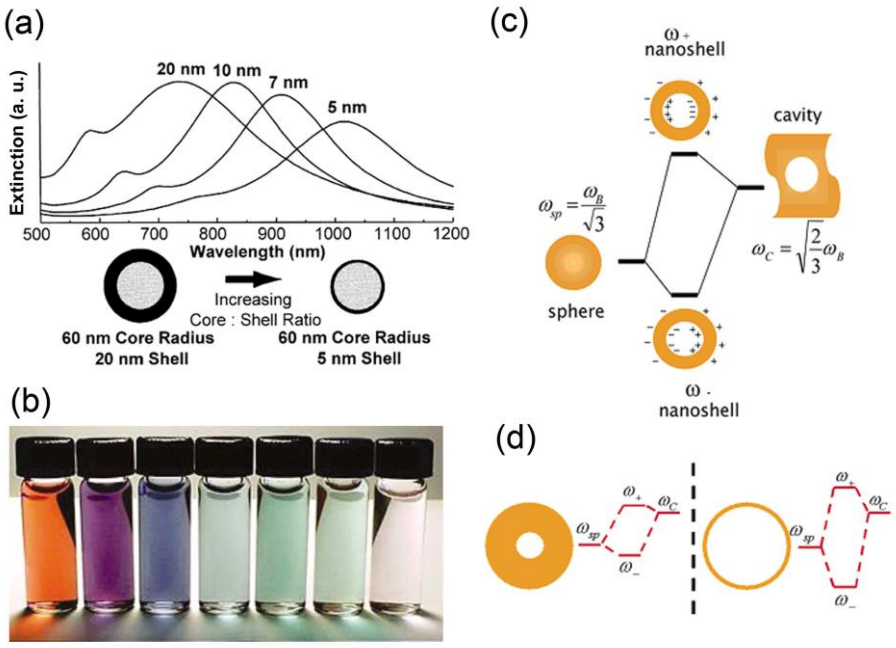

Figure 1.3: (a) Theoretically calculated optical resonances of Au nanoshells as a function of the ratio between the silica core radius and the Au shell thickness. (b) A photograph of aqueous dispersions of Au nanoshells with different frequencies of plasmonic resonances. (c) Plasmon hybridization in metallic nanoshells arises from the interaction between cavity plasmons and sphere plasmons. (d) The strength of the interaction between the sphere and cavity plasmons is dependent on the thickness of the shell. Reprinted from Ref [23, 25].

In 1998, silica/Au core/nanoshell nanoparticles were successfully synthesized by Halas (Figure 1.3a and b).[23] The separate synthesis of the silica core and the Au nanoshell enables a good control of their dimensions. Very tiny Au nanoparticles (seeds) are attached electronically to the silica surface functionalized with amino-propyltriethoxysilane. Subsequent chemical reduction of Au^{3+} to Au^{0} induces a further growth of the Au seeds, which results in the formation of continuous and polycrystalline Au nanoshells with a typical thickness between 5 - 30 nm. During this process, as the gold seeds grow, their plasmon peak becomes slightly red shifted; when the growing gold seeds begin to coalesce and form islands on the nanoparticle surface, the decreasing distance among these islands lead to increased inter-particle plasmon coupling and a red-shifted plasmon resonance.[23] The plasmon-derived optical properties of metallic nanoshells can be understood in light of the plasmon hybridization model of metallic nanoshells.[25] The outer nanoshell surface can be considered as a sphere, while the inner surface of the nanoshell can be considered as a cavity (Figure 1.3c). Similar to the hybridization of atomic orbitals, cavity plasmons and sphere plasmons mix and hybridize, resulting in two new resonances, the "bonding" plasmon and the "anti-bonding" plasmon. The strength of the hybridization is determined by the thickness of the nanoshell. Decreasing the thickness of the nanoshell leads to a stronger interaction, corresponding to a red-shifted resonance (Figure 1.3d), which is coincident with the theoretically calculated results. Silica/Au core/shell nanostructures display many unique optical properties, which, among others, include photothermal performance and production of solar steam nanobubbles.[26,27]

1.2 Fluorescence

1.2.1 Introduction to the fluorescence phenomenon

Nowadays, fluorescence is the most common labelling technique in biological and chemical sciences thanks to its high sensitivity. The excitation and subsequent emission processes of fluorophores are usually illustrated by the Jablonski diagram, as shown in Figure 1.4.[28] Following light absorption, fluorophores are excited to a higher vibrational energy state, either S_1 or S_2. Then, these fluorophores will relax to the lowest vibrational level of S_1 through a rapid process called internal conversion (within 10 ps), which is much faster than the fluorescence emission process. The process of returning from S1 to S0 is the fluorescence emission. Alternatively, fluorophores in the S1 state can also undergo a spin conversion (intersystem crossing) to the first triplet state, T1, resulting in phosphorescence emission.[29]

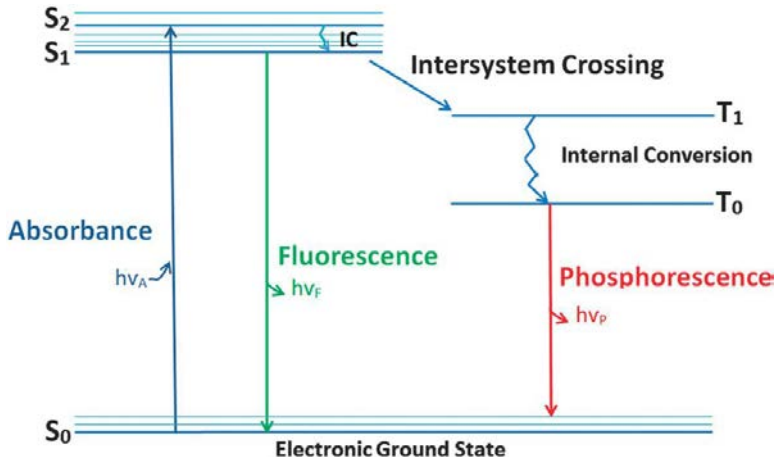

Figure 1.4. Fluorescence absorption and emission processes illustrated by the Jablonski diagram. The singlet ground, first, second electronic states, triplet ground and first triplet state are depicted by S_0, S_1, S_2, T_0 and T_1, respectively. Reprinted from Ref. [28].

1.2.2 Characteristics of Fluorescence Emission

Due to energy losses, the energy of the fluorescence photon is normally smaller than that of the exciting photons. This is displayed by a longer fluorescence wavelength than that of the exciting light (Stokes shift). In recent years, other nonlinear optical processes were discovered,

in which the sequential absorption of two or more photons leads to the emission of light at shorter wavelength than the excitation wavelength; this up-conversion is an anti-Stokes emission.[30] Lifetime and quantum yield are the two most important parameters of fluorescent substances. The fluorescence lifetime (τ) is defined as the time for which the fluorescence intensity decays to 1/e of the initial intensity after excitation. It determines the decay time of the first singlet state, in other words, an average value of the time spent in the excited state, and it is given by,

$$\tau = 1/(k_f+\Sigma k_n) \quad (1\text{-}1)$$

where k_f is the radiative decay rate and Σk_n is the sum of the non-radiative decay rate. The fluorescence quantum yield (Q) is the ratio of the number of photons emitted to the number of photons absorbed. The decay of excited molecules includes radiative and non-radiative transition processes; hence the quantum yield is given by,

$$Q = k_f/(k_f+\Sigma k_n) \quad (1\text{-}2)$$

Higher quantum yield represents stronger fluorescent intensity. The quantum yield can be close to 1 if the rate of radiative decay is much larger than the non-radiative decay rate. A variety of processes during which radiative and/or non-radiative rates are changed can decrease the fluorescence intensity. This is referred to as quenching. It should be noted that an increase of the radiative decay rate will result in higher quantum yields.

1.2.3 Classification of Fluorescent Substances

Fluorescent substances can be divided into several major classes.[31] Organic fluorophores are the first observed fluorescent substances. Nowadays, commercial organic fluorophores with emission spectra ranging from ultraviolet to near-infrared (NIR) are widely utilized as bio-markers and in optoelectronic devices. However, organic fluorophores have broad absorption/emission spectra and low photostability due to their intrinsic photophysical properties. This limits the simultaneous detection of multiple signals and diminishes their effectiveness in long-term imaging. Fluorescent proteins are another type of fluorescent substances. Their fluorescence derives from aromatic amino acids. These fluorescent proteins have been used as fusion tags to study protein dynamics. Such proteins are usually genetically

encoded. This characteristic, combined with their low fluorescent intensity, limits their practical application as injectable target-specific fluorescent probes.[32]

In recent years, inorganic nanoparticles, such as semiconductor nanocrystals (quantum dots, QDs) and up-conversion nanocrystals have been greatly developed. This was motivated by their unique optical properties,[33,34] as for example, broad excitation ranges, narrow emission peaks, spectra spanning the UV to near-infrared, high fluorescence intensity and photostability. Furthermore, the QDs surface can be conjugated with a variety of bio-molecules to enable their application in bio-imaging.[35] In spite of their intrinsic optical advantages, a major concern still remains around QDs, and that is their possible toxicity due to the heavy metals contained in QDs. In the next part, the general characteristics of QDs will be presented in detail.

1.2.4 Colloidal Semiconductors

1.2.4.1 Introduction to Colloidal Semiconductors

Colloidal semiconductors are light-emitting particles commonly synthesized in the solution phase. In the last several decades, they have attracted considerable attention as an important new class of materials in bio-imaging, sensitive detection and optoelectronic devices.[36] When bulk semiconductors absorb energy, an electron in the valence band (VB) can be excited to the conduction band (CB) (the minimum energy required to excite an electron is the band gap energy (E_g)), and make the semiconductor conductive. An electron-hole pair, known as the exciton, is produced during this process. Relaxation of the excited electron back to the hole can give rise to the photon emission. The exciton has a finite size within the crystal defined by the Bohr exciton radius.[37] When the radius of the semiconductor particle is close to or smaller than its Bohr exciton radius, the motion of electrons and holes is greatly spatially confined. This strong dependence on the size is called quantum confinement effect. From the molecular orbital theory, when the crystal size is reduced to a certain value, the electron energy levels of the semiconductor become discontinuous; as a result, the band gap energy continuously increases as the crystal size decreases. Colloidal semiconductors with typical dimensions in the range of 1-100 nm possess size-dependent absorption and fluorescence spectra with discrete electronic transitions. For instance, in the case of CdSe nanocrystals, their emission

can span almost the entire visible spectrum from blue to red simply by varying the size of the nanocrystal from ~2.2 to ~5.5 nm, as shown in Figure 1.5.

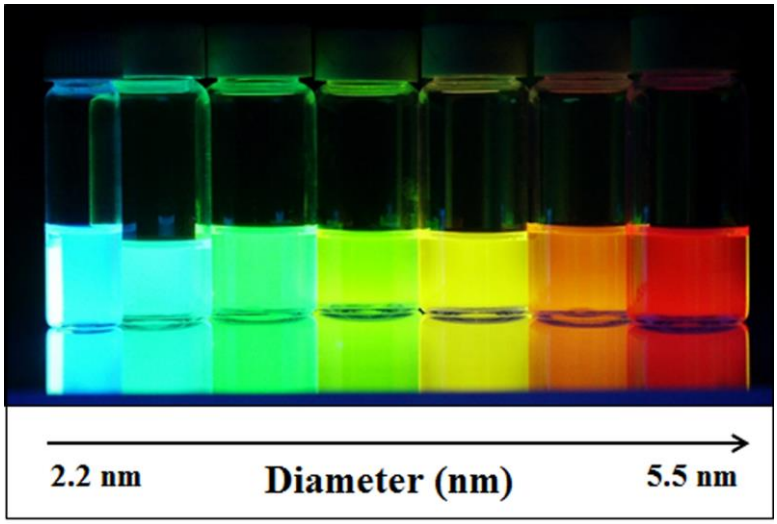

Figure 1.5. Illustration of quantum confinement effects in CdSe colloidal nanocrystals. A red shift in emission is observed for CdSe nanocrystals of increasing size.

1.2.4.2 Nanocrystal Structure

As previously discussed, due to the quantum confinement effect, the nanocrystals' size determines their energy band gap. The number of dimensions of the quantum confinement is dependent on the shape of the semiconductor nanocrystals and has a strong impact on their electronic and optical properties. Two-dimensional (nanoplatelets or quantum wells) and one-dimensional structures (quantum nanorods or nanowires) imply the electrons are confined to only one (the thickness) or two dimensions separately.[38-41] These nanostructures show light-polarization optical properties as a result of their anisotropic structure. Meanwhile, zero-dimensional structures (quantum dots) imply the electrons are confined in all three dimensions. Increasing the number of the confined dimensions will increase the tunability of the band gap.[42]

Colloidal nanocrystals are commonly dispersed in solution. Because of their tiny size, the proportion of surface atoms in the whole nanocrystal is high, leaving many unpassivated dangling bonds on the surface. These bonds can trap charge carriers and cause non-radiative

decay. Ligands adsorbed on the surface of the colloidal nanocrystals can passivate them effectively and prevent their aggregation.[43] The growth of an inorganic shell on nanocrystals is another way to tailor the optical properties. The shell, which is usually another semiconductor material can be deposited in an epitaxial manner. Shell growths with different functions are designed on the cores on the basis of the band gap alignments. Three types can be distinguished, referred to as type-I, type-II and reverse-type-I (Figure 1.6).[42] In type- I, both the electrons and the holes are confined to the core materials because of both deeper VB and CB than those of the shell materials, resulting in enhanced quantum yield and photostability. In reverse type-I, a shell material with both smaller VB and CB is deposited on the core material. This special band alignment induces the electrons and holes to be at least partially delocalized in the shell. In type-II, electrons and holes are segregated between the core and shell materials due to the staggering of VB and CB. A strong red-shift of emission and longer lifetimes are observed in type-II core/shell structures, compared to the core materials.

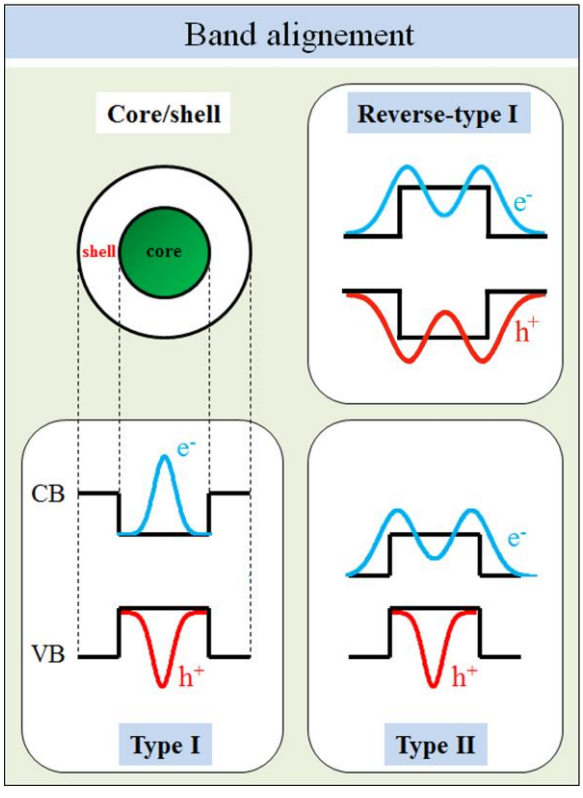

Figure 1.6. Schematic representation of the band alignment of valence band (VB) and conduction band (CB) in different core/shell colloidal semiconductor structures.

1.2.4.3 Optical properties

Colloidal semiconductors suffer from one major drawback, namely 'blinking'.[44,45] Revealed by single nanocrystal studies, this blinking consists in a random fluctuation of their fluorescence intensity between a bright emissive state and a dark non-emissive state. This phenomenon substantially limits their use in bio-imaging and in optoelectronic devices. The blinking phenomenon is thought to arise from two different mechanisms.[46] First, Auger non-radiative processes due to charging and discharging of the nanocrystal cause the energy of the excited exciton to the QD's extra charge rather than radiative recombination (A-type blinking); this process always correlates low fluorescent intensity or even no fluorescence, and short lifetime.[47,48] Second, other non-radiative processes are related to the surface state of nanocrystals (defects, composition), by which 'hot' electrons can be trapped before they relax into emitting core states (B-type blinking).[49,50] Substantial work has been dedicated to the synthesis of non-blinking colloidal nanocrystals, mainly CdZnSe alloys and core/thick-shell CdSe/CdS. Single alloyed nanocrystals do not blink due to a complete suppression of the Auger effect.[51] With regard to thick-shell CdSe/CdS QDs, the delocalization of electrons in the shell leads to a strong decrease of Auger recombination rates and thereby the competition between radiative and Auger recombination, resulting in a neutral bright state and an ionized grey state.[52,53] Nevertheless, Javaux *et al*. demonstrated that the latter is totally inhibited at 30 K, enabling non-blinking nanocrystals with a quantum yield (QY) of 100 %.[54]

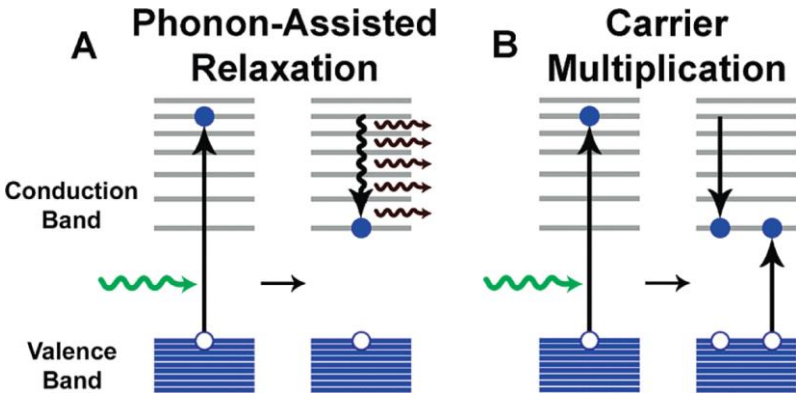

Figure 1.7: Schematic representation of electronic energy relaxation and carrier multiplication in colloidal nanocrystals. (A) An excited carrier relaxes conventionally to the band edge through release of phonons. B) Alternatively, a biexciton is produced by transferring the excess carrier energy to another exciton. Reprinted from Ref [36].

Another process inverse to Auger recombination is carrier multiplication, in which a high energy charge carrier scatters and spends its energy in the creation of a new electron-hole pair, hence forming a biexciton, instead of relaxing to the band edge through the release of phonons, as shown in Figure 1.7.[36] The generation of a biexciton or of multiple excitons from a single high-energy photon can in principle increase the power conversion efficiency and would ultimately improve the efficiency of third-generation solar cells.[55,56]

1.3 The interaction between plasmons and excitons

Hybrid nanomaterials attracted great interest in recent years because they may feature synergistic properties besides the inherent characteristics of the components.[57] Interactions between noble plasmonic metals and excitons can give rise to a variety of interesting phenomena. Basically, one can discern two cases: weak coupling and strong coupling.[58]

1.3.1 Weak coupling between surface plasmons and excitons

In the case of weak coupling, the excitons of the fluorescent substances and the metal surface plasmons are typically considered unperturbed. In this regime, the optical properties of the fluorescent emitters can be controlled by the metal surface plasmons. The oscillating electrons of the metal plasmons can induce multiple responses, such as i)fluorescence enhancement or quenching, ii) changes in fluorescence spectra or iii) strong modification of the radiative lifetime, depending on the hybrid structures.[59]

1.3.1.1 Enhancement of fluorescent intensity

Low fluorescence intensity and photostability greatly limit the applications of fluorescent materials in bio-sensing and bio-imaging applications, as well as in light-emitting devices.[60] Metal-enhanced fluorescence was first proposed in the 80s. Since then, many studies have shown that metal plasmons exhibited a promising potential to tailor the fluorescence behavior.[61-63] In this part, the mechanism of metal-enhanced fluorescence is discussed.

Basically, the excitation near the surface of plasmonic metals can be enhanced by the local electric field; meanwhile the radiative and non-radiative rate of light-emitters can be increased by the Purcell effect and the energy transfer to the metal, thereby changing the whole quantum yield of the light-emitters.[64] Depending on the configuration of the plasmon-fluorescence system, the combination of these two effects can result in a fluorescence enhancement or quenching.

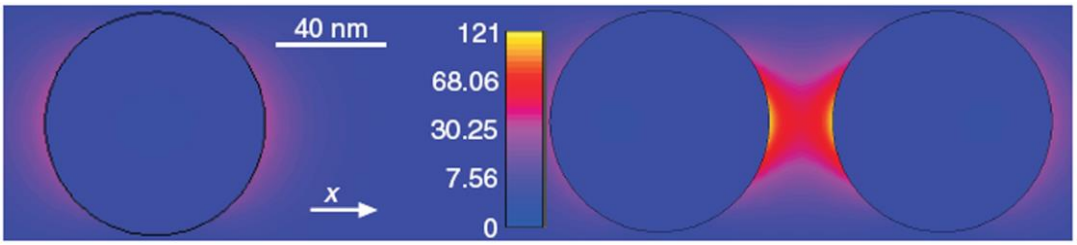

Figure 1.8: (a) Schematic representation of the electric field intensity spatial redistribution produced by a monomer (left) and dimer (right) for 80-nm-diameter gold nanoparticles. The interparticle spacing of the dimer is 23 nm. The incoming light was horizontally polarized at a wavelength of 640 nm. Reprinted from Ref [65].

Higher excitation rate implies more absorption of light and in turn higher fluorescent intensity. The excitation rate of the fluorescent emitters is proportional to the local electric field $|E|^2$. When the noble metals are illuminated by the incident light, the oscillation of the electrons will produce an electric field. This electric field can achieve a maximum, especially when the frequency of the incident light is equal to the frequency of the metal plasmons. Figure 1.8 shows the spatial redistribution of the electric field intensity produced by a monomer (left) and dimer (right) for 80-nm-diameter gold nanoparticles.[65] The incoming light was horizontally polarized at a wavelength of 640 nm. It can be observed that the electric field is maximized in the vicinity of the Au nanoparticle and that the most enhanced specific area is dependent on the direction of the incident light even for an isotropic Au nanosphere. Meanwhile, a domain with an extremely enhanced electric intensity is simulated in the gap of the Au dimer. The enhancement factor E/E_0 (where E_0 is the initial electric field) of the excitation rate of the fluorescent emitters varies with their relative position in the local electric field, with the wavelength of excitation, $E(x_d, \lambda_{ex})$ and with the emitters orientation, e_p. Thereby, the enhancement factor of the excitation rate can be given by,[66]

$$X = |E(x_d, \lambda_{ex})\, e_p|^2/|E_0|^2 \quad (1\text{-}3)$$

In 1940s, Purcell discovered that the rate of spontaneous emission of atoms could be modified when it was resonantly coupled in an electromagnetic cavity, a phenomenon known as Purcell effect.[64] The emitters' own secondary field arrives back at the emitters' location after being scattered in the local environment; this interaction is the origin of the emission dynamics' modification of the light-emitter.[67] Meanwhile an energy transfer from the light-emitter to the plasmons is produced due to the localization of surface plasmons generated by the oscillating near field of the emitter. The scattering and energy transfer together modify both the radiative and non-radiative decay rates of the light-emitter when they are placed in the proximity of metal plasmons, resulting in the modification of the overall quantum yield. It should be noted that the photons can be emitted by the metal through energy transfer to the metal; these photons from the metal are difficult to distinguish from those emitted by the light-emitter itself. The overall emission quantum yield is the sum of these two channels.[59] In the presence of plasmons, the modified lifetime (τ_p) and quantum yield (Q_p) are given below:

$$\tau_p = 1/(k_{f\text{-}p}+\Sigma k_{n\text{-}p}) \quad (1\text{-}4)$$

$$Q_p = k_{f\text{-}p}/(k_{f\text{-}p}+\Sigma k_{n\text{-}p}) \quad (1\text{-}5)$$

Where $k_{f\text{-}p}$ is the modified radiative rate, $k_{n\text{-}p}$ is the modified non-radiative rate. If the increasing speed of the radiative decay rate is higher than that of the non-radiative decay rate, the modified quantum yield will increase. The modification of quantum yield is highly dependent on the intrinsic quantum yield of the light-emitters. In principle, for light-emitters with intrinsic quantum yield close or equal to 100%, the enhancement of the fluorescent intensity can only be achieved by enhancing the excitation rate.[28] Plasmon-enhanced fluorescence is much more effective for low quantum yields. So far the greatest enhancement, 1,300 times brighter, is accomplished when a single dye with a quantum yield of 0.07% is put in an Au bowtie nanoantenna.[15] Besides this, the enhancement of the radiative process reduces the chance of activating photochemical reactions, which are adverse to fluorophores, and hence decreases the photobleaching.

Combining both excitation enhancement and the modification of quantum yield, the ratio between the fluorescence intensity in the presence (I_p) and absence (I_0) of plasmons can be given by:[28]

$$\frac{I_p}{I_0} = X \cdot \frac{Q_p}{Q_0} \tag{1-6}$$

The ratio depends on many parameters including the composition, geometry and size of the metals, the spectral overlap between the plasmons and the emission and/or absorption of the light-emitter, the spacing between the two components and the wavelength of the exciting light.

For a light-emitter placed close to the plasmons, the light-emitter excitation rate will be enhanced when the wavelength of the plasmon resonance is close to the excitation wavelength of the light-emitter. The emission will be enhanced when the wavelength of the plasmon resonance is close to the emission wavelength of the light-emitter.[68] However, the emission peak wavelength is different from the absorption peak wavelength for most light-emitters because of the Stokes shift, so the maximum fluorescence intensity enhancement can be generated when the peak of plasmons is located between the emission and absorption peaks. Besides, plasmon-enhanced fluorescence can display a polarization dependence on the averaged electric field intensity; this is because the electronic field intensity is determined by the relative direction (to the metal) of the exciting light when the structure of the noble metal is anisotropic (such as Au nanorods).[68]

Another very important factor to be considered is the spacing between the two components. In order to obtain the maximum enhancement of the excitation rate, the light-emitter should be as close as possible to the surface of the metal. However, a severe quenching phenomenon is observed when the light-emitters are close enough or 'touch' the metals; in this case, a strong coupling between excitons and surface plasmons can occur. The effect of the distance between the metal and the light-emitter was investigated by Novotny *et al.* utilizing the experimental setup shown in Figure 1.9 (c).[69] Organic dyes are first spin coated on a cleaned glass slide at a very low concentration so as to leave a monolayer of separated dye molecules. The measurements at a single molecule level can be associated to a very low fluorophore concentration. The distance between the metal and the light-emitter is controlled by attaching an Au nanosphere to the end of a pointed optical fiber. When the Au nanosphere gets close to the dye molecule, the fluorescence intensity continuously increases and reaches a maximum at a distance of z = 5 nm. During this process, the excitation rate is enhanced. At the same time, the overall quantum yield also increases because of the faster increasing speed of the radiative

decay rate as compared to that of the non-radiative decay. However, the non-radiative decay rate will increase rapidly if the distance z becomes even smaller, moment at which fluorescence quenching occurs. A variety of dielectric spacer layers including silica, polyelectrolytes or bio-molecules have been widely used to avoid quenching.[18,70]

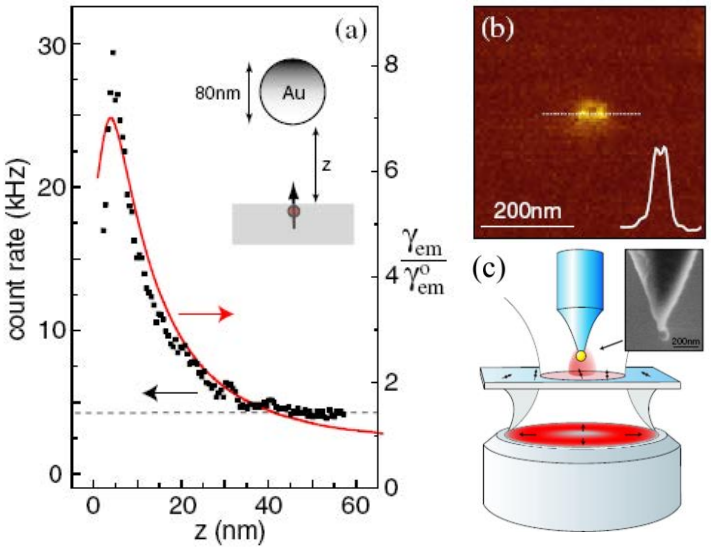

Figure 1.9. (a) Fluorescence rate as a function of particle-surface distance z between an Au nanoparticle and a fluorescent molecule (red curve: theory, dots: experiment). (b) Fluorescence rate image of a single molecule when z = 2nm. (c) Schematic representation of the experimental setup; inset clearly shows that a gold particle is attached to the end of a pointed optical fiber. Reprinted from Ref [69].

1.3.1.2 New phenomena arising from the coupling between excitons and plasmons

Besides the enhancement in fluorescence intensity, many interesting characteristics derived from the interaction between excitons and plasmons have been observed. However, these new phenomena should not be considered isolated from the enhancement in fluorescence intensity because they may be simply different sides of the same underlying physical process.

Most of the fluorescence analyses are based on the fluorescence intensity. However, the intensity is sensible to the external environments and makes the detection of the intensity change not precise. On the other side, a spectral modification, such as a wavelength shift, can

be detected easily. A hybrid nanostructure is fabricated by connecting Au nanospheres and CdTe nanowires via molecular linkers (Figure 1.10a).[71] The excitons in the CdTe nanowires drift and diffuse because of the non-uniform diameter of the CdTe nanowire. In the presence of Au nanospheres, the exciton lifetime decreases and not all excitons have enough time to decay to the minimum potential, leading to a red emission shift. Attaching target proteins to molecular linkers can alter the distance between Au and CdTe, and thereby result in a shift of the emission wavelength (Figure 1.10b and c). This technology can resolve difficulties in the quantification of fluorescence intensity under different optical conditions.

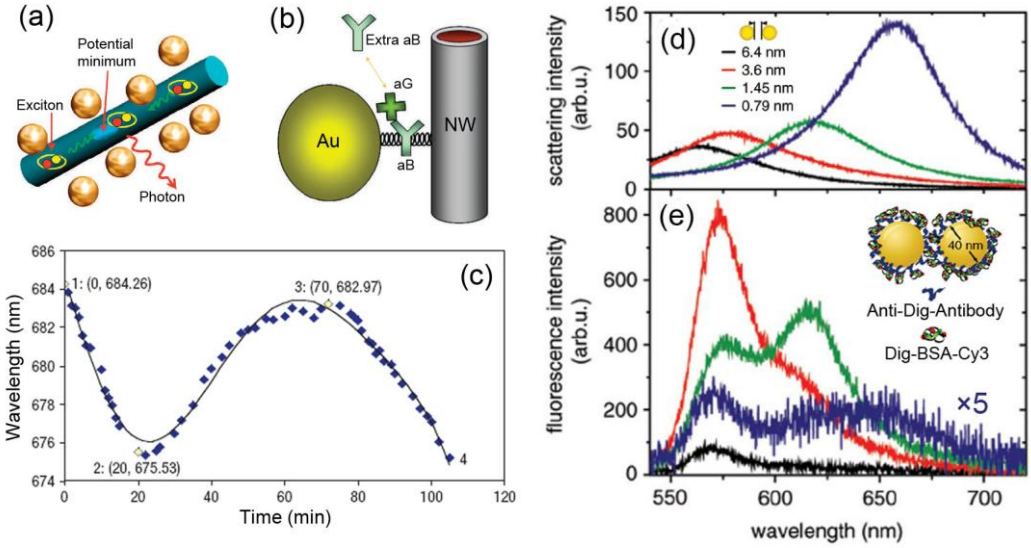

Figure 1.10. (a) Schematic representation of a hybrid of Au nanospheres and CdTe nanowires; the increase of the radiative decay rate leads to a blue shift of emission wavelength. (b) The separation between Au and CdTe can be changed when target proteins are combined with molecular linkers. (c) Reversible shift of the emission wavelength. (d) Experimental scattering spectra and (e) experimental fluorescence spectra of single dimer with Cy3 molecules being placed in the gaps (as shown by the inset in e); the spectra with identical colors are measured from the same dimer. Reprinted from Ref [71, 72].

The spectral shape can also be modified by the interaction between excitons and plasmons. One example is the observation of reshaped spectral outline from dye molecules when they are placed in the gaps of Au nanoparticle dimers (Figure 1.10 d and e).[72] Decreasing the distance between the two nanoparticles leads to a redshift in the longitudinal mode resonance; this is due to the increasingly strong coupling between their plasmons. The dye molecules in the gaps of Au dimers are forced to emit preferentially at the dimers' resonance frequency. Usually, both the ground and excited states of light emitters carry multiple vibrational energy levels other than one excited electronic state. The decay rates of the excitons from different

pairs of the vibrational energy levels are different; thereby the excited molecules will decay preferentially to the transitions, which have a decay rate that matches the frequency of the dimers' plasmons, thus displaying a reshape in emission spectra.

As mentioned above, photons can be emitted from light-emitters into free space or by transferring the energy of the excitons to the metal. In most studies, the independent sources of these radiations are difficult to distinguish. Lukin *et al.* managed to observe the photon emitting at the end of Ag nanowire by locating a quantum dot in the proximity of an Ag nanowire (Figure 1.11).[73] Due to the thin Ag nanowires' tight field confinement and the low velocity of plasmons, the Ag nanowire can directly capture most of the emission from the QDs into the guided surface plasmons, and release these energies to photons at the tip of the Ag nanowire. This will make the tips of the Ag nanowire to light up. When the QD in the red circle in Figure 1.11 b is uniquely excited by a laser, the other two bright spots are exactly located at the tips of the coupled Ag nanowire (Channel III). The energy of the excitons can also be transferred to a metal film and emit plasmon-coupled photons.[74]

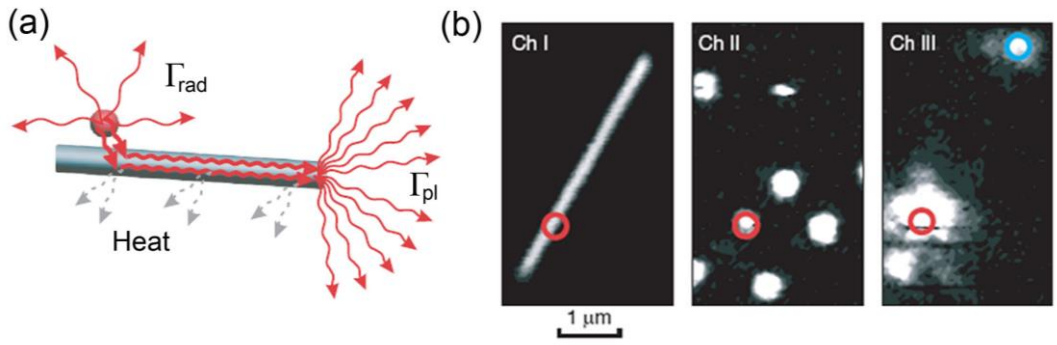

Figure 1.11. (a) The QD can emit into the free space directly or into the guided surface plasmons of the Ag nanowire by radiative coupling due to the tight field confinement and low velocity of plasmons. (b) Channel I: Ag nanowire image. Channel II: optical images of QDs; the red circle marks the location of the coupled QD. Channel III: Only the QD in the red circle is excited by a laser; the bright spot in the red circle corresponds to the free emission of QD; while the other two bright spots arise from the radiative coupling between QD and the Ag nanowire. Reprinted from Ref [73].

Optical metallic plasmonic nanoantennas attracted great attentions in recent years because of their ability to control and manipulate optical fields at the nanometer scale. The nanoantenna is a transducer between free radiation and localized energy; they can highly enhance local fields and direct single-molecule emission.[75] Locating a quantum dot in the near

field of a nanofabricated Yagi-Uda antenna can strongly polarize and direct the fluorescence of the quantum dot into a narrow direction, which can be controlled by tuning the size and structure of the antenna.[76]

The optical properties of quantum dots including blinking and carrier multiplication can also be changed by the adjacent plasmonic metals. When single thick-shell CdSe/CdS nanocrystals or QD/SiO_2 nanoparticles are deposited on an Au film, extremely reduced blinking is observed.[18,77] The suppressed fluctuation of the fluorescence can be explained by the accelerated radiative decay rate, which makes the radiative decay surpass the Auger non-radiative decay. Surface plasmons of a rough Au film can also significantly enhance multi-photon emission of nearby coupled QDs while suppressing the single photon emission at the same time.[78]

1.3.2 Strong coupling between surface plasmons and excitons

In the regime of strong coupling, surface plasmons and excitons are coupled directly; both the exciton wave functions and surface plasmon modes are modified. A new exciton-photon coupled state, the polariton is formed. In this polariton state, the energy is shared and oscillates in the two components. As of today, organic dyes and QDs have been used to obtain a strong coupling with metal films.[13,14,79] Specifically, selective growth of gold tips onto semiconductor nanorods and tetrapods was accomplished by Banin *et al.*[80,81] However, almost no fluorescence can be detected in such semiconductor/metal heterostructures. Recent studies on the hybrid CdS/Au nanostructures indicate that ultrafast energy transfer from the semiconductor to the metal causes fluorescence quenching.[82] On the opposite, it has also been shown that the mixing of electronic states at the interface between semiconductorsıan d metals leads to the significant suppression of both plasmon and exciton emission.[83] *In situ* studies of nucleation and growth of Au on CdSe/CdS nanorods by Shevchenko et al. indicate that rapid formation of Au−S sites at the surface of CdSe/CdS nanorods during the synthesis acts as a trap for the hole (faster than 3 ps), and thereby causes a marked photoluminescence quenching.[84] The strong coupling between excitons and plasmons provides a fundamental framework for applications that rely on optimizing nanoscale light-matter interactions, such as optical nonlinear devices.[85]

References

(1) Jones, M. R.; Osberg, K. D.; Macfarlane, R. J.; Langille, M. R.; Mirkin, C. A.: Templated techniques for the synthesis and assembly of plasmonic nanostructures. *Chemical Reviews* **2011**, *111*, 3736-3827.

(2) Lu, X. M.; Rycenga, M.; Skrabalak, S. E.; Wiley, B.; Xia, Y. N.: Chemical synthesis of novel plasmonic nanoparticles. *Annu Rev Phys Chem* **2009**, *60*, 167-192.

(3) Willets, K. A.; Van Duyne, R. P.: Localized surface plasmon resonance spectroscopy and sensing. *Annu Rev Phys Chem* **2007**, *58*, 267-297.

(4) Kretschm.E: Determination of optical constants of metals by excitation of surface plasmons. *Z Phys* **1971**, *241*, 313-324.

(5) Salomon, L.; Bassou, G.; Aourag, H.; Dufour, J. P.; de Fornel, F.; Carcenac, F.; Zayats, A. V.: Local xxcitation of surface plasmon polaritons at discontinuities of a metal film: theoretical analysis and optical near-field measurements. *Physical Review B* **2002**, *65*, 125409.

(6) Ye, X. C.; Jin, L. H.; Caglayan, H.; Chen, J.; Xing, G. Z.; Zheng, C.; Vicky, D. N.; Kang, Y. J.; Engheta, N.; Kagan, C. R.; Murray, C. B.: Improved size-tunable synthesis of monodisperse gold nanorods through the use of aromatic additives. *Acs Nano* **2012**, *6*, 2804-2817.

(7) Link, S.; El-Sayed, M. A.: Spectral properties and relaxation dynamics of surface plasmon electronic oscillations in gold and silver nanodots and nanorods. *J Phys Chem B* **1999**, *103*, 8410-8426.

(8) Tang, F.; Ma, N.; Wang, X. Y.; He, F.; Li, L. D.: Hybrid conjugated polymer-Ag@PNIPAM fluorescent nanoparticles with metal-enhanced fluorescence. *Journal of Materials Chemistry* **2011**, *21*, 16943-16948.

(9) Liu, N. G.; Prall, B. S.; Klimov, V. I.: Hybrid gold/silica/nanocrystal-quantum-dot superstructures: synthesis and analysis of semiconductor-metal interactions. *J Am Chem Soc* **2006**, *128*, 15362-15363.

(10) Reineck, P.; Gomez, D.; Ng, S. H.; Karg, M.; Bell, T.; Mulvaney, P.; Bach, U.: Distance and wavelength dependent quenching of molecular fluorescence by Au@SiO_2 core-shell nanoparticles. *Acs Nano* **2013**, *7*, 6636-6648.

(11) Peng, B.; Zhang, Q.; Liu, X. F.; Ji, Y.; Demir, H. V.; Huan, C. H. A.; Sum, T. C.; Xiong, Q. H.: Fluorophore-doped core-multishell spherical plasmonic nanocavities: resonant energy transfer toward a loss compensation. *Acs Nano* **2012**, *6*, 6250-6259.

(12) Fu, Y.; Zhang, J.; Lakowicz, J. R.: Plasmon-enhanced fluorescence from single fluorophores end-linked to gold nanorods. *J Am Chem Soc* **2010**, *132*, 5540-5541.

(13) Ni, W. H.; Chen, H. J.; Su, J.; Sun, Z. H.; Wang, J. F.; Wu, H. K.: Effects of dyes, gold nanocrystals, pH, and metal Ions on plasmonic and molecular resonance coupling. *J Am Chem Soc* **2010**, *132*, 4806-4814.

(14) Munechika, K.; Chen, Y.; Tillack, A. F.; Kulkarni, A. P.; Plante, I. J. L.; Munro, A. M.; Ginger, D. S.: Spectral control of plasmonic emission enhancement from quantum dots near single silver nanoprisms. *Nano Lett* **2010**, *10*, 2598-2603.

(15) Kinkhabwala, A.; Yu, Z. F.; Fan, S. H.; Avlasevich, Y.; Mullen, K.; Moerner, W. E.: Large Single-molecule fluorescence enhancements produced by a bowtie nanoantenna. *Nat Photonics* **2009**, *3*, 654-657.

(16) Mahmoudi, M.; Shokrgozar, M. A.: Multifunctional stable fluorescent magnetic nanoparticles. *Chem Commun* **2012**, *48*, 3957-3959.

(17) Bardhan, R.; Grady, N. K.; Cole, J. R.; Joshi, A.; Halas, N. J.: Fluorescence enhancement by Au nanostructures: nanoshells and nanorods. *Acs Nano* **2009**, *3*, 744-752.

(18) Ma, X. D.; Tan, H.; Kipp, T.; Mews, A.: Fluorescence enhancement, blinking suppression, and gray states of individual semiconductor nanocrystals close to gold nanoparticles. *Nano Lett* **2010**, *10*, 4166-4174.

(19) Oregan, B.; Gratzel, M.: A Low-Cost, High-efficiency solar-cell based on dye-sensitized colloidal TiO_2 films. *Nature* **1991**, *353*, 737-740.

(20) Sugawara, Y.; Kelf, T. A.; Baumberg, J. J.; Abdelsalam, M. E.; Bartlett, P. N.: Strong coupling between localized plasmons and organic excitons in metal nanovoids. *Phys Rev Lett* **2006**, *97*, 266808.

(21) Dintinger, J.; Klein, S.; Bustos, F.; Barnes, W. L.; Ebbesen, T. W.: Strong coupling between surface plasmon-polaritons and organic molecules in subwavelength hole arrays. *Physical Review B* **2005**, *71*, 035424.

(22) Pompa, P. P.; Martiradonna, L.; Della Torre, A.; Della Sala, F.; Manna, L.; De Vittorio, M.; Calabi, F.; Cingolani, R.; Rinaldi, R.: Metal-enhanced fluorescence of colloidal nanocrystals with nanoscale control. *Nat Nanotechnol* **2006**, *1*, 126-130.

(23) Oldenburg, S. J.; Averitt, R. D.; Westcott, S. L.; Halas, N. J.: Nanoengineering of optical resonances. *Chemical Physics Letters* **1998**, *288*, 243-247.

(24) Zhou, H. S.; Honma, I.; Komiyama, H.; Haus, J. W.: Controlled synthesis and quantum-size effect in gold-coated nanoparticles. *Physical Review B* **1994**, *50*, 12052-12056.

(25) Wang, H.; Brandl, D. W.; Nordlander, P.; Halas, N. J.: Plasmonic nanostructures: artificial molecules. *Accounts of Chemical Research* **2007**, *40*, 53-62.

(26) Hirsch, L. R.; Stafford, R. J.; Bankson, J. A.; Sershen, S. R.; Rivera, B.; Price, R. E.; Hazle, J. D.; Halas, N. J.; West, J. L.: Nanoshell-mediated near-infrared thermal therapy of tumors under magnetic resonance guidance. *Proc Natl Acad Sci USA* **2003**, *100*, 13549-13554.

(27) Neumann, O.; Urban, A. S.; Day, J.; Lal, S.; Nordlander, P.; Halas, N. J.: Solar vapor generation enabled by nanoparticles. *Acs Nano* **2013**, *7*, 42-49.

(28) Darvill, D.; Centeno, A.; Xie, F.: Plasmonic fluorescence enhancement by metal nanostructures: shaping the future of bionanotechnology. *Physical Chemistry Chemical Physics* **2013**, *15*, 15709-15726.

(29) Lakowicz, J. R.: Principles of fluorescence spectroscopy **2006** *Third Edition*.

(30) Haase, M.; Schäfer, H.: Upconverting nanoparticles. *Angewandte Chemie International Edition* **2011**, *50*, 5808-5829.

(31) Kobayashi, H.; Ogawa, M.; Alford, R.; Choyke, P. L.; Urano, Y.: New strategies for fluorescent probe design in medical diagnostic imaging. *Chemical Reviews* **2009**, *110*, 2620-2640.

(32) Ando, R.; Mizuno, H.; Miyawaki, A.: Regulated fast nucleocytoplasmic shuttling observed by reversible protein highlighting. *Science* **2004**, *306*, 1370-1373.

(33) Murray, C. B.; Norris, D. J.; Bawendi, M. G.: Synthesis and characterization of nearly monodisperse CdE (E = sulfur, selenium, tellurium) semiconductor nanocrystallites. *J Am Chem Soc* **1993**, *115*, 8706-8715.

(34) Wang, F.; Han, Y.; Lim, C. S.; Lu, Y.; Wang, J.; Xu, J.; Chen, H.; Zhang, C.; Hong, M.; Liu, X.: Simultaneous phase and size control of upconversion nanocrystals through lanthanide doping. *Nature* **2010**, *463*, 1061-1065.

(35) Muro, E.; Pons, T.; Lequeux, N.; Fragola, A.; Sanson, N.; Lenkei, Z.; Dubertret, B.: Small and stable sulfobetaine zwitterionic quantum dots for functional live-cell imaging. *J Am Chem Soc* **2010**, *132*, 4556-4557.

(36) Smith, A. M.; Nie, S.: Semiconductor nanocrystals: structure, properties, and band gap engineering. *Accounts of Chemical Research* **2009**, *43*, 190-200.

(37) Talapin, D. V.; Rogach, A. L.; Shevchenko, E. V.; Kornowski, A.; Haase, M.; Weller, H.: Dynamic distribution of growth rates within the ensembles of colloidal II−VI and III−V semiconductor nanocrystals as a factor governing their photoluminescence efficiency. *J Am Chem Soc* **2002**, *124*, 5782-5790.

(38) Ithurria, S.; Dubertret, B.: Quasi 2D colloidal CdSe platelets with thicknesses controlled at the atomic level. *J Am Chem Soc* **2008**, *130*, 16504-16505.

(39) Ithurria, S.; Tessier, M. D.; Mahler, B.; Lobo, R. P. S. M.; Dubertret, B.; Efros, A. L.: Colloidal nanoplatelets with two-dimensional electronic structure. *Nat Mater* **2011**, *10*, 936-941.

(40) Peng, X.; Manna, L.; Yang, W.; Wickham, J.; Scher, E.; Kadavanich, A.; Alivisatos, A. P.: Shape control of CdSe nanocrystals. *Nature* **2000**, *404*, 59-61.

(41) Zhong, H.; Scholes, G. D.: Shape tuning of type II CdTe-CdSe colloidal nanocrystal heterostructures through seeded growth. *J Am Chem Soc* **2009**, *131*, 9170-9171.

(42) Reiss, P.; Protière, M.; Li, L.: Core/shell semiconductor nanocrystals. *Small* **2009**, *5*, 154-168.

(43) Pokrant, S.; Whaley, K. B.: Tight-binding studies of surface effects on electronic structure of CdSe nanocrystals: the role of organic ligands, surface reconstruction, and inorganic capping shells. *Eur. Phys. J. D* **1999**, *6*, 255-267.

(44) Nirmal, M.; Dabbousi, B. O.; Bawendi, M. G.; Macklin, J. J.; Trautman, J. K.; Harris, T. D.; Brus, L. E.: Fluorescence intermittency in single cadmium selenide nanocrystals. *Nature* **1996**, *383*, 802-804.

(45) Empedocles, S.; Bawendi, M.: Spectroscopy of single CdSe nanocrystallites. *Accounts of Chemical Research* **1999**, *32*, 389-396.

(46) Galland, C.; Ghosh, Y.; Steinbruck, A.; Sykora, M.; Hollingsworth, J. A.; Klimov, V. I.; Htoon, H.: Two types of luminescence blinking revealed by spectroelectrochemistry of single quantum dots. *Nature* **2011**, *479*, 203-207.

(47) Efros, A. L.; Rosen, M.: Random telegraph signal in the photoluminescence intensity of a single quantum dot. *Phys Rev Lett* **1997**, *78*, 1110-1113.

(48) Klimov, V. I.; Mikhailovsky, A. A.; McBranch, D. W.; Leatherdale, C. A.; Bawendi, M. G.: Quantization of multiparticle Auger rates in semiconductor quantum dots. *Science* **2000**, *287*, 1011-1013.

(49) Zhao, J.; Nair, G.; Fisher, B. R.; Bawendi, M. G.: Challenge to the charging model of semiconductor-nanocrystal fluorescence intermittency from off-State quantum yields and multiexciton blinking. *Phys Rev Lett* **2010**, *104*, 157403.

(50) Rosen, S.; Schwartz, O.; Oron, D.: Transient fluorescence of the off state in blinking CdSe/CdS/ZnS semiconductor nanocrystals is not governed by Auger recombination. *Phys Rev Lett* **2010**, *104*, 157404.

(51) Wang, X. Y.; Ren, X. F.; Kahen, K.; Hahn, M. A.; Rajeswaran, M.; Maccagnano-Zacher, S.; Silcox, J.; Cragg, G. E.; Efros, A. L.; Krauss, T. D.: Non-blinking semiconductor nanocrystals. *Nature* **2009**, *459*, 686-689.

(52) Mahler, B.; Spinicelli, P.; Buil, S.; Quelin, X.; Hermier, J. P.; Dubertret, B.: Towards non-blinking colloidal quantum dots. *Nat Mater* **2008**, *7*, 659-664.

(53) Chen, Y.; Vela, J.; Htoon, H.; Casson, J. L.; Werder, D. J.; Bussian, D. A.; Klimov, V. I.; Hollingsworth, J. A.: "Giant" multishell CdSe nanocrystal quantum dots with suppressed blinking. *J Am Chem Soc* **2008**, *130*, 5026-5027.

(54) Javaux, C.; Mahler, B.; Dubertret, B.; Shabaev, A.; Rodina, A. V.; Efros, A. L.; Yakovlev, D. R.; Liu, F.; Bayer, M.; Camps, G.; Biadala, L.; Buil, S.; Quelin, X.; Hermier, J. P.: Thermal activation of non-radiative Auger recombination in charged colloidal nanocrystals. *Nat Nanotechnol* **2013**, *8*, 206-212.

(55) Klimov, V. I.: Spectral and dynamical properties of multilexcitons in semiconductor nanocrystals. *Annu Rev Phys Chem* **2007**, *58*, 635-673.

(56) Park, Y. S.; Bae, W. K.; Padilha, L. A.; Pietryga, J. M.; Klimov, V. I.: Effect of the Core/Shell interface on Auger recombination evaluated by single-quantum-dot spectroscopy. *Nano Lett* **2014**, *14*, 396-402.

(57) Agranovich, V. M.; Gartstein, Y. N.; Litinskaya, M.: Hybrid resonant organic–inorganic nanostructures for optoelectronic applications. *Chemical Reviews* **2011**, *111*, 5179-5214.

(58) Achermann, M.: Exciton-Plasmon interactions in metal-semiconductor nanostructures. *J Phys Chem Lett* **2010**, *1*, 2837-2843.

(59) Ming, T.; Chen, H. J.; Jiang, R. B.; Li, Q.; Wang, J. F.: Plasmon-controlled fluorescence: beyond the intensity enhancement. *J Phys Chem Lett* **2012**, *3*, 191-202.

(60) Burns, A.; Sengupta, P.; Zedayko, T.; Baird, B.; Wiesner, U.: Core/shell fluorescent silica nanoparticles for chemical sensing: towards single-particle laboratories. *Small* **2006**, *2*, 723-726.

(61) Siiman, O.; Lepp, A.: Protonation of the methyl-orange derivative of aspartate adsorbed on colloidal silver - a surface-enhanced resonance raman-scattering and fluorescence emission study. *J Phys Chem-Us* **1984**, *88*, 2641-2650.

(62) Lakowicz, J. R.: Radiative decay engineering 5: metal-enhanced fluorescence and plasmon emission. *Anal Biochem* **2005**, *337*, 171-194.

(63) Lakowicz, J. R.; Fu, Y.: Modification of single molecule fluorescence near metallic nanostructures. *Laser Photonics Rev* **2009**, *3*, 221-232.

(64) Pound, R. V.; Purcell, E. M.: Measurement of magnetic resonance absorption by nuclear moments in a solid. *Phys Rev* **1946**, *69*, 681-681.

(65) Acuna, G. P.; Moller, F. M.; Holzmeister, P.; Beater, S.; Lalkens, B.; Tinnefeld, P.: Fluorescence enhancement at docking sites of DNA-directed self-assembled nanoantennas. *Science* **2012**, *338*, 506-510.

(66) Liaw, J.; Chen, C.; Chen, J.: Plasmonic effect of gold nanospheroid on spontaneous emission. *Progress In Electromagnetics Research B* **2011**, *31*, 2891-2959.

(67) Bharadwaj, P.; Deutsch, B.; Novotny, L.: Optical antennas. *Adv Opt Photonics* **2009**, *1*, 438-483.

(68) Ming, T.; Zhao, L.; Yang, Z.; Chen, H. J.; Sun, L. D.; Wang, J. F.; Yan, C. H.: Strong polarization dependence of plasmon-enhanced fluorescence on single gold nanorods. *Nano Lett* **2009**, *9*, 3896-3903.

(69) Anger, P.; Bharadwaj, P.; Novotny, L.: Enhancement and quenching of single-molecule fluorescence. *Phys Rev Lett* **2006**, *96*, 113002.

(70) Jin, Y. D.; Gao, X. H.: Plasmonic fluorescent quantum dots. *Nat Nanotechnol* **2009**, *4*, 571-576.

(71) Lee, J.; Hernandez, P.; Lee, J.; Govorov, A. O.; Kotov, N. A.: Exciton-plasmon interactions in molecular spring assemblies of nanowires and wavelength-based protein detection. *Nat Mater* **2007**, *6*, 291-295.

(72) Ringler, M.; Schwemer, A.; Wunderlich, M.; Nichtl, A.; Kurzinger, K.; Klar, T. A.; Feldmann, J.: Shaping emission spectra of fluorescent molecules with single plasmonic nanoresonators. *Phys Rev Lett* **2008**, *100*, 203002.

(73) Akimov, A. V.; Mukherjee, A.; Yu, C. L.; Chang, D. E.; Zibrov, A. S.; Hemmer, P. R.; Park, H.; Lukin, M. D.: Generation of single optical plasmons in metallic nanowires coupled to quantum dots. *Nature* **2007**, *450*, 402-406.

(74) Wang, Y.; Yang, T.; Pourmand, M.; Miller, J. J.; Tuominen, M. T.; Achermann, M.: Time-resolved surface plasmon polariton coupled exciton and biexciton emission. *Opt Express* **2010**, *18*, 15560-15568.

(75) Novotny, L.; van Hulst, N.: Antennas for light. *Nat Photonics* **2011**, *5*, 83-90.

(76) Curto, A. G.; Volpe, G.; Taminiau, T. H.; Kreuzer, M. P.; Quidant, R.; van Hulst, N. F.: Unidirectional emission of a quantum dot coupled to a nanoantenna. *Science* **2010**, *329*, 930-933.

(77) Canneson, D.; Mallek-Zouari, I.; Buil, S.; Quelin, X.; Javaux, C.; Mahler, B.; Dubertret, B.; Hermier, J. P.: Strong purcell effect observed in single thick-shell CdSe/CdS nanocrystals coupled to localized surface plasmons. *Physical Review B* **2011**, *84*, 245423.

(78) LeBlanc, S. J.; McClanahan, M. R.; Jones, M.; Moyer, P. J.: Enhancement of multiphoton emission from single CdSe quantum dots coupled to gold films. *Nano Lett* **2013**, *13*, 1662-1669.

(79) Ni, W. H.; Yang, Z.; Chen, H. J.; Li, L.; Wang, J. F.: Coupling between molecular and plasmonic resonances in freestanding dye-gold nanorod hybrid nanostructures. *J Am Chem Soc* **2008**, *130*, 6692-6693.

(80) Mokari, T.; Rothenberg, E.; Popov, I.; Costi, R.; Banin, U.: Selective growth of metal tips onto semiconductor quantum rods and tetrapods. *Science* **2004**, *304*, 1787-1790.

(81) Saunders, A. E.; Popov, I.; Banin, U.: Synthesis of hybrid CdS-Au colloidal nanostructures. *J Phys Chem B* **2006**, *110*, 25421-25429.

(82) Wu, K.; Zhu, H.; Liu, Z.; Rodríguez-Córdoba, W.; Lian, T.: Ultrafast charge separation and long-lived charge separated state in photocatalytic CdS–Pt nanorod heterostructures. *J Am Chem Soc* **2012**, *134*, 10337-10340.

(83) Khon, E.; Mereshchenko, A.; Tarnovsky, A. N.; Acharya, K.; Klinkova, A.; Hewa-Kasakarage, N. N.; Nemitz, I.; Zamkov, M.: Suppression of the plasmon resonance in Au/CdS colloidal nanocomposites. *Nano Lett* **2011**, *11*, 1792-1799.

(84) Demortiere, A.; Schaller, R. D.; Li, T.; Chattopadhyay, S.; Krylova, G.; Shibata, T.; Claro, P. C. D.; Rowland, C. E.; Miller, J. T.; Cook, R.; Lee, B.; Shevchenko, E. V.: In situ optical and structural studies on photoluminesence quenching in CdSe/CdS/Au heterostructures. *J Am Chem Soc* **2014**, *136*, 2342-2350.

(85) Zhang, J. T.; Tang, Y.; Lee, K.; Ouyang, M.: Tailoring light-matter-spin interactions in colloidal hetero-nanostructures. *Nature* **2010**, *466*, 91-95.

Chapter 2 Synthesis of Quantum Dots and Their Incorporation in Silica

2.1 Synthesis of QDs

2.1.1 Introduction

Since the breakthrough of the synthesis of high quality colloidal QDs (such as CdS, CdSe and CdTe) by injecting organometallic precursors into the growth solution at high temperature was first reported by Murray *et al.*,[1] synthetic methods for the production of QDs have been greatly developed to improve the physical properties of core-only nanoparticles. The synthesis of core/shell nanoparticles, which involves the homogeneous growth of a crystalline structure on top of a core, is one of the most effective strategies to tune the final nanoparticles' properties.[2-4] The epitaxial overgrowth with another semiconductor shell can not only serve to passivate the surface of the core, but can also enlarge the obtained emission spectral range by a selective choice of the core and shell materials.[5,6] A method named Successive Ion Layer Adsorption Reaction (SILAR) process was developed to synthesize high quality core/shell QDs. Nanoparticles' size dispersion and secondary nucleation can be controlled through this method.[7,8] Recently, core/thick-shell CdSe/CdS nanocrystals have attracted interest in virtue of their reduced blinking.[9,10] In this case, the growth of a thick CdS shell via the SILAR method would be extremely time-consuming because of the high number of injections with long time intervals that would be required. A protocol, which relies upon the continuous injection of shell precursors to the core solution has been developed in our lab to produce these core/thick shell QDs within a few hours.[11]

In this section, we show the synthesis of the different QD types used in this thesis. CdSe/CdS core/shell QDs were synthesized by depositing a shell of CdS with different thicknesses via successive injection of the precursors on CdSe nanocrystals. CdSe/CdS/ZnS core/shell/shell QDs were obtained by combining the injection method for the growth of CdS with the SILAR process for the growth of ZnS.

2.1.2 Precursors preparation

S-ODE: A sulfur stock solution in 1-octadecene (ODE) was prepared by heating 320 mg of sulfur in 100 mL of degassed ODE at 120 °C until complete dissolution. The concentration of S-ODE is 0.1 M.

Se-ODE: A selenium stock solution in ODE (Se-ODE 0.1 M) was prepared by first suspending 790 mg of selenium in 10 mL of ODE. This mixture was then injected in small quantities to 90 mL of degassed ODE at 170 °C while rising progressively the temperature until 205°C. The solution was then kept at 205 °C for 30 min.

Cadmium oleate: 0.5 M $Cd(oleate)_2$ in oleic acid was synthesized by heating 3.2 g of CdO in 50 mL of oleic acid at 160 °C under Ar for 1 h until all the CdO was dissolved. Then, this solution was degassed under vacuum at 70 °C for 30 min.

Cadmium myristate was prepared following a previously published procedure. 1.23 g of cadmium nitrate tetrahydrate (5.0 mmol) was dissolved in 40 ml of methanol; another solution was made by dissolving 3.13 mg of sodium myristate (13.1 mmol) in 250 ml of methanol. After complete dissolution, the cadmium nitrate solution was mixed with the sodium myristate solution, giving a white precipitate. This precipitate is filtered, washed with methanol and dried under vacuum for one night.

Zinc oleate: 0.5 M $Zn(oleate)_2$ in oleic acid was synthesized by heating 2.03 g of ZnO in 50 mL of oleic acid at 280 °C under Ar for 45 min until all the ZnO was dissolved. This solution was then degassed under vacuum at 80 °C for 30 min.

2.1.3 Synthesis of 6 nm-in-radius-CdSe/CdS core/shell QDs

2.1.3.1 Synthesis of CdSe QDs

CdSe nanocrystals were prepared following a protocol invented by Cao.[12] 0.3 mmol of cadmium myristate and 0.15 mmol of selenium powder were dispersed in 16 mL of ODE, degassed under vacuum at room temperature for 30 min, and heated up to 240 °C under argon flow for 8 min. 200 µL of oleic acid were added and the solution was cooled down to room temperature. CdSe nanocrystals (emission λ_{max} = 564 nm) were obtained as a colloidal

suspension in ODE (C = 2.86×10^{-5} M, radius = 1.55 nm)[13,14] and used directly for the CdS shell growth as follows.

2.1.3.2 Formation of a CdS shell on CdSe cores

A precursor solution for the growth of the CdS shell was made by mixing 24 mL of 0.1 M S-ODE in ODE and 5 mL of a 0.5 M solution of $Cd(oleate)_2$ in oleic acid. 2 mL of oleylamine were added to 4 mL of the CdSe nanocrystals solution in ODE (C = 2.86×10^{-5} M) and heated to 260 °C for 20 min under Ar flow. 4.5 mL of the precursor solution were added dropwise within 2 h. The temperature was raised up to 310 °C and another 22.5 mL of the precursor solution was injected at a rate of 15 mL/h. The mixture was cooled down to room temperature and the nanocrystals dispersed in ODE were precipitated with ethanol. The precipitate was taken up in 10 mL of hexane and 40 mL of ethanol were added to precipitate the QDs. This washing process was repeated one more time. The CdSe/CdS QDs were taken up in hexane and characterized optically and by electronic microscopy (Figure 2.1). Their final radius was 6.0±0.5 nm, corresponding to a CdS shell thickness of 4.5±0.5 nm.

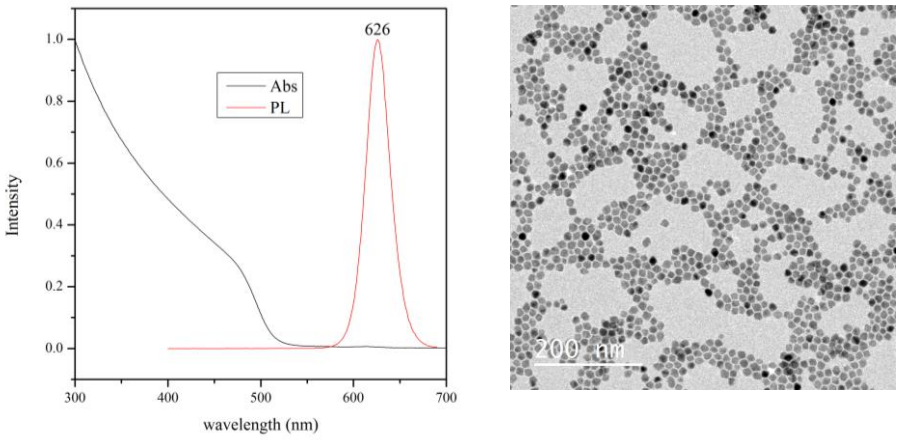

Figure 2.1. Absorption and photoluminescence spectra (left) and TEM image (right) of 6-nm-in-radius CdSe/CdS core/shell QDs.

2.1.4 Synthesis of 15 nm-in-radius-CdSe/CdS core/shell QDs

2.1.4.1 Synthesis of CdSe cores

CdSe cores were synthesized as per a protocol adapted by Mahler from Yang *et al.* with slight modifications.[12,15] A dispersion of selenium powder (12 mg) in ODE (8 mL) was added in a three-necked flask to cadmium myristate (174 mg) and additional ODE (8 mL) was further introduced. The mixture was degassed for 30 min under vacuum and then the flask was filled with argon and heated up to 240 °C. After 25 min, 570-nm-emitting cores were obtained. Oleic acid (200 µL) was injected at this temperature and the solution was heated up to 260 °C. At this temperature, oleylamine (2 mL) was injected and the reaction was further stirred for 20 min. The temperature was raised to 280 °C and 4 mL of a mixture of Se-ODE (0.1 M, 5 mL) and cadmium oleate (0.5 M, 1 mL) were injected dropwise (36 mL/h), while progressively rising the temperature until 305 °C. After the addition of the precursors, the solution was rapidly cooled down to room temperature. The 630-nm-emitting CdSe QDs (2.9 nm in radius) were washed with ethanol and then taken up in hexane (10 mL).

2.1.4.2 Formation of a CdS shell on CdSe cores

In a three-necked flask, a mixture of freshly-made CdSe cores (40 nmol), ODE (5 mL) and cadmium myristate (10 mg) was degassed for 30 min at 70 °C under vacuum. The flask was then filled with argon and heated up to 260 °C. At this temperature, oleylamine (2 mL) was injected and the reaction was further stirred for 20 min. 4.5 mL of a mixture of S-ODE (0.1 M, 16.5 mL) and cadmium oleate (0.5 M, 3.5 mL) were added dropwise (2.25 mL/h). After injection, the temperature was raised to 310 °C. At this temperature, the remaining 15.5 mL of the precursor solution were added dropwise (7 mL/h). After injection, 22 mL of the reaction medium were withdrawn, and another 20 mL of a mixture of S-ODE (0.1 M, 16.5 mL) and cadmium oleate (0.5 M, 3.5 mL) were added dropwise (7 mL/h) to the QDs remaining in the flask. The solution was then cooled down to room temperature. The core/shell CdSe/CdS QDs were finally washed with ethanol and redispersed in hexane (QDs concentration: 1.42 µM). The CdSe/CdS QDs were characterized optically and by electronic microscopy (Figure 2.2). Their final radius was ~ 15 nm, corresponding to a CdS shell thickness of 12.1 nm.

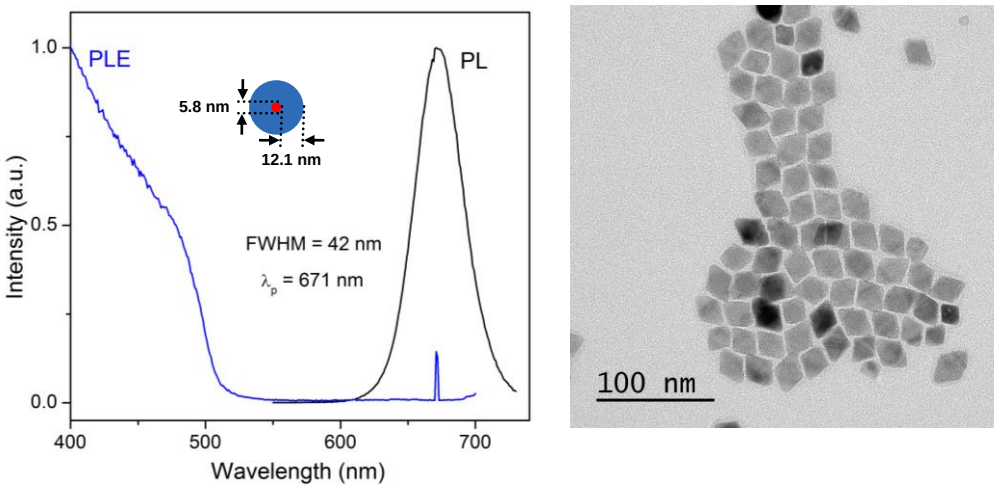

Figure 2.2. Photoluminescence (PL) and PL Excitation (PLE) spectra (Left) and TEM image (Right) of CdSe/CdS 15 nm-in-radius-QDs.

2.1.5 Synthesis of CdSe/CdS/ZnS

2.1.5.1 Synthesis of CdSe/CdS

The synthesis of the cores was carried out in a 100 ml three-necked round-bottomed flask under argon atmosphere. 170 mg of Cd(myristate)$_2$ (0.3 mmol) were introduced in the flask and then 7.5 mL of ODE were added. The mixture was stirred and degased under vacuum at room temperature for 30 min. The reaction was then put under Ar and heated up to 240°C, followed by the injection of 12 mg of Se dispersed in 1 mL of ODE. The reaction was heated for 5 min. Then, 100 µL of oleic acid were added, followed by the addition of 10 mL of ODE and 10 mL of oleylamine. Thereafter, a Cd(OA)$_2$/S-ODE mixture was injected at 9 mL/h. The reaction was monitored to stop the injection once 610 nm of emission was achieved. The reaction was left to cool down to room temperature. The CdSe/CdS QDs were washed with ethanol and then dispersed into 10 mL of ODE for the next step.

CdSe/CdS QDs with emission peaks at 550 and 650 nm were synthesized by tuning the size of CdSe. The deposition of CdS was performed as the synthesis of QD-610 nm; the reaction was monitored to stop the injection once 550 or 650 nm of emission was achieved.

2.1.5.2 ZnS shell growth

The shell growth of two and a half monolayers of ZnS was done by SILAR.[8] The amount of $Zn(oleate)_2$ 0.1M in ODE and S-ODE 0.1M required for each monolayer were calculated from the concentration and size of the CdSe cores previously estimated. 600 nmol of CdSe/CdS QDs were introduced in a 100 ml three-necked flask and diluted with ODE to a total volume of 20 mL, followed by the addition of 10 mL of oleylamine. The solution was degased under vacuum at room temperature for 30 min. The reaction was then put under Argon. The amounts of 0.1 M $Zn(oleate)_2$ in ODE and of 0.1 M S-ODE required for the formation of the first ZnS monolayer were introduced with syringes. The reaction was heated at 230°C for 20 min. The amount of 0.1 M $Zn(oleate)_2$ necessary for the formation of the next layer was injected over 30 seconds. After 10 min at 230°C, the amount of 0.1 M S-ODE required for the formation of the next layer was injected over 30 seconds and the reaction was left 10 min at 230°C. Finally, the amount of 0.1 M $Zn(oleate)_2$ necessary for the formation of the last layer was injected over 30 seconds and the reaction was left 10 min at 230°C. The reaction was finally cooled down to room temperature. The CdSe/CdS/ZnS core/shell/shell QDs were washed with ethanol and then dispersed into 10 mL of hexane. Figure 2.3 shows the TEM images and emission spectra of the obtained monodispersed CdSe/CdS/ZnS QDs. The average sizes of QDs with emission colors at 550, 610 and 650 nm are 15, 12 and 15 nm respectively.

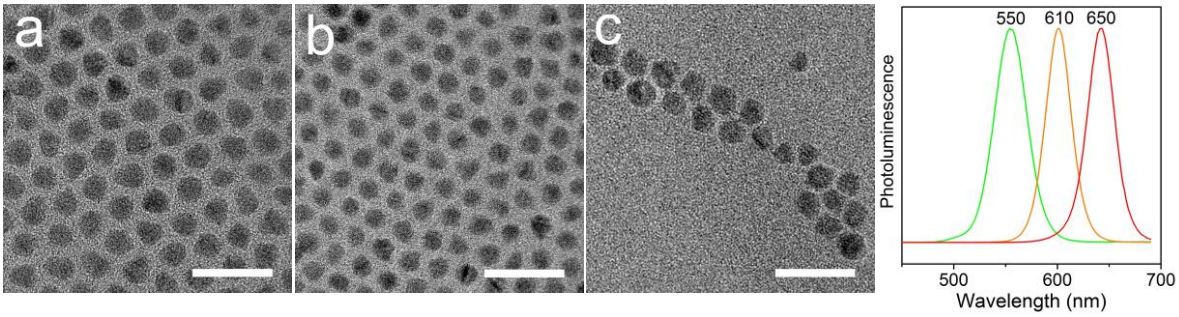

Figure 2.3. TEM images of CdSe/CdS/ZnS QDs with emissions at a) 550 nm; b) 610 nm; c) 650 nm; d) corresponding photoluminescence spectra. Scale bars: 50 nm.

2.2 Synthesis of QD/SiO_2

2.2.1 Introduction

Silica coating techniques for nanoparticles (NPs) are attractive since the silica shell can protect the NPs from the external environment, thus improving their chemical and physical stability.[16-18] The surface chemistry of SiO_2 facilitates the functionalization with many groups for further use.[19-22] Besides, it is especially important for *in vivo* applications since the cross-linked SiO_2 shell can decrease toxicity arising from the release of heavy metal ions.[23]

The coating of hydrophobic QDs by a thin layer of silica was initially achieved through a ligand exchange with thiol-silanes, followed by the polymerization of the siloxane function.[24] Further growth and tuning of the silica shell could then be performed using tetraethyl orthosilicate (TEOS) as the SiO_2 precursor (Stöber method).[25] As a representative example, Nann *et al.* succeeded in encapsulating CdSe/ZnS QDs in silica shells having a thickness ranging from 15 to 40 nm.[25] Bakalova developed another method: single QD micelles were first stabilized by hydrophobic silica precursors, followed by an extension of the silica layer to form a silica shell around the micelle. Up to 92% of obtained QD/SiO_2 consists of one single QD in the SiO_2 shell.[26] However, these multi-steps approaches require a careful control over the experimental conditions, such as the pH value, the quantity of silanes or of TEOS.

QDs/SiO_2 can also be obtained by applying water-in-oil (W/O) reverse micro-emulsion solution methods. Both hydrophilic and hydrophobic QDs have been successfully encapsulated in SiO_2 beads via this method.[16,18,27-33] The incorporation mechanism of hydrophobic QDs in SiO_2 is illustrated in Scheme 2.1 by Meijerink *et al.*[30] First, the original organic ligands on the hydrophobic QDs surface are replaced by the surfactant or by hydrolyzed TEOS molecules. The introduction of ammonia will produce more hydrolyzed TEOS molecules, which will replace all the surfactant molecules around QDs. Water and ammonia molecules are present between the TEOS-coated QD and the surfactant molecules layer, where the SiO_2 growth takes place via further hydrolysis and condensation of TEOS. Compared to the ligand exchange method, the reverse-emulsion method is less complicated without ligands exchange and much more reproducible. The obtained QD/SiO_2 NPs display highly uniform dispersion and the thickness of SiO_2 can be tuned easily and precisely by changing the quantity of TEOS.

In this section, our synthetic approach towards the obtainment of monodisperse, size-tunable SiO_2 nanospheres is presented. These nanoparticles contain unique pre-synthesized CdSe/CdS QDs (two radius: 6 and 15 nm) exactly at their center and are made by the reverse emulsion solution method. The SiO_2 layer thickness was regulated from 12 to 60 nm. Thicker SiO_2 layers can be obtained by further growth of SiO_2 *via* the Stöber method. The QD/SiO_2 core/shell nanoparticles will be referred to as 'R/T_1 nanoparticles', where R and T_1 are the CdSe/CdS QD radius and the SiO_2 shell thickness, respectively, expressed in nanometer (nm).

Scheme 2.1: Schematic representation of the incorporation mechanism of hydrophobic QDs (in orange) in SiO_2 spheres by the reverse microemulsion method. Reprinted from [30].

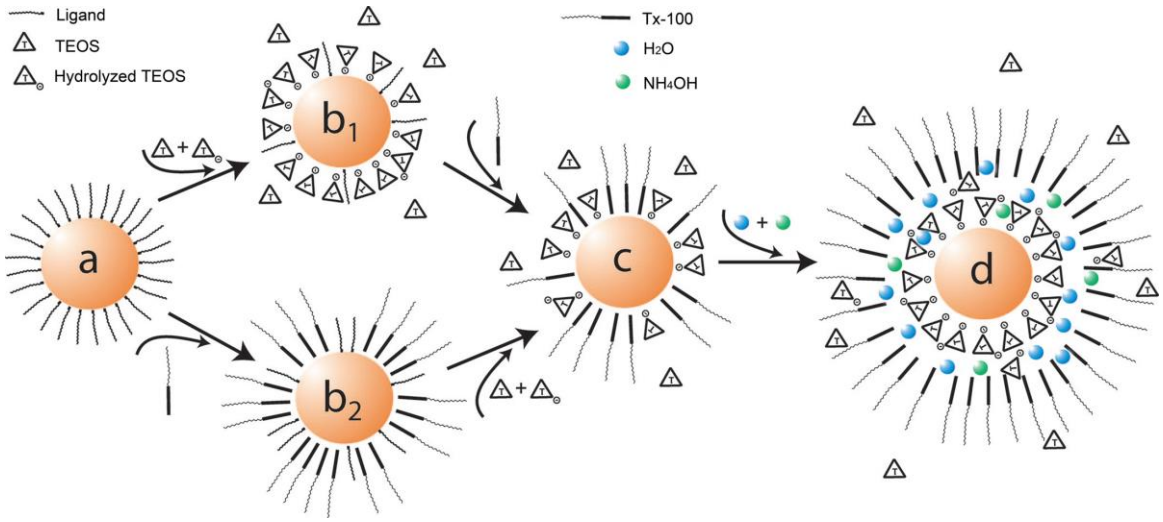

2.2.2 Selection of surfactant

The reverse emulsion solution is generally formed from polyoxyethylene (5) nonylphenylether (Igepal CO-520) or poly(ethylene glycol) p-(1,1,3,3-tetramethylbutyl)-phenyl ether (Triton X-100) as the surfactant.[18,34] First of all, Igepal CO-520 and Triton X-100 were used and compared with regard to their effect on the final QD/SiO_2 size.

2.2.2.1 Synthesis of QD/SiO_2 NPs with Igepal CO-520

In a typical synthesis, 350 mg of Igepal CO-520 were dissolved in 6 mL of cyclohexane. Subsequently, 0.20 nmol of 6 nm-in-radius-QDs (in 100 μL of hexane) were added, followed by the addition of 200 μL of ammonia solution (29.4 wt % in water) and 20 μL of TEOS under stirring. The mixture was stirred for 12 hours at room temperature. Then, depending on the desired SiO_2 shell thickness, variable amounts of TEOS were added, and the solution was further stirred for 12 h to bring about the encapsulation process. The QD/SiO_2 nanoparticles were precipitated by adding 3 mL of ethanol to the reaction solution. This solution was centrifuged and the supernatant was removed. The QD/SiO_2 were washed successively with 20 mL of a butanol/hexane 1/1 mixture (v/v), 20 mL of an isopropanol/hexane 1/1 mixture (v/v), 20 mL of an ethanol/hexane 1/1 mixture (v/v), and 20 mL of ethanol. QD/SiO_2 NPs were dispersed in 10 mL of water, further washed twice with water and finally redispersed in 15 mL of methanol.

2.2.2.2 Synthesis of QD/SiO_2 NPs with Triton X-100

The procedure is similar to the protocol in the section ***2.2.2.1****. The quantities of the reaction materials are as follows: 6 nm-in-radius-QDs, 0.16 nmol (in 75 μL of hexane) or 15 nm-in-radius-QDs, 0.16 nmol (in 120 μL of hexane); Triton X-100, 1.89 g; hexanol, 1.47 g; cyclohexane, 7.5 mL; water, 0.38 mL; NH_4OH (29.4 wt % in water), 60 μL; TEOS, 60 μL. Variable amounts of TEOS (from 70 to 640 μL) depending on the desired SiO_2 shell thickness were added and the solution was further stirred for 24 h at room temperature to achieve the encapsulation process.*

2.2.2.3 The effect of the surfactant on the QD/SiO_2 NPs size

As shown in Figure 2.4 a, 6/12 QD/SiO_2 NPs were successfully synthesized through a one-step TEOS addition (20 μL) when Igepal CO-520 was used as the surfactant; more than 95% of SiO_2 beads contain only one QD at the center. The SiO_2 thickness can be increased to 19 nm by the second addition of 30 μL of TEOS (Figure 2.4 b). However, the SiO_2 thickness did not increase when more TEOS was introduced to the growth solution. The emulsion system with Igepal CO-520 is sensitive to the alcohol content; the high concentration of TEOS will produce much ethanol, which can increase the polydispersity of QD/SiO_2 NPs or even destroy

the micelle system.[35] Osseao-Asare *et al.* demonstrated that monodispersed SiO_2 nanospheres with radii in the range of 20 to 35 nm were synthesized within reverse Igepal CO-520 micelles by tuning the ratio between the quantities of water and surfactant.[36] In the case of QD/SiO_2 synthesis, however, it appears complicated to adjust the QDs quantity to the ratio between water and Igepal CO-520 so as to make SiO_2 beads containing a unique QD.

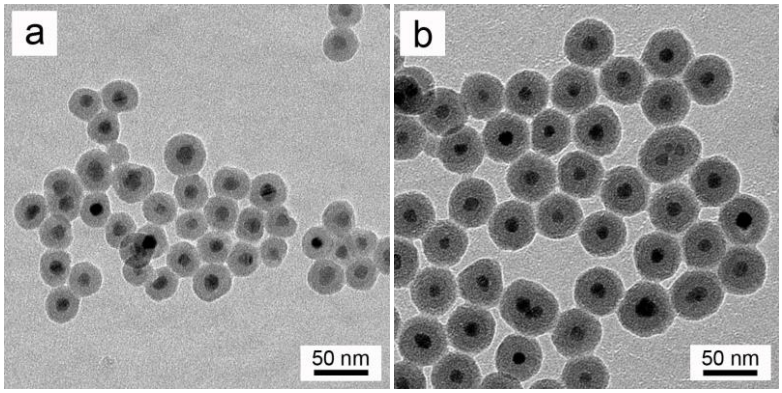

Figure 2.4. TEM images of 6/T1 QD/SiO_2 NPs synthesized in an Igepal CO-520 emulsion solution with various SiO_2 thicknesses; a) 12 nm; b) 19 nm.

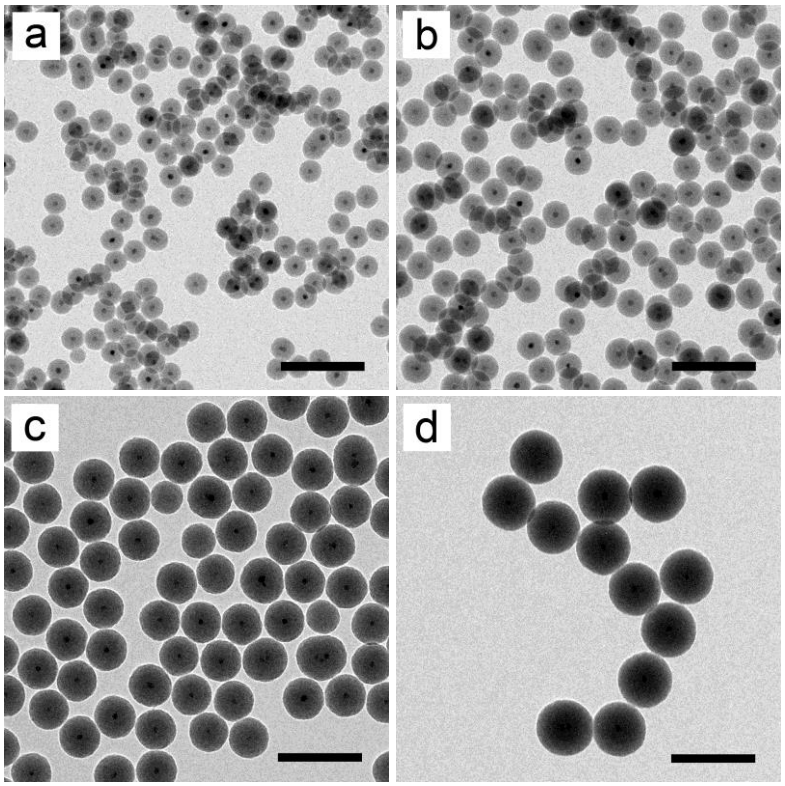

Figure 2.5. TEM images of 6/T_1 QD/SiO_2 NPs synthesized in a Triton X-100 emulsion solution with various SiO_2 thicknesses obtained through the addition of the corresponding amount of TEOS: a) 21.5 nm (60 µL); b) 29 nm (130 µL); c) 42 nm (310 µL); d) 60 nm (700 µL).

When Triton X-100 was used as the surfactant, the introduction of 1-hexanol helped Triton X-100 dissolving in cyclohexane and also acted as a co-surfactant, which can improve the uniformity of the emulsion system. This micro-emulsion was less sensitive to the alcohol produced by the TEOS hydrolysis.[35] The first addition of TEOS (60 µL) made the SiO_2 layer grow to 21.5 nm (Figure 2.5 a) (diameter of the resulting QD/SiO_2 NPs: 55 nm). Different amounts of TEOS were added (from 70 to 640 µL) to obtain thicker SiO_2 layers (from 31.5 to 60 nm), as shown in Figure 2.5. 95% of obtained QD/SiO_2 beads contained only one dot at the center. Note that the maximal SiO_2 thickness accessible via this protocol is 60 nm, as shown in Figure 2.5d, most probably due to the size of the surfactant micelles. When 15-nm-in-radius-QDs were added to the emulsion solution, as shown in Figure 2.6, these huge QDs were also successfully coated with SiO_2 shells. Less than 5% of individual QD/SiO_2 contained two or three QDs at the center. The thickness of SiO_2 was tuned from 12 to 50 nm by adding different quantities of TEOS.

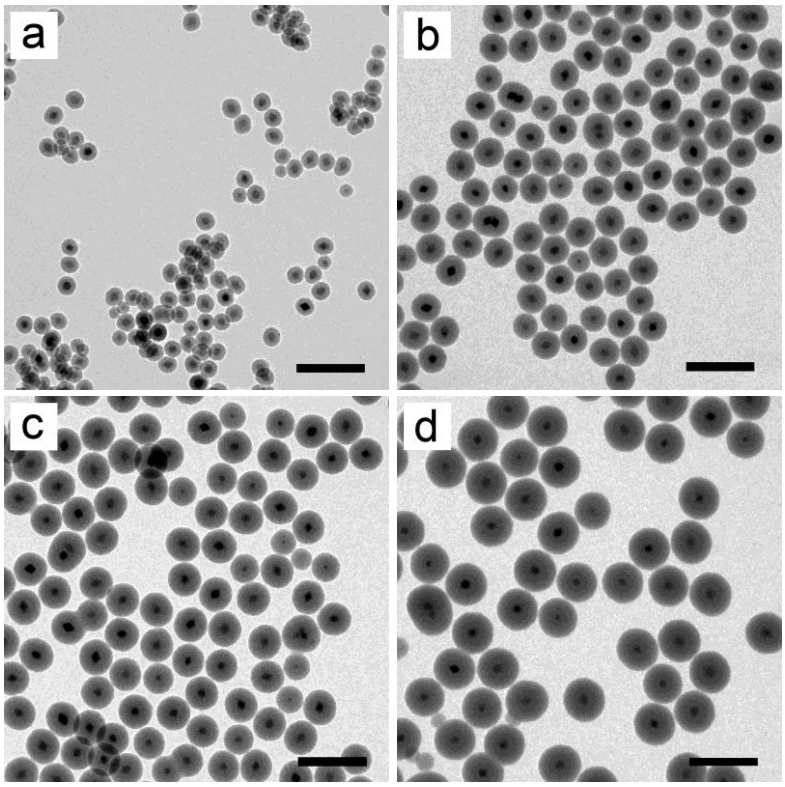

Figure 2.6. TEM images of 15/T_1 QD/SiO_2 NPs synthesized in a Triton X-100 emulsion solution with various SiO_2 thicknesses obtained through the addition of the corresponding amount of TEOS: a) 12 nm (60 µL); b) 27.5 nm (240 µL); c) 35 nm (460 µL); d) 47 nm (940 µL). Scale bars: 200 nm

2.2.3 Effect of the QDs amount

In last section, more than 95% of individual QD/SiO_2 contained only single QDs at the center can be obtained. These QD/SiO_2 NPs will be covered with a continuous gold nanoshell, which enables us to study the coupling of plasmons and fluorescence at single particle level. In order to clarify the effect of the QDs amount on the QDs number incorporated in SiO_2 beads, different quantities of 15-nm-in-radius-QDs were added to the reverse emulsion solution of the protocol in the section **2.2.2.2**. When the amount of QDs was increased from 0.16 nmol to 0.26 nmol, the corresponding amount of TEOS was also increased in the same ratio. TEM images of the obtained QD/SiO_2 NPs are presented in Figure 2.7. The proportion of QD/SiO_2 beads containing multiple QDs at their center did not increase significantly within the investigated QD quantity range. These results combined with the incorporation of QDs of different sizes indicate that QDs act as heterogeneous nucleation points for SiO_2 deposition, which is consistent with the mechanism elucidated by Meijerink *et al*.[30]

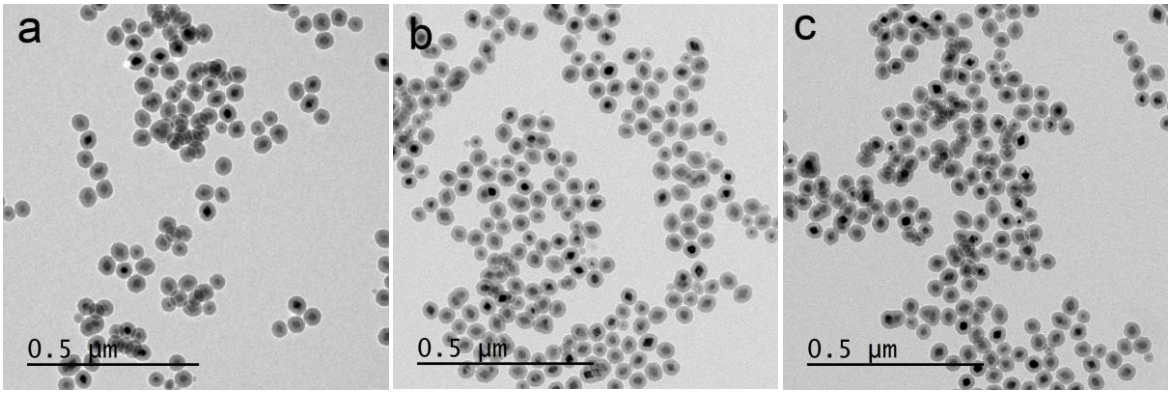

Figure 2.7. TEM images of 15-nm-in-radius-QD/SiO_2 when QDs of different amounts were added: a) 0.16 nmol; b) 0.21 nmol; c) 0.26 nmol.

However, when 1.2 nmol of 6-nm-in-radius-QDs were introduced (10 times higher than that used in the section **2.2.2.2**), the proportion of QD/SiO_2 NPs which contained multiple QDs increased and the morphology of QD/SiO_2 became irregular (Figure 2.8a). When the QD amount continuously increased to 2.4 nmol (20 times higher than that used in the section **2.2.2.2**), the high QD concentration made the micelle system unstable, resulting in serious aggregation of QD/SiO_2 (Figure 2.8b). This indicates that SiO_2 nanospheres that have multiple QDs encapsulated at their center cannot be achieved by simply increasing the QDs amount in this reverse emulsion system.

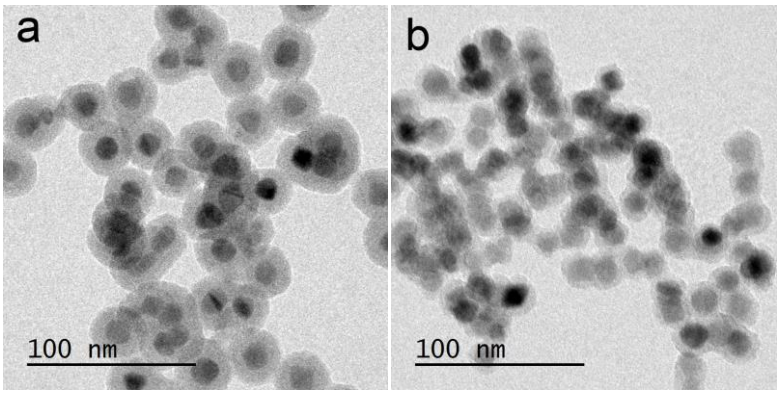

Figure 2.8. TEM images of 6-nm-in-radius-QD/SiO_2 when QDs of different amounts were added: a) 1.2 nmol; b) 2.4 nmol.

2.2.4 Growth of thicker SiO_2 layer *via* Stöber method

As explained in the previous paragraph, there was a limit in the achievable SiO_2 size when using the reverse emulsion method. The conventional Stöber method could then be used to obtain larger silica nanoparticles, starting from the QD/SiO_2 beads synthesized via reverse micro-emulsion.[37] Two sizes of QD/SiO_2 NPs were chosen to act as seeds: 25 and 62 nm in radius.

2.2.4.1 Regrowth of silica on QD/SiO_2 NPs (radius-62 nm)

6 nm-in-radius-QD/SiO_2 NPs (radius: 62 nm, 1.0 mL from the previously-described 15-mL methanol dispersion) were centrifuged and redispersed in 8.0 mL of water. This solution was then slowly added to a mixture of 40.0 mL of ethanol and 600 µL of ammonia solution (29.4 wt % in water). When this solution became homogeneous, 44, 49 and 54 µL of TEOS in ethanol (v/v = 1/9) were added every 4 hours. The reaction solution was kept stirring overnight in a closed system.

2.2.4.2 Regrowth of silica on QD/SiO_2 NPs (radius-25 nm)

The procedure is similar to the protocol in the section ***2.2.4.1****; the quantities of the reaction materials are as follows: 6 nm-in-radius-QD/SiO_2 NPs (radius: 25 nm) from the previously-*

described 15-mL methanol dispersion, 300 µL; water, 2.47 mL; ethanol, 12.8 mL; ammonia solution (29.4 wt % in water), 185 mL; and 15 µL of TEOS in ethanol (v/v = 1/9) were added. Another 15 µL of TEOS in ethanol (v/v = 1/9) were added after 4 hours. The reaction solution was kept stirring overnight in a closed system.

2.2.4.3 The effect of the QD/SiO_2 starting size on the silica regrowth

As an example, 6/60 QD/SiO_2 NPs were grown to 6/65 NPs (Figure 2.9); although a slight NPs aggregation could be observed. It should be noted that this effect is all the more important as the size of starting QD/SiO_2 NPs decreases: when 6/19 NPs were regrown, the thickness of the SiO_2 layer effectively became bigger after the addition of TEOS, but severe aggregation and no separated QD/SiO_2 beads occurred (Figure 2.10). The distance between two adjacent QD cores in each aggregate being approximately 50 nm (which equals the diameter of QD/SiO_2 NPs before regrowth) indicates that the beads were already aggregated before TEOS addition. This could be explained by surfactant molecules coming from the emulsion process and remaining onto the silica surface of the NPs. Compared to small QD/SiO_2 NPs, big QD/SiO_2 beads are easier to separate via sonication. The separation of QD/SiO_2 NPs favors the removal of the surfactant, and thereby decreases the aggregation of QD/SiO_2 NPs before the regrowth of SiO_2.

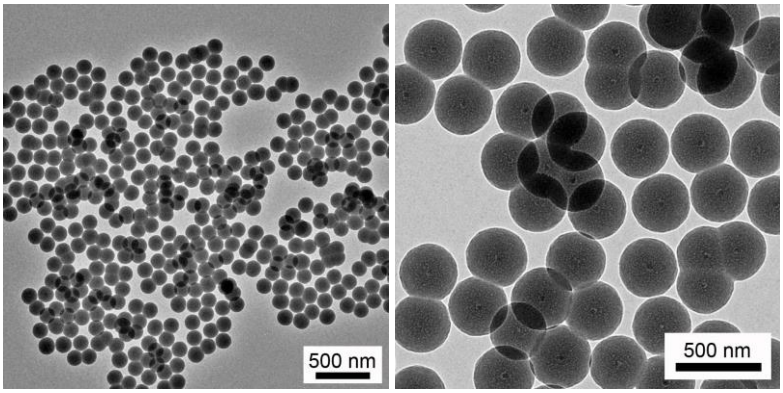

Figure 2.9. TEM images of 6/60 QD/SiO_2 NPs regrown via the Stöber method.

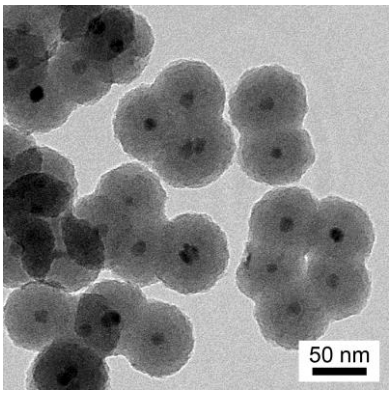

Figure 2.10. TEM images of 6/19 QD/SiO_2 NPs regrown the via Stöber method.

2.2.5 Conclusions

A variety of core/shell QDs including CdSe/CdS and CdSe/CdS/ZnS have been synthesized. These monodispersed QDs have different sizes (resulting from the core size and the shell thickness) and emission colors. They serve as core materials for the various encapsulation strategies described in this thesis.

Two types of CdSe/CdS QDs (radius: 6 and 15 nm) have been successfully encapsulated in SiO_2 beads through a reverse micro-emulsion method. Under optimized conditions, 95% of QD/SiO_2 beads contain unique QD at their center, a fact that facilitates coupling investigations at single QD level. As we will show in the following chapter, these QD/SiO_2 NPs can be covered by a continuous gold nanoshell to realize the coupling between QD emission and plasmon resonance in gold nanoshells. The thickness of the SiO_2 layer – one important parameter to maximize the plasmon coupling – can be precisely adjusted by tuning the quantity of the SiO_2 precursor TEOS.

References

(1) Murray, C. B.; Norris, D. J.; Bawendi, M. G.: Synthesis and characterization of nearly monodisperse CdE (E = sulfur, selenium, tellurium) semiconductor nanocrystallites. *J Am Chem Soc* **1993**, *115*, 8706-8715.

(2) Hines, M. A.; Guyot-Sionnest, P.: Synthesis and characterization of strongly luminescing ZnS-Capped CdSe nanocrystals. *J Phys Chem-Us* **1996**, *100*, 468-471.

(3) Peng, X. G.; Schlamp, M. C.; Kadavanich, A. V.; Alivisatos, A. P.: Epitaxial growth of highly luminescent CdSe/CdS core/shell nanocrystals with photostability and electronic accessibility. *J Am Chem Soc* **1997**, *119*, 7019-7029.

(4) Reiss, P.; Protiere, M.; Li, L.: Core/Shell semiconductor nanocrystals. *Small* **2009**, *5*, 154-168.

(5) Mews, A.; Eychmueller, A.; Giersig, M.; Schooss, D.; Weller, H.: Preparation, characterization, and photophysics of the quantum dot quantum well system cadmium sulfide/mercury sulfide/cadmium sulfide. *The Journal of Physical Chemistry* **1994**, *98*, 934-941.

(6) Battaglia, D.; Li, J. J.; Wang, Y.; Peng, X.: Colloidal two-dimensional systems: CdSe Quantum shells and wells. *Angewandte Chemie International Edition* **2003**, *42*, 5035-5039.

(7) Li, J. J.; Wang, Y. A.; Guo, W.; Keay, J. C.; Mishima, T. D.; Johnson, M. B.; Peng, X.: Large-scale synthesis of nearly monodisperse CdSe/CdS core/shell nanocrystals using air-stable reagents via successive ion layer adsorption and reaction. *J Am Chem Soc* **2003**, *125*, 12567-12575.

(8) Xie, R.; Kolb, U.; Li, J.; Basché, T.; Mews, A.: Synthesis and characterization of highly luminescent CdSe−Core CdS/$Zn_{0.5}Cd_{0.5}S$/ZnS Multishell Nanocrystals. *J Am Chem Soc* **2005**, *127*, 7480-7488.

(9) Mahler, B.; Spinicelli, P.; Buil, S.; Quelin, X.; Hermier, J. P.; Dubertret, B.: Towards non-blinking colloidal quantum dots. *Nat Mater* **2008**, *7*, 659-664.

(10) Chen, Y.; Vela, J.; Htoon, H.; Casson, J. L.; Werder, D. J.; Bussian, D. A.; Klimov, V. I.; Hollingsworth, J. A.: "Giant" multishell CdSe nanocrystal quantum dots with suppressed blinking. *J Am Chem Soc* **2008**, *130*, 5026-5027.

(11) Javaux, C.; Mahler, B.; Dubertret, B.; Shabaev, A.; Rodina, A. V.; Efros, A. L.; Yakovlev, D. R.; Liu, F.; Bayer, M.; Camps, G.; Biadala, L.; Buil, S.; Quelin, X.; Hermier, J.

P.: Thermal activation of non-radiative Auger recombination in charged colloidal nanocrystals. *Nat Nanotechnol* **2013**, *8*, 206-212.

(12) Yang, Y. A.; Wu, H. M.; Williams, K. R.; Cao, Y. C.: Synthesis of CdSe and CdTe nanocrystals without precursor injection. *Angew Chem Int Edit* **2005**, *44*, 6712-6715.

(13) Yu, W. W.; Qu, L.; Guo, W.; Peng, X.: Experimental determination of the xxtinction coefficient of CdTe, CdSe, and CdS nanocrystals. *Chem Mater* **2003**, *15*, 2854-2860.

(14) Leatherdale, C. A.; Woo, W. K.; Mikulec, F. V.; Bawendi, M. G.: On the absorption cross section of CdSe nanocrystal quantum dots. *The Journal of Physical Chemistry B* **2002**, *106*, 7619-7622.

(15) Mahler, B.; Lequeux, N.; Dubertret, B.: Ligand-controlled polytypism of thick-shell CdSe/CdS nanocrystals. *J Am Chem Soc* **2010**, *132*, 953-959.

(16) Selvan, S. T.; Tan, T. T.; Ying, J. Y.: Robust, non-cytotoxic, silica-coated CdSe quantum dots with efficient photoluminescence. *Adv Mater* **2005**, *17*, 1620-+.

(17) Zhang, T. T.; Stilwell, J. L.; Gerion, D.; Ding, L. H.; Elboudwarej, O.; Cooke, P. A.; Gray, J. W.; Alivisatos, A. P.; Chen, F. F.: Cellular effect of high doses of silica-coated quantum dot profiled with high throughput gene expression analysis and high content cellomics measurements. *Nano Lett* **2006**, *6*, 800-808.

(18) Yang, Y. H.; Jing, L. H.; Yu, X. L.; Yan, D. D.; Gao, M. Y.: Coating aqueous quantum dots with silica via reverse microemulsion method: Toward size-controllable and robust fluorescent nanoparticles. *Chem Mater* **2007**, *19*, 4123-4128.

(19) Santra, S.; Yang, H. S.; Holloway, P. H.; Stanley, J. T.; Mericle, R. A.: Synthesis of water-dispersible fluorescent, radio-opaque, and paramagnetic CdS : Mn/ZnS quantum dots: A multifunctional probe for bioimaging. *J Am Chem Soc* **2005**, *127*, 1656-1657.

(20) Chen, F. Q.; Gerion, D.: Fluorescent CdSe/ZnS nanocrystal-peptide conjugates for long-term, nontoxic imaging and nuclear targeting in living cells. *Nano Lett* **2004**, *4*, 1827-1832.

(21) Graf, C.; Dembski, S.; Hofmann, A.; Ruhl, E.: A general method for the controlled embedding of nanoparticles in silica colloids. *Langmuir* **2006**, *22*, 5604-5610.

(22) Yang, H. S.; Santra, S.; Walter, G. A.; Holloway, P. H.: Gd-III-functionalized fluorescent quantum dots as multimodal imaging probes. *Adv Mater* **2006**, *18*, 2890-2894.

(23) Hu, X. G.; Gao, X. H.: Silica-polymer dual layer-encapsulated quantum dots with remarkable stability. *Acs Nano* **2010**, *4*, 6080-6086.

(24) Bruchez, M.; Moronne, M.; Gin, P.; Weiss, S.; Alivisatos, A. P.: Semiconductor nanocrystals as fluorescent biological labels. *Science* **1998**, *281*, 2013-2016.

(25) Nann, T.; Mulvaney, P.: Single quantum dots in spherical silica particles. *Angew Chem Int Edit* **2004**, *43*, 5393-5396.

(26) Zhelev, Z.; Ohba, H.; Bakalova, R.: Single quantum dot-micelles coated with silica shell as potentially non-cytotoxic fluorescent cell tracers. *J Am Chem Soc* **2006**, *128*, 6324-6325.

(27) Yang, Y. H.; Gao, M. Y.: Preparation of fluorescent SiO2 particles with single CdTe nanocrystal cores by the reverse microemulsion method. *Adv Mater* **2005**, *17*, 2354-+.

(28) Yu, C. H.; Caiulo, N.; Lo, C. C. H.; Tam, K.; Tsang, S. C.: Synthesis and fabrication of a thin film containing silica-encapsulated face-centered tetragonal FePt nanoparticles. *Adv Mater* **2006**, *18*, 2312-2314.

(29) Tan, T. T.; Selvan, S. T.; Zhao, L.; Gao, S. J.; Ying, J. Y.: Size control, shape evolution, and silica coating of near-infrared-emitting PbSe quantum dots. *Chem Mater* **2007**, *19*, 3112-3117.

(30) Koole, R.; van Schooneveld, M. M.; Hilhorst, J.; Donega, C. D.; 't Hart, D. C.; van Blaaderen, A.; Vanmaekelbergh, D.; Meijerink, A.: On the incorporation mechanism of hydrophobic quantum dots in silica spheres by a reverse microemulsion method. *Chem Mater* **2008**, *20*, 2503-2512.

(31) Jing, L. H.; Yang, C. H.; Qiao, R. R.; Niu, M.; Du, M. H.; Wang, D. Y.; Gao, M. Y.: Highly fluorescent CdTe@SiO_2 particles prepared *via* reverse microemulsion method. *Chem Mater* **2010**, *22*, 420-427.

(32) Yi, D. K.; Selvan, S. T.; Lee, S. S.; Papaefthymiou, G. C.; Kundaliya, D.; Ying, J. Y.: Silica-coated nanocomposites of magnetic nanoparticles and quantum dots. *J Am Chem Soc* **2005**, *127*, 4990-4991.

(33) Guerrero-Martinez, A.; Perez-Juste, J.; Liz-Marzan, L. M.: Recent progress on silica coating of nanoparticles and related nanomaterials. *Adv Mater* **2010**, *22*, 1182-1195.

(34) Darbandi, M.; Thomann, R.; Nann, T.: Single quantum dots in silica spheres by microemulsion synthesis. *Chem Mater* **2005**, *17*, 5720-5725.

(35) Chang, S. Y.; Liu, L.; Asher, S. A.: Preparation and properties of tailored morphology, monodisperse colloidal silica cadmium-sulfide nanocomposites. *J Am Chem Soc* **1994**, *116*, 6739-6744.

(36) Osseoasare, K.; Arriagada, F. J.: Preparation of SiO_2 nanoparticles in a nonionic reverse micellar system. *Colloid Surface* **1990**, *50*, 321-339.

(37) Stober, W.; Fink, A.; Bohn, E.: Controlled growth of monodisperse silica spheres in micron size range. *J Colloid Interf Sci* **1968**, *26*, 62-69.

Chapter 3 Generalized Synthesis of QD/SiO_2/Au Core/shell/shell Nanoparticles

3.1 Introduction

Most of the studies on the coupling between QDs excitons and metallic plasmons have used metallic films, patterned metals or metal nanoparticles as the plasmon sources, while colloidal discrete single QD/metal hybrids would be extremely attractive for both fundamental research and practical applications.[1-5] We particularly focused on the synthesis of QD/metal core/shell colloidal heterostructures. The plasmonic gold layer could indeed increase the excitation rate and decrease the fluorescence lifetimes of the QD, conferring new optical properties to the fluorescent nanocrystal.[6,7] On another hand, the gold layer could act as a shield (due to the inertness of this material) to prevent the effect of fluorescence quenchers such as oxygen, and thereby increase the photochemical robustness of the corresponding nanoparticle.[8] The plasmon resonance of the metallic nanoshell can be adjusted easily, in a broad range from visible light to the infrared region, by tuning the ratio between the internal and the external radii of the gold layer.[9,10] This rather facile adjustment makes easier the optimization of the coupling between the QD exciton and gold surface plasmons.

To the best of our knowledge, only two significant studies have led so far to single QD/metal hybrids. First integrated single core/shell QD/gold nanoparticles were synthesized by Gao and co-workers, and published in 2009.[11] A 2-3-nm gold shell could be formed by the reduction of gold(III) ions immobilized by a cationic polymer (poly-L-histidine, PLH) adsorbed on CdSe/ZnS-based micelle-like structures. Spacing between the QD core and the gold shell could be adjusted by using an extra layer-by-layer coating of polyelectrolyte bilayers, before the cationic polymer adsorption (Figure 3.1). This led to QD/Au nanoparticles displaying both fluorescence and scattering properties, with increased photostability. However, this process showed some technical limitations. The bilayer coating proved to be extremely time-consuming and low-yielding, and limited to two rounds. On the other hand, it does not seem effective to allow access to a wide variety of distances between the fluorophore and the plasmonic shell, since the polymeric bilayer is no more than 1-nm thick. Tuning of the gold

shell thickness appears also to be a tough work, due to the single layer adsorption of the gold ions leading to the gold shell. Eventually, no effective coupling between plasmons of the gold nanoshell and the fluorescence of QDs was demonstrated. Zhang *et al.* managed to grow a gold nanoshell on $NaYF_4/SiO_2$ NPs by applying PLH as the template, but we were not able to reproduce these results.

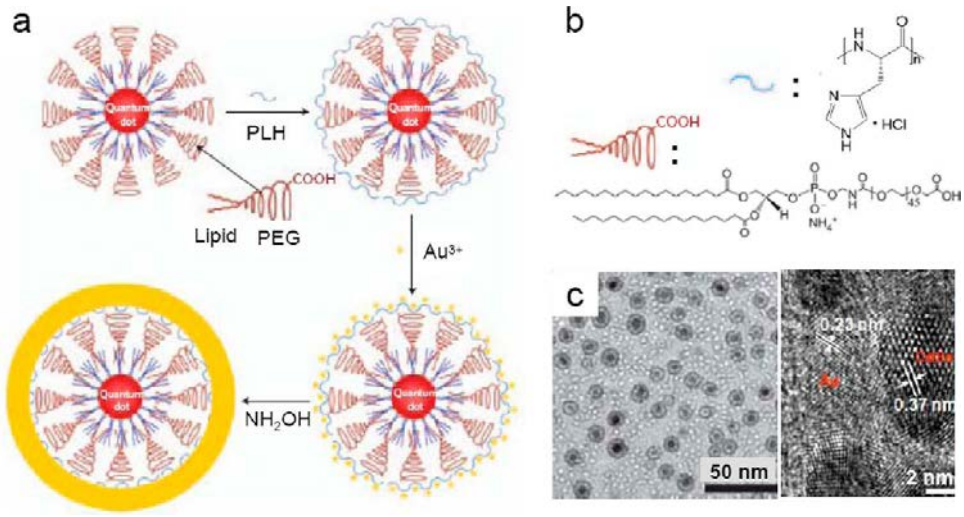

Figure 3.1. (a) Scheme of Au-shell-encapsulated QDs synthesized by Gao *et al.* A lipid-PEG-COOH (purple) was used to make hydrophobic QDs water-soluble. This was followed by the adsorption of a polymer (PLH, blue) for the immobilization of Au^{3+} ions. Au nucleation was formed on the PLH template by introducing the reducing agent, leading to the formation of a thin gold shell. (b) Molecular structures of lipid-PEG-COOH and PLH. (c) TEM and HRTEM images of the synthesized QD/Au core/shell NPs. Reprinted from Ref [11].

More recently, Dasgupta *et al.* presented a method to cover Si QDs with gold nanoshells.[12] The Si QDs were synthesized by etching of the silica layer of Si/SiO_2 core/shell NPs, resulting in Si QDs surfaces that were rich in Si-H bonds. Exposing these new-made Si QDs to mild UV light in an aqueous solution caused the dissociation the surface Si-H bonds and gave rise to dangling bonds, which provided preferential sites for gold NPs nucleation and growth in a non-epitaxial manner, leading to gold nanoshells. Clear signatures of QD/Au core/shell nanostructures were identified on the basis of HRTEM observations. The gold coverage enhanced the photostability of Si QDs. However, both the lifetime and the fluorescence intensity decreased, because the gold nanoshell was in direct contact with the Si QD surface and created new non-radiative decay routes. This effect is well-known in the case of other semiconductor QDs, where this direct contact between gold and QDs can lead to a

total quenching of the fluorescence.[13,14] Additionally, it has been shown that the fluorescence of QDs dispersed using small mercapto-molecules could be completely quenched by Au^{3+} ions because these quenchers could access the QD surface too easily during the synthesis.[11]

Besides, the ability of adjusting the plasmon resonance is limited in both the above-mentioned examples, due to the difficulty to control the dimensions of the gold layer and the spacing between the QDs and the plasmon source. These limitations prevent the adjustment of the coupling because the plasmon resonance, the QDs absorption and emission wavelengths cannot be tuned easily.

In this chapter, we describe a general method for the chemical deposition of a gold shell on the previously synthesized QD/SiO_2 NPs to obtain single colloidal QD/SiO_2/Au core/shell/shell heterostructures (their fluorescent and plasmonic properties will be the subject of the next chapter). In particular, we will show that the gold shell thickness can be finely controlled. The gold nanoshell growth process itself was inspired by the work of Halas *et al.*[9,15,16]

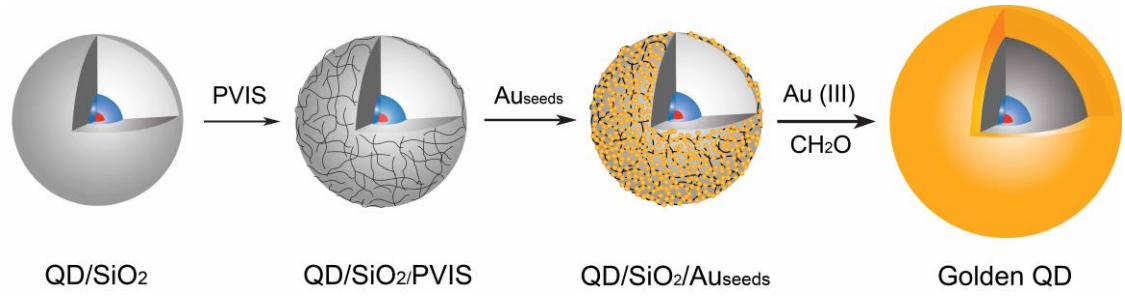

Figure 3.2. Scheme of the different steps leading from QD/SiO_2 to golden QDs (Au-shell-encapsulated QDs); PVIS: poly(1-vinylimidazole-*co*-vinyltrimethoxysilane).

The synthetic route is a three-step process (Figure 3.2). First, QD/SiO_2 NPs are functionalized with chemical moieties having a strong affinity for gold. Then, tiny gold nanoparticles ("gold seeds") are adsorbed onto the NPs, to act as nucleation sites for the deposition of the gold nanoshell. Finally, these gold seeds are grown and merged by the reduction of gold(III) ions to gold(0). The synthesis results in a continuous polycrystalline gold shell around QD/SiO_2 NPs. In this section, unless otherwise specified, we will illustrate the deposition of gold onto QD/SiO_2 NPs having a diameter of 100 nm. In the following, the QD/SiO_2/Au core/shell/shell nanoparticles ("golden QDs") will be referred to as '$R/T_1/T_2$ nanoparticles', where R, T_1 and T_2 are respectively the CdSe/CdS QD radius, the silica shell

thickness and the gold shell thickness, expressed in nanometers (nm). 100-nm-in-diameter QD/SiO_2 NPs will thus be described as 15/35 NPs.

More specifically in our study, a polymer has been developed to maximize the density of the gold seeds adsorbed onto the surface of silica. We will show that it helps to improve the homogeneity of the corresponding gold nanoshell and to get thin gold nanoshells. The rate of gold(III) reduction can also be controlled to give a fine tuning of the gold layer thickness. We now propose to underline the effects of these various experimental parameters on the final thickness and texture of the gold nanoshell.

3.2 Functionalization of QD/SiO_2 NPs

First, we started with the functionalization of QD/SiO_2 NPs as illustrated below:

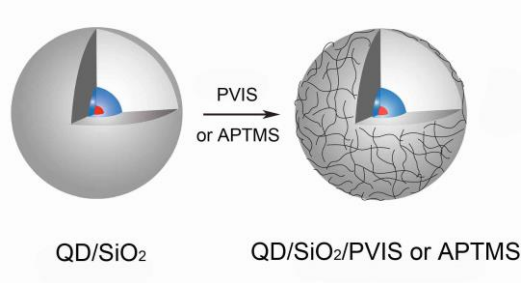

Figure 3.3. Scheme of the functionalization of QD/SiO_2 NPs with silanes for the adsorption of the gold seeds; PVIS: poly(1-vinylimidazole-*co*-vinyltrimethoxysilane); APTMS: aminopropyltrimethoxysilane.

Aminosilanes, such as (3-aminopropyl)trimethoxysilane (APTMS) and (3-aminopropyl)-triethoxysilane (APTES) have been widely used to functionalize the surface of SiO_2 beads (through covalent siloxane linkage) in order to adsorb gold seeds.[16] Under the adsorption conditions (pH = 4.5), the amine moieties grafted on silica are fully protonated, but they can still immobilize tris(hydroxymethyl)phosphine-coated gold seeds (see section 3.3.1) *via* hydrogen bonds between the amino and the hydroxyl groups. Note that direct complexation of gold by the amine lone pair of electrons cannot be totally excluded, provided proton exchanges take place (which is likely to occur between the protonated amino group and the hydroxymethyl function). The surface coverage amounts up to 25-30%.[16,17]

However, to improve the homogeneity of the gold layer, and access thin gold shells, a higher adsorption and coverage of gold seeds is required. Matsui *et al.* took advantage of

imidazole strong affinity for gold to fabricate gold nanowires from histidine-rich peptide nanotubes.[11,18,19] Based on the same rationale, we synthesized a polymer, the poly(1-vinylimidazole-*co*-vinyltrimethoxysilane), we called PVIS, to maximize the adsorption of the gold seeds, and compared its properties to these of APTMS.

PVIS is a polymer resulting from the statistical copolymerization of 1-vinylimidazole (to adsorb gold seeds) and vinyltrimethoxysilane (to attach onto silica) in a 93/7 ratio (see reaction and structure in Figure 3.3). Compared to aminosilanes, PVIS can still be covalently bound to silica beads, but affords a higher density of adsorbing functions.

3.2.1 Synthesis of poly(1-vinylimidazole-co-vinyltrimethoxysilane), PVIS

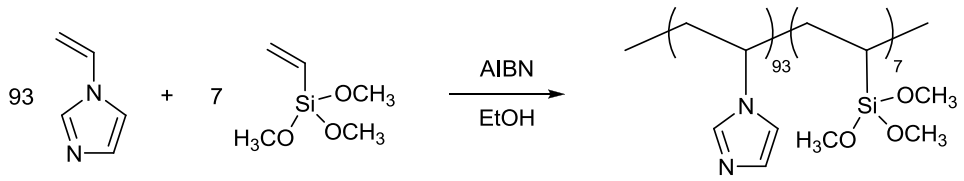

Figure 3.4. Synthesis and structure of poly(1-vinylimidazole-*co*-vinyltrimethoxysilane): PVIS.

1-vinylimidazole (4.38 g, 46.5 mmol) and vinyltrimethoxysilane (0.519 g, 3.5 mmol) were dissolved in ethanol (10 mL). The solution was degassed under argon for 30 min and then heated at 75 °C. A solution of recrystallized AIBN (25 mg, 0.15 mmol) in ethanol (5 mL) was injected into the reaction medium. After 24 h, the polymer was precipitated into diethyl ether (500 mL), washed with diethyl ether and finally dried under vacuum. Thermogravimetric analysis confirmed the respective monomer incorporations into the statistical copolymer were in agreement with the ratio initially introduced (1-vinylimidazole/vinyltrimethoxysilane: 93/7).[20]

After this synthesis, PVIS was covalently grafted (*via* siloxane bridges) onto the silica surface of QD/SiO_2 NPs. In parallel, APTMS, a typical aminosilane used for the adsorption of gold seeds, was grafted onto QD/SiO_2 NPs in the same way for later comparison.

3.2.2 Functionalization of the surface of QD/SiO_2 NPs with PVIS or APTMS

QD/SiO_2 NPs (2 mL from the previous 15-mL methanol dispersion in Chapter 2, estimated concentration C ≈ 4.0 nM) were dispersed in methanol (10 mL), followed by the addition of either of or PVIS (5 mg/m^2 silica, determined using gold seeds adsorption, see section 3.2.2.3) or APTMS (1.6 µL, 5 mg/m^2 silica).[16] *Then the mixture was heated up to 65 °C for 1.5 h. The reacting medium was cooled down to room temperature, and either QD/SiO_2/PVIS NPs or QD/SiO_2/APTMS NPs were washed 4 times with methanol. The respective NPs were finally redispersed in methanol (2 mL).*

Once the functionalization of the silica has been achieved, tiny gold seeds were adsorbed onto the surface of QD/SiO_2/silane NPs.

3.3 Gold seeds adsorption

The adsorption of the gold seeds consists in two steps: first, the preparation of the small gold colloids; second, the adsorption itself on functionalized QD/SiO_2 NPs (Figure 3.5).

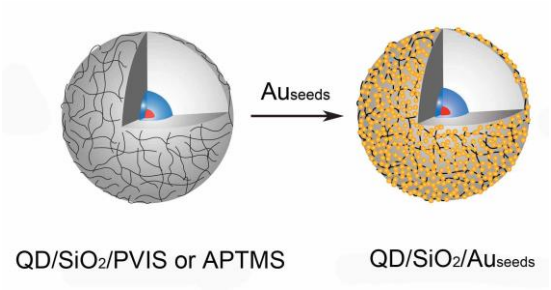

Figure 3.5. Scheme of the gold seeds adsorption onto QD/SiO_2/silane NPs.

3.3.1 Preparation of the gold seeds solution

The gold colloids we will later use as seeds (1-3 nm in diameter) were prepared according to Duff *et al.*,[21] by the reduction of gold(III) ions using THPC in an alkaline solution. The reducing agent THPC is a hydroxymethyl-substituted phosphonium. The mechanism of the

gold(III) reduction by THPC is still unclear but some reactions that are likely to occur can be deduced from the known THPC chemistry as followed (equations 4-1 and 4-2):[21]

$$P(CH_2OH)_4^+ + OH^- \rightarrow P(CH_2OH)_3 + CH_2O + H_2O \quad (4\text{-}1)$$

$$3\ P(CH_2OH)_3 + 2\ AuCl_4^- + 6\ HO^- \rightarrow 3\ O{=}P(CH_2OH)_3 + 2\ Au + 8\ Cl^- + 3\ H_2O \quad (4\text{-}2)$$

The most active reducing agent, namely the phosphine $P(CH_2OH)_3$, is generated by the alkaline elimination of one hydroxymethyl moiety. But the reduction of gold (III) is probably assisted by the other reducing agent formed according to equation 4-1, formaldehyde CH_2O. Indeed, this mild reducing species is known to reduce gold(III) in the presence of gold(0).[22] Consequently, the phosphine $P(CH_2OH)_3$ is not totally consumed by the reduction reaction and the remaining molecules can adsorb onto the gold seeds formed: they act as ligands *via* the complexation of gold by the phosphine free electron pair, making the seeds well dispersed in water. Nevertheless, in alkaline conditions, this phosphine derived from THPC has also a reducing ability that can cause water reduction into hydrogen according to the following chemical equation (4-3):

$$P(CH_2OH)_3 + H_2O \rightarrow O{=}P(CH_2OH)_3 + H_2 \quad (4\text{-}3)$$

Consequently, the THPC-alkali solution will deactivate over time and must be used directly after the preparation.

Typically, under rapid stirring, NaOH (0.2 M in water, 450 µL) and THPC (68 mM in water, 300 µL; stock solution prepared by diluting 120 µL of a 80 wt.% THPC aqueous solution into 10 mL of water) were successively added to water (13.65 mL), and the mixture was stirred for 5 min. $HAuCl_4$ (25 mM in water, 600 µL) was added dropwise and the solution was stirred for 15 min. The gold seeds solution obtained was aged at 4 °C for at least 2 weeks before use. When stored at 4 °C, this gold seeds suspension could be used within 3 months.

Gold colloids quality can be monitored by UV-Vis spectroscopy (Figure 3.6): the appearance of a plasmonic peak at ~ 530 nm indicates that the seeds have ripened (a plasmonic resonance appears for gold NPs having a diameter at least ~ 4 nm)[22] and are not suitable anymore for the growth of a gold shell.[15]

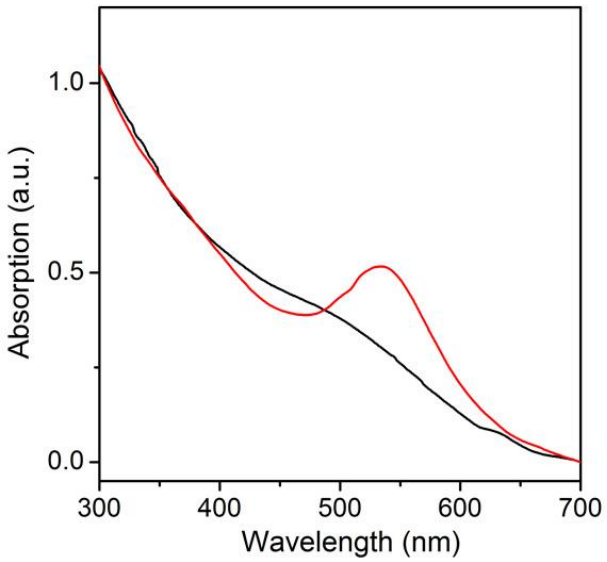

Figure 3.6. Absorption spectra of gold seeds solutions aged for 2 weeks (black line) or 1 year (red line).

Unless otherwise specified, only gold seeds with aging time between 2 weeks and 3 months were used in the different adsorption experiments presented below. Note that no difference in the behavior of these gold seeds could be observed within this aging time range.

3.3.2 Adsorption of the gold seeds onto QD/SiO_2 NPs

Either QD/SiO_2/PVIS or QD/SiO_2/APTMS NPs (100 µL from the previous 2-mL methanol dispersion, estimated concentration C ≈ 4 nM) were dispersed in the gold colloids (3 mL) and stirred for 1 h at room temperature. All of the free gold seeds remaining in solution were removed by 2-3 washings with water. QD/SiO_2/Au_{seeds} NPs were finally redispersed in water (1 mL) and used directly after preparation to grow the gold nanoshell.

3.3.3 Determination of the optimal amount of PVIS for the functionalization of QD/SiO_2 NPs

We first examined the quantity of PVIS required to saturate the surface of QD/SiO_2 NPs (Figure 3.7), following the corresponding adsorption of aged gold seeds. We proceeded using increasing amounts of polymer relative to QD/SiO_2 NPs during the functionalization step, and monitored the volume of gold adsorbed after the seeds adsorption using UV-Vis spectroscopy. Indeed, Mie theory indicates that the volume of gold can be estimated from its UV absorption at 350 nm, once the QDs absorption has been deconvoluted.[23] Indeed, for nanoparticles whose size is smaller than the light wavelength (here, gold seeds), on the basis of Mie scattering theory, the absorption value is only determined by the volume of the nanoparticles. However, in the case of plasmonic nanoparticles, the absorption value used for the volume calculation should be away from the plasmon absorption. Thereby, we pick the absorption value at 350 nm to assess the quantity of adsorbed gold seeds.

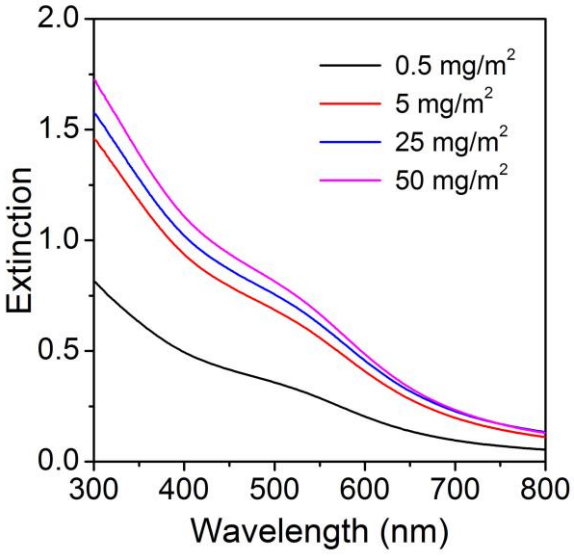

Figure 3.7. Extinction spectra of QD/SiO_2/PVIS/Au_{seeds} NPs for increasing surface concentrations of PVIS (from 0.5 mg to 50 mg per silica surface unit, same concentrations of NPs in each case).

In each case, the QD/SiO_2 NPs concentration was the same. Thereby, we can compare the relative quantities of adsorbed gold seeds using directly the absorption value of QD/SiO_2/Au_{seeds} at 350 nm. Beyond 5 mg of polymer per square meter of silica surface, no significant increase in the absorption of the NPs at 350 nm was observed, indicating that the volume of gold seeds adsorbed per NP has reached a maximum. In other words, the silica is

fully functionalized for such a surface concentration of PVIS. Consequently we used this surface concentration of PVIS for all next adsorption experiments.

3.3.4 Effect of the functionalizing agent on the amount of adsorbed gold seeds

Either PVIS or APTMS were grafted on QD/SiO_2 NPs under the same conditions (see section 3.2.2), and the respective functionalized NPs were incubated with an aged gold seeds dispersion. After careful washings, corresponding typical TEM images (Figure 3.8a and b) illustrate that the density of adsorbed gold seeds is much higher in the case of PVIS-functionalized QD/SiO_2 beads than in the case of APTMS functionalization.

More quantitatively, the absorption spectra shown in Figure 3.8c allow distinguishing between the absorption due to QDs (non-functionalized NPs, dashed lines) and the absorption due to gold seeds (supplementary absorption represented by solid lines compared to respective dashed lines). The concentrations in NPs being identical in each case, we can thus estimate the respective gold amounts per NP: PVIS leads to an unprecedented seed coverage that is 3.2 times higher than in the case of APTMS functionalization. As the average seeds coverage is ~ 25% in the case of aminosilane-type functionalizing agents,[9,16] we can thus estimate the seeds coverage to be ~ 80% with PVIS.

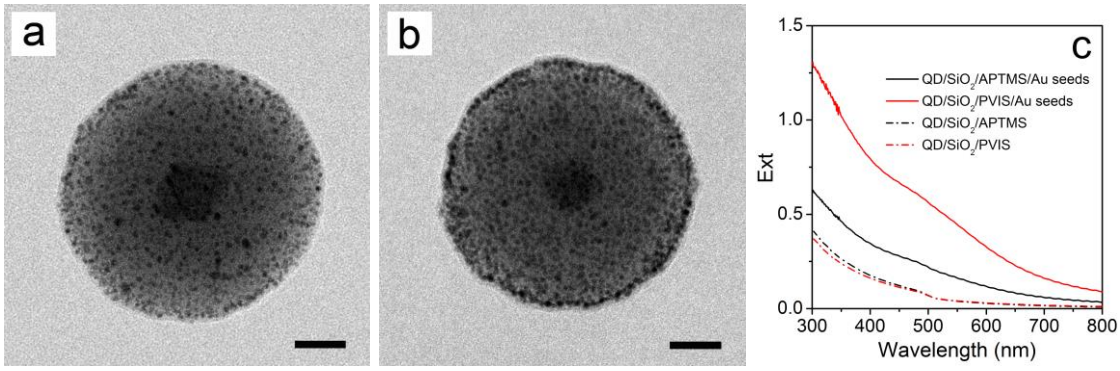

Figure 3.8. Typical TEM images of 15/35 QD/SiO_2/Au_{seeds} NPs with a) APTMS or b) PVIS as the functionalizing agent; c) Corresponding extinction spectra before (dashed lines) and after (solid lines) adsorption of aged old seeds at the same NPs concentration. Scale bars: 20 nm.

Thanks to a higher density of adsorbing functions (here, imidazole moieties), it is thus possible to enhance the number of seeds adsorbed per NP. This major result has a great importance concerning the growth and the thickness of the gold nanoshell. But the effect of gold seed coverage on the formation of the nanoshell will be discussed in a later section (see section 3.4.4.1), once the other parameters of the growth process have been optimized.

Using PVIS, we assume that the main interaction which drives the gold seeds adsorption is the complexation of gold by the imidazole moieties, thanks to the π-electron system of their aromatic ring. Indeed, at the adsorption pH (~ 4.5), the imidazole group (pK_a ~ 5) is only partially protonated and thereby hydrogen bonds, which are not particularly favored, cannot be considered as the major interactions involved.

To further try and increase the number of gold seeds adsorbed with PVIS, we turned to adsorption experiments performed at a lower pH.

3.3.5 Effect of the pH on the amount of adsorbed gold seeds

3.3.5.1 PVIS-functionalized QD/SiO_2 NPs

The pH of the seeds solution was lowered from 4.5 to a value of 3.5, at which we can expect the imidazole groups to be fully protonated. We could thus combine their electrostatic properties (hydrogen bond with phosphine-coated gold seeds *via* the interaction between the protonated imidazole groups and the hydroxyl groups of $P(CH_2OH)_3$) with the already existing complexation interaction.

The adsorption solution of pH = 3.5 was prepared by introducing 15 µL of 0.1 M aqueous HCl into 1.5 mL of 2-week-aged gold seeds solution; then, the adsorption of gold seeds on QD/SiO_2 was performed according to the protocol described in section 3.3.2.

QD/SiO_2/PVIS/Au_{seeds} NPs resulting from these modified adsorption conditions have been characterized by TEM and compared to the NPs obtained at pH = 4.5 (Figure 3.9). The corresponding images show in both cases a dense coverage of gold seeds, which seems to be slightly enhanced at pH = 3.5 compared to pH = 4.5. However, it is difficult to conclude with certainty on the influence of pH from the TEM images observation. That is the reason why we moved to a more quantitative analysis.

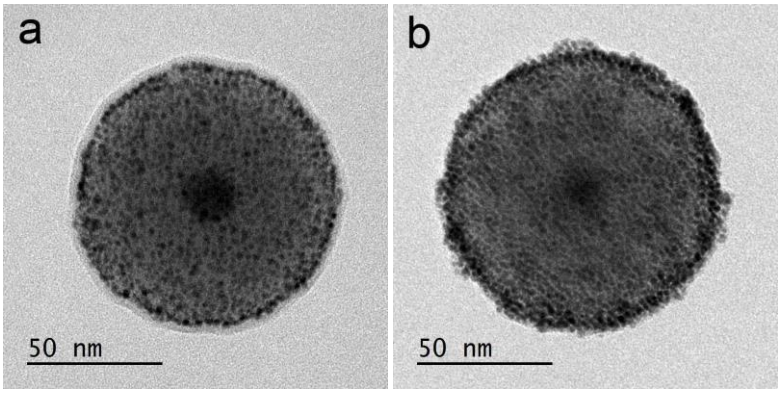

Figure 3.9. Typical TEM images of 15/35 QD/SiO_2/PVIS/Au_{seeds} NPs obtained using an aged gold seeds solution at pH ~4.5 (a) and 3.5 (b).

In order to clarify the adsorption behavior of the gold seeds, the adsorption isotherms of aged gold seeds were measured in solutions at pH = 3.5 or 4.5. These adsorption isotherms represent the amount of adsorbed seeds as a function of the amount of non-adsorbed seeds. As already mentioned, they can be constructed using gold absorption at 350 nm, since the seeds absorption at 350 nm is proportional to the gold volume. Note that to extract the absorption of the gold seeds from the UV-Vis spectrum, the absorption value at 350 nm of our NPs was deconvoluted from the QD absorption, and normalized by the concentration of the QD/SiO_2/Au_{seeds} NPs.

Various amounts of QD/SiO_2/PVIS NPs (from 140 to 15 µL, estimated concentrations: 4 nM) were dispersed in 1.5 mL of aged gold colloids. This solution was stirred for 1 h and centrifuged. For each sample, the supernatant was separated and the absorption spectrum was measured. Then the QD/SiO_2/Au_{seeds} NPs were washed with water 3 times and redispersed in 1.9 mL of water. 200 µL of this QD/SiO_2/Au_{seeds} solution were dispersed in 1.8 mL of water and the absorption spectrum was measured. The absorption value of adsorbed Au seeds was normalized to the same QD/SiO_2/PVIS NPs concentration as when 100 µL of QD/SiO_2/PVIS NPs were used.

The resulting adsorption isotherms at pH = 4.5 and 3.5 are presented below (Figure 3.10). They show in both cases that the average number of adsorbed seeds keeps relatively stable (taking into account measurements uncertainties) as the ratio between the volume of QD/SiO_2/PVIS NPs and the volume of the gold seeds solution changes. So, even for the lowest amount of seeds introduced, the adsorption has already reached a saturation plateau,

indicating that there is a monolayer adsorption in both cases. But the absorption value at 350 nm corresponding to this plateau is 1.3 times higher at pH = 3.5 than at pH = 4.5. Consequently, these results demonstrate that the seeds coverage at pH = 3.5 is slightly denser than at pH = 4.5.

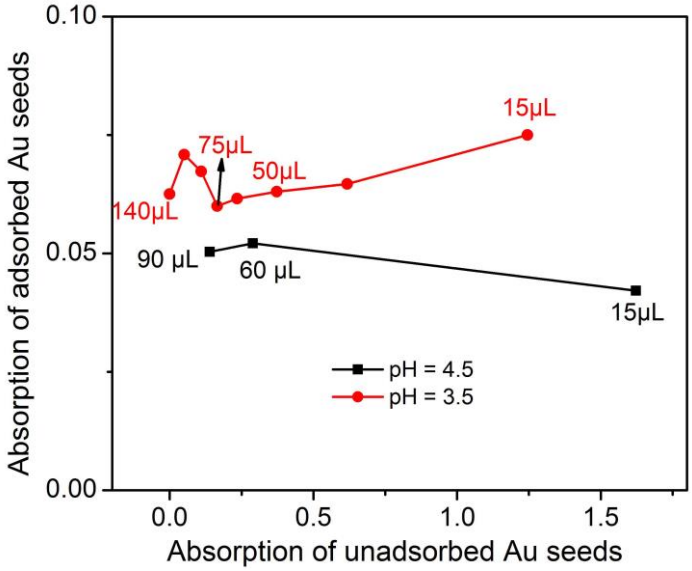

Figure 3.10. Adsorption isotherm of aged gold seeds on 6/44 QD/SiO_2/PVIS NPs at pH =3.5 (red dots) and pH = 4.5 (black squares). The absorption of adsorbed gold seeds was calculated as follows: the absorption value at 350 nm of QD/SiO_2 NPs was subtracted from the absorption value of QD/SiO_2/Au_{seeds} NPs at 350 nm. The inset volumes indicate the quantities of QD/SiO_2/PVIS NPs used.

These conclusions are in agreement with the assumptions we made concerning the behavior of PVIS. Nevertheless, the quite weak difference between the adsorptions at pH = 3.5 or 4.5 indicates the complexation by the imidazole group predominates over the electrostatic interactions.

To further confirm our rationale and for comparison, we also carried out the adsorption of seeds at pH = 3.5 on APTMS-functionalized QD/SiO_2 NPs.

3.3.5.2 APTMS-functionalized QD/SiO_2 NPs

The protocol used for the adsorption of seeds at pH = 3.5 using APTMS-functionalized NPs was identical to the one described in previous section 3.3.5.1. In that case, as the amine function (pK_a ~ 10) is already fully protonated at pH = 4.5 and as the adsorption completely

relies on electrostatic interactions, we do not expect any dramatic change in the gold seeds adsorption.

The TEM image of the resulting QD/SiO_2/APTMS/Au_{seeds} NPs are presented below (Figure 3.11), and compared to the results obtained at pH = 4.5. As expected, when APTMS was used as the functionalizing agent, no significant change in the gold seeds adsorption could be observed as the pH decreased.

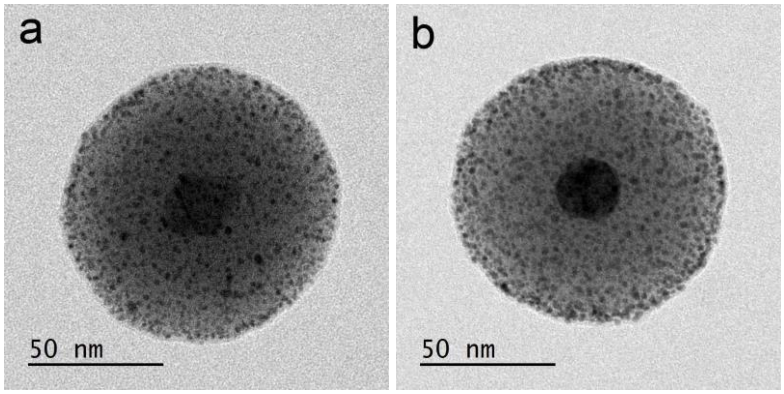

Figure 3.11. Typical TEM image of 15/35 QD/SiO_2/APTMS/Au_{seeds} NPs obtained using a 2-week-aged gold seeds solution at pH = ~4.5 (a) and 3.5 (b).

As explicitly indicated in section 3.3.1, all preceding experiments have been performed using aged gold seeds. Here we want to show the properties of freshly-made seeds (immediately used after the preparation) toward adsorption, compared to the aged one and as a function of a few parameters tested above (functionalizing agent, pH).

3.3.6 Fresh gold seeds adsorption

3.3.6.1 Effect of the functionalizing agent on the amount of adsorbed fresh gold seeds

Applying the protocol described above (section 3.3.2, pH = 4.5), freshly-made seeds could also adsorb onto silica. The resulting NPs are illustrated by the TEM images below (Figure 3.12). As for aged gold seeds, the coverage obtained with PVIS-functionalized QD/SiO_2 NPs is much higher than with APTMS-functionalized NPs.

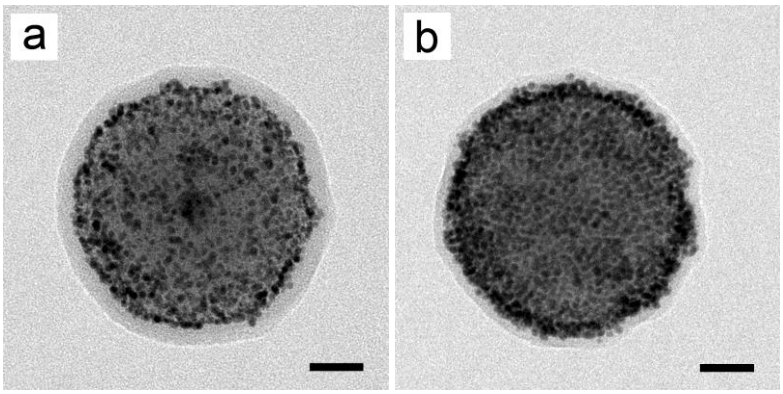

Figure 3.12. Typical TEM images of 6/42 QD/SiO_2/fresh Au_{seeds} NPs obtained with a) APTMS or b) PVIS as the functionalizing agent at pH = ~4.5. Scale bars: 20 nm.

The behavior of fresh gold seeds toward the adsorption seems so far quite similar to the behavior of aged gold seeds. Let us now compare their respective adsorption properties with the same functionalizing agent, namely PVIS.

3.3.6.2 Effect of the gold seeds aging on the amount of PVIS-adsorbed gold seeds

In order to compare the adsorption behavior of the freshly-made and aged gold seeds, the adsorption isotherms were measured in the respective colloidal suspensions at pH = 4.5.

Various amounts of QD/SiO_2/PVIS NPs (from 90 to 15 µL, estimated concentration C ≈ 4 nM) were dispersed in 1.5 mL of new-made gold colloids. This solution was stirred for 1 h and centrifuged. Then the adsorption isotherms were obtained in the same method as section 3.3.5.1. The absorption value of adsorbed Au seeds was normalized to the same QD/SiO_2/PVIS NPs concentration as when100 µL of QD/SiO_2/PVIS NPs were used.

The resulting adsorption isotherms of freshly-made and aged gold seeds at pH = 4.5 are presented in Figure 3.13. As the ratio between the volume of QD/SiO_2/PVIS NPs and the volume of the gold seeds solution changes, the average number of adsorbed seeds in both cases keeps relatively stable (taking into account measurements uncertainties), indicating that there is a monolayer adsorption in both cases. However the coverage of gold seeds obtained with the freshly-made gold seeds solution is slightly higher. We have seen above (see section

3.3.1) that the phosphine ligands ($P(CH_2OH)_3$) can be oxidized to phosphine oxides ($O=P(CH_2OH)_3$) in water, which probably takes place during the aging process. This oxidation would lead to a less strong complexation of gold seeds by $O=P(CH_2OH)_3$ (coordination by one electron lone pair of the oxide oxygen) instead of the original complexation between gold and $P(CH_2OH)_3$. Consequently, the phosphine oxide ligands are mostly displaced when the aged gold seeds are complexed by the imidazole groups of PVIS, whereas part of the phosphine ligands can stay on the freshly-made gold seeds and favor electrostatic interactions *via* hydrogen bonds, thus enhancing a little the seeds coverage in this latter case.

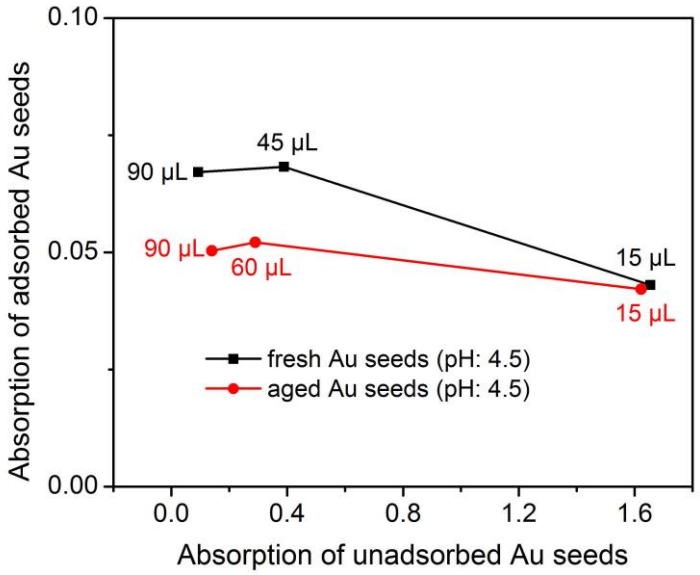

Figure 3.13. Adsorption isotherm of aged gold seeds (red dots) or fresh gold seeds (black squares) on 6/44 QD/SiO_2/PVIS NPs at pH = 4.5. The adsorbed gold seeds absorption was calculated as follows: the absorption value at 350 nm of QD/SiO_2 NPs was subtracted from the absorption value of $QD/SiO_2/Au_{seeds}$ NPs at 350 nm. The inset volumes indicate the quantities QD/SiO_2/PVIS NPs used.

As a higher H^+ concentration would promote the protonation of PVIS imidazole groups and therefore, increase the gold seeds coverage (see the experiment with aged seeds in section 3.3.2), we decided to try and perform the adsorption of freshly-made gold seeds at a lower pH (~3.5).

3.3.6.3 Effect of the pH on the amount of PVIS-adsorbed fresh gold seeds

As discussed above, we can expect the imidazole groups to be fully protonated when the pH of the seeds solution is lowered from 4.5 to 3.5. In order to clarify the adsorption behavior of the fresh gold seeds, the adsorption isotherms of fresh gold seeds were measured in solutions at pH = 3.5 or 4.5 as in section 3.3.5.1.

Various amounts of QD/SiO_2/PVIS NPs (from 140 to 15 µL, estimated concentrations: 4 nM) were dispersed in 1.5 mL of new-made gold colloids at pH = 4.5 or 3.5. Then the adsorption isotherms were obtained in the same method as section 3.3.5.1. The absorption value of adsorbed Au seeds was normalized to the same QD/SiO_2/PVIS NPs concentration as when 100 µL of QD/SiO_2/PVIS NPs were used.

The resulting adsorption isotherms at pH = 4.5 and 3.5 are presented in Figure 3.14.

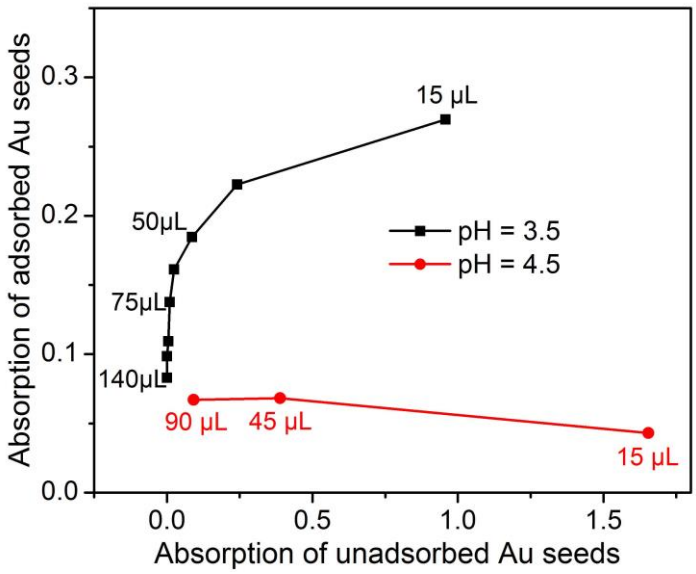

Figure 3.14. Adsorption isotherms of the freshly-made gold seeds on 6/44 QD/SiO_2/PVIS NPs at pH = 4.5 (red dots) or pH = 3.5 (black squares). The adsorbed gold seeds absorption was calculated as follows: the absorption value at 350 nm of QD/SiO_2 NPs was subtracted from the absorption value of QD/SiO_2/Au_{seeds} NPs at 350 nm. The inset volumes indicate the quantities QD/SiO_2/PVIS NPs used.

Compared to pH = 4.5 (monolayer adsorption at this pH value, as shown in section 3.3.6.2), the average quantity of adsorbed fresh gold seeds increased rapidly as the volume of QD/SiO_2/PVIS NPs decreased from 140 µL to 15 µL in 1.5 mL of freshly-made gold colloids

at pH = 3.5 and no saturation plateau was observed. The line shape of the isotherm is the characteristic of a multilayer adsorption, which is confirmed by the TEM image of the corresponding QD/SiO_2/Au_{seeds} NPs (for a volume of 15 µL of NPs added at pH = 3.5, Figure 3.14) as shown in Figure 3.15. According to the size of the seeds (2-3 nm in diameter), the thickness of the seeds shell is ~ 12 nm, corresponding to ~ 5-6 layers of seeds.

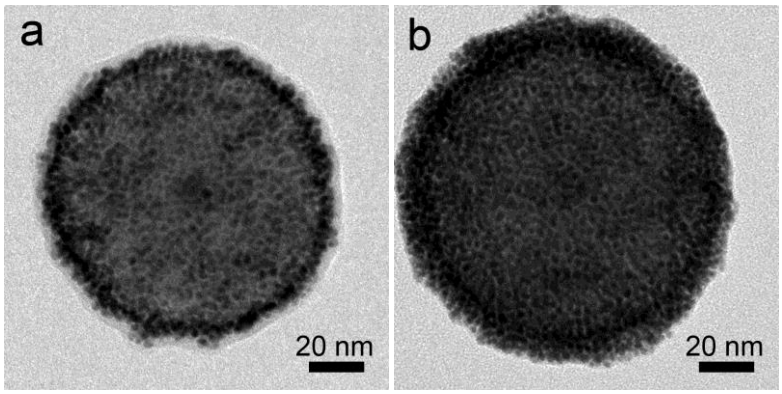

Figure 3.15. Typical TEM images of 6/44 QD/SiO_2/fresh Au_{seeds} obtained after adsorption at (a) pH = 4.5 (for a volume of 15 µL of NPs added, Figure 3.14) and (b) pH = 3.5 (for a volume of 15 µL of NPs, Figure 3.14).

The mechanism of this multilayer adsorption remains unclear to us. But a possible explanation is proposed below. When the pH of the freshly-made gold seeds solution was adjusted to 3.5, the complexation interaction (between imidazole groups and gold) and the hydrogen bond interaction (between hydroxyl groups in $P(CH_2OH)_3$ on gold and protonated imidazole groups) can together lead to a very dense layer of gold seeds. Thus, another very dense $P(CH_2OH)_3$-coated seeds layer can be obtained *via* hydrogen bonds, this time between the hydroxyl groups themselves, resulting in a multilayer adsorption of gold seeds.

When the freshly-made gold seeds solution was used at pH = 4.5, the imidazole groups were poorly protonated and the adsorption of gold seeds was only due to the complexation of gold by the imidazole groups. In this case, the layer of adsorbed gold seeds may be not dense enough to have a dense external $P(CH_2OH)_3$ layer, resulting in a monolayer gold seeds adsorption. Another explanation would involve more directly the pH value (3.5) that could favor the formation of hydrogen bonds between the hydroxyl functions of the phosphine ligands.

In this part, we showed that the polymer we have synthesized, PVIS, enables us to achieve a much higher gold seeds coverage than APTMS, one of the most used aminosilanes for the adsorption of gold seeds, regardless of the pH value. The adsorption experiments involving aged or freshly-made gold seeds, at pH = 4.5 or 3.5, do not make appear important differences, except at pH = 3.5 for the freshly-made seeds (multilayer adsorption).

However, in the typical conditions of a gold nanoshell growth from QD/SiO_2/PVIS/Au_{seeds} NPs (see next section), the fresh gold seeds proved to be much less prompt to gold deposition than the aged ones: when aged gold seeds were used, the color of the medium changed from almost colorless to blue (the color of golden QDs in aqueous solution) only 20 min after the introduction of CH_2O; on the contrary, when the fresh gold seeds were used, it took much more time to obtain this blue color. Moreover, adsorbed freshly-made seeds lead to an important side self-nucleation of gold during the gold growth; most probably because they are more easily displaced than the aged ones from the surface of QD/SiO_2 NPs (see section 3.3.6.2). A possible explanation can be deduced from Oldenberg hypotheses, based on the gold seeds preparation chemistry.[24] The phosphine ligand obtained as a product in the chemical equation 4-2 can strongly bind to gold and form a protecting layer on the gold seed surface, allowing only hydrogen bond between $P(CH_2OH)_3$ and the imidazole groups (no complexation of gold possible). During aging, oxidation of this phosphine would lead to a less bound phosphine oxide ligand (more easily displaced) that would not prevent the complexation of the seeds by the imidazole function. Consequently, aging would afford strongly adsorbed aged gold seeds that do not detach during the gold growth.

For the reasons indicated above, the freshly-made seeds were not considered as suitable for the growth of gold nanoshells.[15] We will therefore discuss the formation of continuous gold nanoshells and its optimization on QD/SiO_2/Au_{seeds} NPs obtained using PVIS as the functionalization agent and an aged gold seeds dispersion at pH = 4.5 (Figure 3.8b). The effect of the gold seeds coverage (density and number of layers) on the formation of the nanoshell will be discussed in a later section, once the optimization of the growth process has been discussed.

3.4 Growth of the gold nanoshell from QD/SiO_2/Au_{seeds} NPs

Gold nanoshells are generally grown by the reduction of a gold plating solution on gold-seeded NPs as shown in Figure 3.16. Consequently, the choices of the reducing agent and method are essential. As examples, formaldehyde is a typical reducing agent used by Halas and co-workers, due to its mild reducing power;[15,25] whereas van Blaaderen *et al.* employed a stronger reducing agent, hydroxylamine hydrochloride, to grow gold nanoshells *via* an dropwise injection method.[26]

In this section, unless otherwise specified, we will show the optimization of the gold layer deposition on QD/SiO_2/PVIS/aged Au_{seeds} NPs at pH = 4.5.

Figure 3.16. Scheme showing the formation of a continuous gold nanoshell from a QD/SiO_2/Au_{seeds} NP.

3.4.1 Reduction methods tested

We tested three methods, ordered by increasing reducing power: method 1 was based on a one-shot injection of formaldehyde in a QD/SiO_2/Au_{seeds} NPs dispersion in the gold plating solution; method 2 consisted in a dropwise co-addition of hydroxylamine and the gold plating solution to the NPs dispersion, followed by a one-shot injection of formaldehyde; and method 3 proceeded *via* a dropwise addition of hydroxylamine in the gold plating solution NPs dispersion.

Preparation of the gold plating solution: *the gold plating solution was prepared by adding $HAuCl_4$ (25 mM in water, 750 µL) to K_2CO_3 (1.8 mM in water, 50 mL). After 30 min of stirring (the light yellow solution turned to colorless), the plating solution was stored at 4 °C*

for a minimum of 24 h before use. When stored at 4 °C, this solution was to be used within 1 month after the preparation.

Method 1: fast addition of CH_2O. *$QD/SiO_2/PVIS/Au_{seeds}$ NPs (100 µL from the 1-mL water dispersion, estimated concentration C ≈ 0.4 nM) were added to gold plating solution (2.5 mL), then CH_2O (37 wt.% in water, 12.5 µL) was added in one portion under stirring within 15 min. $QD/SiO_2/Au$ nanoshells hybrids were centrifuged, washed with water, and redispersed in water (2 mL).*

Method 2: dropwise co-addition of NH_2OH and the gold plating solution, followed by fast addition of CH_2O. *$QD/SiO_2/PVIS/Au_{seeds}$ (800 µL from the 1-mL water dispersion, estimated concentration C ≈ 0.4 nM) were dispersed in water (1.2 mL), then gold plating solution (4 mL) and NH_2OH•HCl (5 mM in water, 480 µL) were added dropwise to the dispersion within 20 min, at the same time but using separate syringes. The mixture was stirred for 5 min and centrifuged. The NPs were washed with water and redispersed in water (1.6 mL). 100 µL of this NPs dispersion were added to gold plating solution (2.0 mL), and CH_2O (37 wt.% in water, 11.25 µL) was added dropwise under stirring within 15 min. The dispersion was centrifuged, and the $QD/SiO_2/Au$ nanoshells hybrids were washed with water and redispersed in water (2 mL).*

Method 3: slow addition of NH_2OH. *$QD/SiO_2/PVIS/Au_{seeds}$ (100 µL from the 1-mL water dispersion, estimated concentration C ≈ 0.4 nM) were dispersed in gold plating solution (2.5 mL), and NH_2OH•HCl (1.87 mM in water, 1.25 mL) was added dropwise within 45 min. The mixture was stirred for 10 min and centrifuged. The $QD/SiO_2/Au$ nanoshells hybrids were washed with water and redispersed in water (2 mL).*

The NPs obtained after the gold nanoshell growth are $QD/SiO_2/Au$ nanoshells hybrids, which will be called thereafter "golden QDs".

The aim of these three methods was to grow gold nanoshells that are continuous, as smooth as possible, and whose thicknesses are identical for all of the NPs. Method 1 should proceed smoothly, with a slow growth of the seeds, thus favoring a simultaneous growth. In method 2, the objective is to grow the seeds as rapidly and simultaneously as possible until they merge, using a strong reducing agent, and finish the growth with a smooth thickening of the shell. Using method 3, we wanted to verify if the growth of the seeds using a strong reducing agent

could be better controlled by a dropwise addition. In other words, the global objective of this set of experiments was to be able to avoid any overgrowth of certain seeds, that is, to make all the seeds grow at the same rate, so that the resulting gold shell is as thin and smooth as possible.

3.4.2 Results, interpretations and choice of the reduction method

SEM images of golden QDs synthesized *via* methods 1, 2 and 3 (Figure 3.17 a, b and c respectively) show that all the gold nanoshells are continuous, but have different characteristics as far as the roughness and the shell thickness are concerned.

From the SEM analysis, gold nanoshells synthesized *via* method 1 display a smooth surface and a narrow size distribution; those obtained *via* method 2 show a narrow size distribution as well, but exhibit a rough gold surface; and in the case of method 3, the gold nanoshell growth leads to a quite wide size range of the corresponding NPs, and their surface state varies from smooth to rough. As a conclusion, we can say from the SEM observation that hydroxylamine (the strong reducing agent) leads to the overgrowth of some seeds, resulting in particularly rough surfaces. So far, method 1 is thus the one that best fits our specifications.

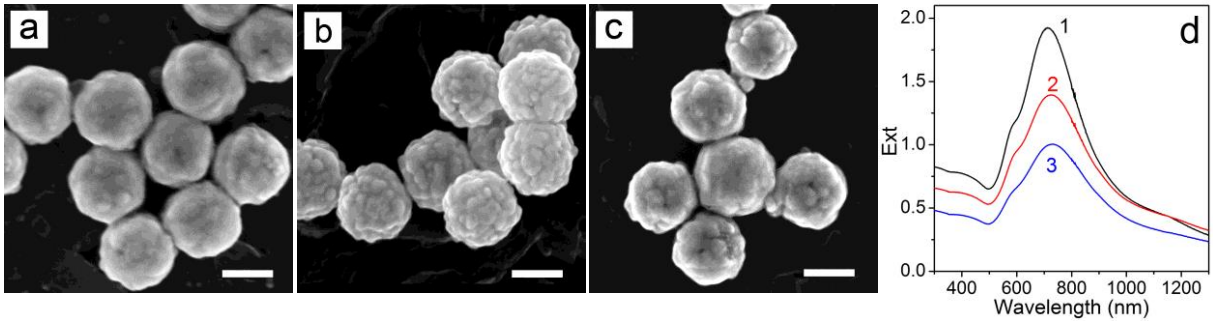

Figure 3.17. Influence of the reduction method on the gold nanoshell growth. SEM images of golden QDs NPs synthesized by a) Method 1: one-shot injection of CH_2O; b) Method 2: co-addition of hydroxylamine and the gold plating solution, followed by one-shot injection of CH_2O; c) Method 3: dropwise addition of hydroxylamine; and the corresponding extinction spectra without normalization (d, same NPs concentration for each method). Scale bars: 100 nm.

More precisely, the absorption spectra corresponding to the NPs obtained *via* the three methods allow us to better understand and interpret what occurs during these syntheses. Indeed, the absorption spectrum of our golden QDs has been modeled by B. Habert during his

PhD (see the simulation part in the appendix; collaboration with François Marquier and Jean-Jacques Greffet from the Institut d'Optique Graduate School) and the main conclusions follow. To sum up: i) as already indicated, the extinction at 350 nm (once the absorption of the QD has been removed) is proportional to the amount of gold on the NP; ii) the full width at half maximum increases when the size dispersion widen; and iii) NPs that have aggregated to form dimers absorb at near-infrared wavelengths (~ 1100 nm).

Let us now analyze these three parts of the absorption spectra. As these spectra have been recorded with the same concentration in NPs, the QDs contribution in the absorption at 350 nm is identical in all cases (Figure 3.17d). We can thus deduce that the NPs resulting from method 1 incorporated more gold than the NPs obtained via method 2, themselves including more gold than the ones grown with method 3. Method 1 is therefore the most efficient, since it allows the best incorporation of gold from the reduction of gold ions. This analysis is further confirmed by the extent of the side self-nucleation of gold nanoparticles observed during the growth process: the self-nucleation was more important with method 3 than with method 2, and more important with method 2 than with method 1.

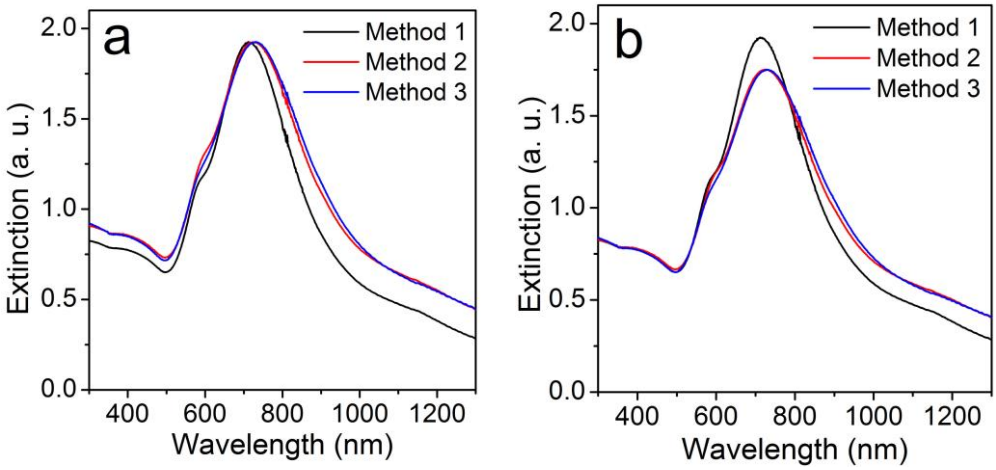

Figure 3.18. Extinction spectra of gold nanoshells obtained *via* the three different methods, being normalized by a) extinction values at plasmonic peak maximum wavelength and b) extinction values at 350 nm.

The plasmonic peaks are located almost at the same wavelength for the three methods and the full widths at half maximum of the plasmonic peaks for methods 1, 2 and 3 are respectively 222, 268 and 271 nm. They can be compared more directly if the extinction spectra are normalized at the plasmonic peak maximum absorption (Figure 3.18a). This

indicates that gold nanoshells grown by method 1 are much more monodispersed than the others. In other words, their thickness distribution is narrower.

Finally, during the deposition of the gold layer, the formation of dimers (that absorbs at ~ 1100 nm from the simulations) could be observed (see SEM images in Figure 3.17). According to the extinction spectra of the NPs synthesized by methods 1, 2 and 3 normalized at the extinction value at 350 nm (Figure 3.18b), the gold nanoshells obtained using method 1 suffered less from aggregation during the growth process than those synthesized by method 2 and 3 (~ same amount of dimers, judging from the absorption at 1100 nm).

Based on the above analyses that confirm the first SEM observations, reduction method 1 is the one that affords the best control of the growth of the gold nanoshells. Consequently, this method was chosen to further optimize our gold growth process.

3.4.3 PVP-K12-assisted gold nanoshell growth

The size of starting gold seeds (~ 2-3 nm in diameter) makes it theoretically possible to get very thin gold nanoshells. However, the growth of the seeds is individually hardly controlled, resulting in an inhomogeneous growth that requires often additional gold precursor to obtain a continuous shell. In this case unfortunately, side self-nucleation of gold nanoparticles dramatically increases, thus preventing efficient growth of the gold layer.

On another hand, in a general manner, as-synthesized golden QDs NPs suffer from facile aggregation (even if stored at 4°C) because there are almost no more ligands remaining on their surface. In order to further improve growth method 1 and overcome these limitations, a polymer, poly(vinylpyrrolidone) (PVP-K12; number average molecular weight: 3,500 g/mol; Figure 3.19), was introduced during the growth process. PVP is a water-soluble polymer bearing hydrophilic lactam (cyclic amide) functions, thus favoring the dispersion in water. Additionally, PVP can absorb onto specific crystal faces as ligands and thereby should improve the colloidal stability of golden QDs.[27]

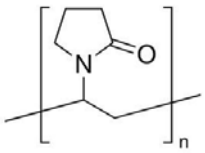

Figure 3.19. Structure of poly(vinylpyrrolidone), PVP.

Kim *et al.* introduced PVP to bind to gold(III) during a gold shell growth process, thus allowing an adjustment of the reduction rate to have a good control of the gold deposition.[28] So we try to grow gold nanoshell using a PVP-modified version of method 1. For fair comparison, identical gold nanoshell growths were carried out without the addition of PVP.

A QD/SiO_2/PVIS/Au_{seeds} NPs dispersion (100 µL from the 1-mL water dispersion, estimated concentration C ≈ 0.4 nM) was diluted in gold plating solution (resp. 1 mL or 3 mL), followed by the addition of PVP-K12 (0.35 wt.% in water, resp. 40 µL or 120 µL). CH_2O (37 wt.% in water, 5 µL per mL of gold plating solution) was added in one portion, and stirred for 30 min under stirring and the dispersion was centrifuged. Golden QDs were washed with water and redispersed in water (2 mL). For the gold nanoshell growths carried out without the addition of PVP (identical process), the reaction solution was stirred for 15 min after the addition of CH_2O.

The resulting golden QDs (TEM images) and their absorption spectra are presented in Figure 3.20 below. As shown in Figures 3.20 a1 and b1, for 1 mL of gold plating solution, no continuous gold nanoshell could be obtained without PVP; whereas in the presence of PVP, all of the gold nanoshells were already continuous, with a thickness around 12 nm. In both cases, self-nucleation was negligible.

Increasing the volume of the gold plating solution to 3 mL allowed, in the absence of PVP, to obtain a complete and relatively smooth nanoshell (thickness ~ 24 nm, Figure 3.20 a2), while PVP-assisted growth gave once again a continuous shell, whose thickness is comparable to the latter (~ 24 nm), but exhibits a more pronounced roughness (Figure 3.20 b2). As evidenced by the higher extinction value at 350 nm (Figure 3.20, right), the volume of gold in NPs grown with PVP is greater than for those grown without, which is consistent with the important side self-nucleation of gold particles observed in the latter case (no secondary nucleation in the PVP-assisted process). Nevertheless, it may appear contradictory with the same apparent shell thicknesses observed in both cases. We assume that the roughness of the

PVP-grown shell can account for its unexpectedly low apparent thickness, compared to NPs grown without PVP. The plasmonic resonance of PVP-grown shells is also consistent with this assumption. As the corresponding NPs incorporated more gold than those grown without PVP (for a continuous shell in both cases), we could expect the plasmonic resonance of the former to be more blue-shifted than that of the latter (see section 1.1.4 in Chapter 1). However, simulated extinction spectra taking into account the gold roughness (see the simulation part in the appendix) showed this blue-shift effect is much less important with such a gold surface state.

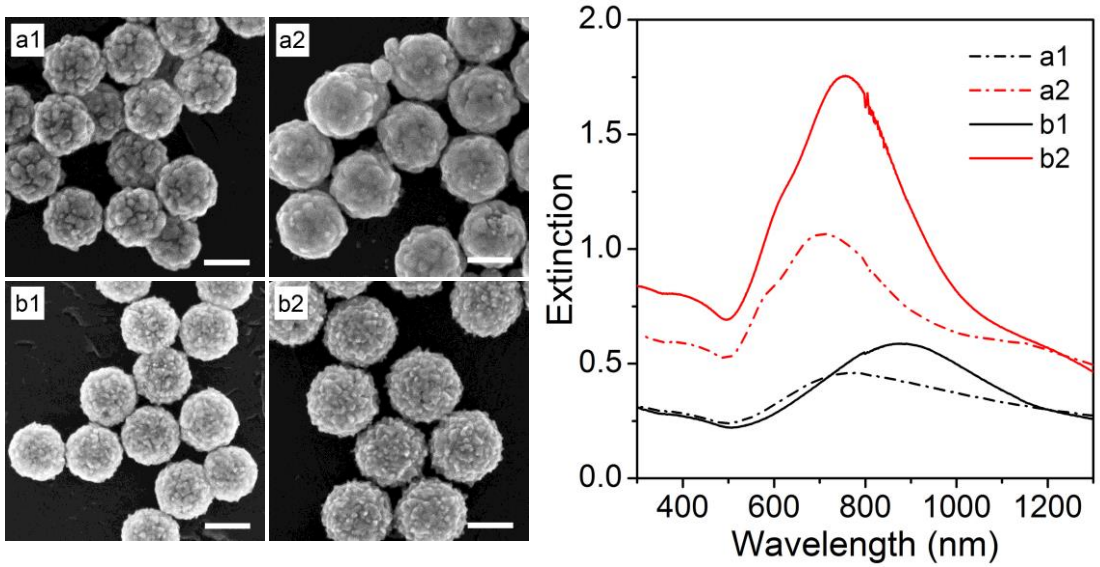

Figure 3.20. Effect of PVP-K12 on gold growth. Left: SEM images of golden QDs NPs synthesized from QD/SiO_2 NPs without (a) or with PVP (b), and 1 mL (1) or 3 mL (2) of gold plating solution (washed samples). Scale bars: 100 nm. Right: corresponding extinction spectra without normalization, but for the same NPs concentration.

As far as the ligand properties of PVP are concerned, golden QDs NPs prepared with PVP show a long-term colloidal stability when dispersed in polar solvents: at least ~ 1 year when stored at 4 ^{o}C, compared to a few days without PVP.

PVP thus plays two major roles during the gold growth. First, it can complex gold(III) ions, slowing down their reduction rate. The growth rate of the gold seeds is consequently better controlled and homogeneous, which allows access to thin continuous gold shells, as well as much less gold waste through secondary self-nucleation. Second, PVP can adsorb onto the gold surface of golden QDs NPs and act as stabilizing ligand, thus conferring to the NPs an

enhanced colloidal stability in water. This adsorption may also account for the roughness observed, which could arise from a PVP-directed growth of gold at specific crystal facets.

The effect of PVP on the growth rate can be compared to a side effect of PVIS we had observed at the beginning of our study. We noticed that, when a large excess of PVIS was used during the functionalization process, no gold shell growth could be obtained from $QD/SiO_2/Au_{seeds}$ NPs. We can indeed expect that an excess of PVIS has a similar effect to PVP and slows the growth rate, down to complete inhibition of the process in this case: PVIS can probably bind more tightly to the seeds and consequently, totally prevent their growth. As complementary results in the case of PVP, the use of an excess of PVP-K12 or the use of PVP-K15 (number average molecular weight = 10,000 g/mol) at the same concentration as in the authentic process greatly decreased the growth rate of the gold seeds and thereby extended the reaction time obviously (the beginning of the reaction is clearly marked by the appearance of a characteristic blue color). Although slower, these processes did not afford any particular improvement in the formation of the gold nanoshells. As gold(III) ions are fluorescence quenchers, a too slow reduction of gold(III) ions could be detrimental to the QDs fluorescence and should be avoided. Hence, we neither used neither an excess of PVP-K12 nor PVP-K15.

So far, PVP-K12-assisted gold nanoshell growth *via* method 1 has proved to be the most efficient to control the gold nanoshell growth. In the following sections, we will therefore study the effect of the gold seeds coverage on the gold nanoshells formation using this optimized method.

3.4.4 Effect of the gold seeds coverage density

3.4.4.1 Gold seeds coverages obtained with APTMS or PVIS

The optimized gold nanoshell growth (PVP-assisted method 1) was performed on $QD/SiO_2/Au_{seeds}$ NPs samples obtained from the functionalization with either APTMS or PVIS.

100 µL of $QD/SiO_2/Au_{seeds}$ NPs having either low (APTMS) or high coverage of gold seeds (PVIS) (estimated concentration $C \approx 0.4$ nM) were mixed respectively with the same amount

of gold plating solution and a nanoshell was grown following PVP-assisted method 1 (see section 3.4.3).

The experiment was repeated with increasing amounts of the gold plating solution (from 0.75 to 3 mL), and the resulting extinction and SEM images of golden QDs with 1 and 3 mL of gold plating solution are illustrated in Figure 3.21. To be clearer, the corresponding plasmon resonance wavelength was reported as a function of the volume of the gold plating solution introduced in the process (Figure 3.22).

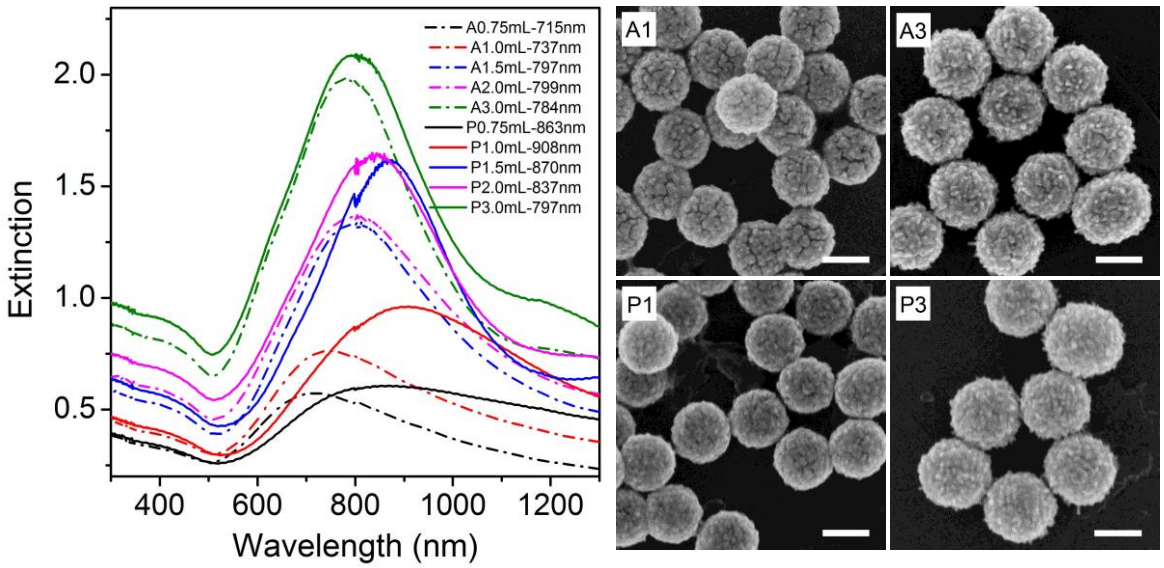

Figure 3.21. Effect of the coverage of gold seeds to the formation of the gold nanoshells. Left: Evolution of the extinction spectra of the golden QDs as a function of the volume of the gold plating solution for golden QDs grown from QD/SiO_2/APTMS/aged Au_{seeds} NPs (dashed line) or QD/SiO_2/PVIS/aged Au_{seeds} NPs (solid line) at pH = 4.5; the volume of QD/SiO_2/Au_{seeds} used was 100 µL. Right: SEM images of the golden QDs corresponding to different points of the figure shown on the left. Scale bars: 100 nm.

According to section 1.1.4 in Chapter 1, during gold nanoshell growth, the reduction of gold ions enlarges gold seeds and progressively decreases the distance between them: the interparticle plasmon coupling increases, resulting in a red-shift of the plasmon resonance. Once the nanoshell is continuous, further deposition of gold increases the thickness of the gold layer and causes a blue-shift of the plasmon absorption.[19] The continuity and thickening of the growing gold nanoshell can thus be monitored using absorption measurements.

As suggested above, the maximum wavelength reached by the gold nanoshells before blue-shift indicates that the gold shell is continuous; and the higher is the wavelength, the thinner is

the shell. Experimentally, PVIS-coated QD/SiO_2/Au_{seeds} NPs can be embedded in a continuous shell using a lesser amount of gold (1 mL of gold plating solution, P1, confirmed by SEM image) than for APTMS-coated NPs (1.5 mL of gold plating solution, A1.5; SEM confirmed the nanoshell are not continuous for 1 mL of gold plating solution, A1). Consequently, a high coverage of gold seeds allows access to thinner complete gold shells (as confirmed by plasmon resonance at 908 nm, P1) compared to a lower coverage of seeds (805 nm, A1.5). Functionalization of the silica surface by PVIS, through the density of seeds adsorbed, thus affords an important control on the thickness of the gold layer deposited.

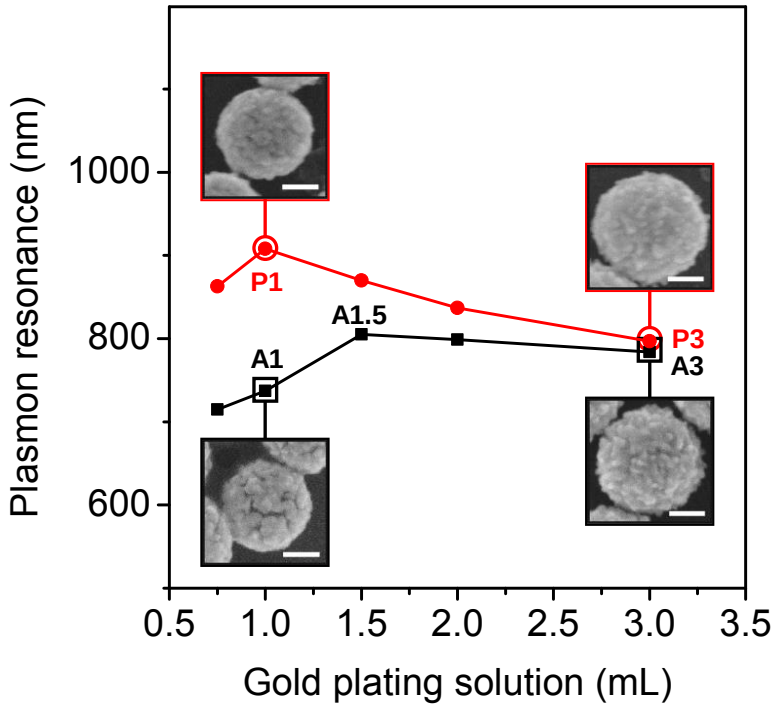

Figure 3.22. Effect of the coverage of gold seeds on the formation of the gold nanoshells. Evolution of the surface plasmon resonance wavelength of the gold nanoshells as a function of the amount of gold plating solution introduced when APTMS (black curve and squares) or PVIS (red curve and dots) was used as the functionalization agent (volume of QD/SiO_2/aged Au_{seeds} = 100 µL), pH = 4.5); A1, A3, P1, P3: SEM images of the golden QDs associated to the corresponding points of the figure. Scale bars: 50 nm.

Then, for increasing amounts of gold, the respective gold nanoshells are thicker (lower corresponding plasmon resonance wavelengths) and comparable thicknesses of the shells are obtained for 3 mL of the gold plating solution (resonances at ~ 800 nm, P3, A3 and associated SEM images, Figure 3.22).

According to this discussion, using the dense coverage of gold seeds afforded by PVIS-functionalization enables a better tuning of the thickness of the gold layer deposited, since thinner shells are accessible, compared to the coverage obtained with APTMS functionalization.

3.4.4.2 Gold seeds coverages obtained with PVIS at different pH values

As discussed in section 3.3.5, the addition of HCl (pH = 3.5) could slightly increase the aged gold seeds coverage on silica when PVIS was used as the functionalization agent. In order to determine whether this slightly higher gold seeds coverage had a significant effect on the gold growth, gold nanoshells were deposited on the QD/SiO_2/PVIS/aged Au_{seeds} NPs obtained from the gold seeds adsorption at pH = 3.5 (see Figure 3.9). The procedure was identical to that of the preceding section. The results were then compared to the gold nanoshells grown from QD/SiO_2/PVIS/aged Au_{seeds} NPs obtained from the gold seeds adsorption at pH = 4.5.

100 µL of QD/SiO_2/PVIS/Au_{seeds} NPs (obtained from the aged gold seeds adsorption at pH = 3.5, estimated concentration C ≈ 0.4 nM) were mixed with the gold plating solution and a nanoshell was grown following PVP-assisted method 1, as in section 3.4.4.1.

The evolutions of the extinction spectra and of the gold nanoshells surface plasmon resonance as a function of the volume of gold plating solution are shown in Figure 3.23 (a) and (b) respectively, and compared to the results obtained at pH = 4.5. They prove that QD/SiO_2/PVIS NPs covered with a slightly higher density of gold seeds (resulting from the adsorption of aged gold colloids at pH = 3.5) do not improve significantly the adjustment of the thickness of the deposited gold layer. Indeed, the highest plasmon resonance wavelength observed (corresponding to the thinnest shell accessible) is almost the same (~ 900 nm) in both cases. Furthermore, the thickening of the shell, indicated by the consecutive blue-shift of the plasmon resonance, is faster with the gold-seeded NPs obtained at pH = 3.5 than with those obtained at pH = 4.5. The control of the thickness of the gold layer is consequently a little less fine and the gold-seeded NPs formed at pH = 4.5 still afford the best control of the gold growth.

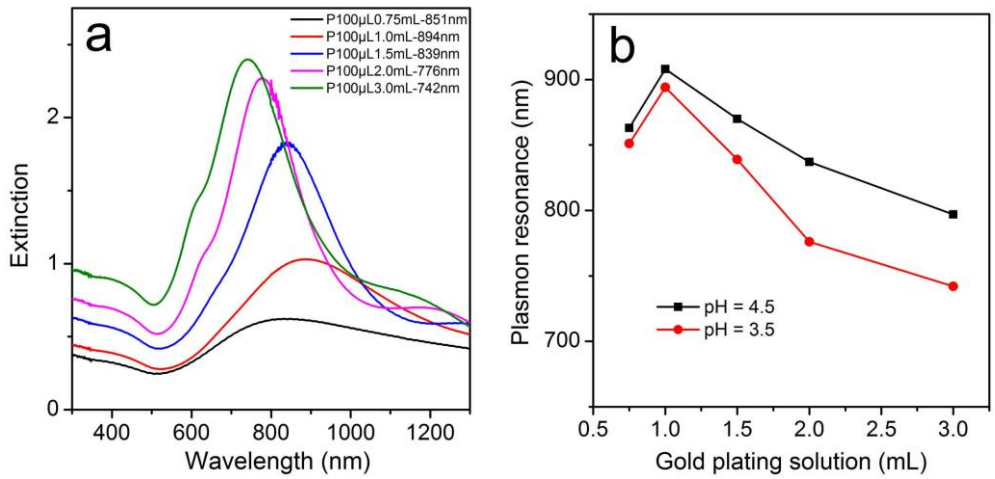

Figure 3.23. Effect of the coverage of gold seeds on the formation of gold nanoshells. a): Evolution of the extinction spectrum of the golden QDs as a function of the volume of the gold plating solution for golden QDs grown from QD/SiO_2/PVIS/aged Au_{seeds} NPs at pH = 3.5; the volume of QD/SiO_2/Au_{seeds} NPs used was 100 µL. b) Evolution of the surface plasmon resonance wavelength of the gold nanoshells grown from QD/SiO_2/PVIS/aged Au_{seeds} NPs obtained at pH = 4.5 (black squares) or pH = 3.5 (red dots) as a function of the amount of gold plating solution.

3.4.5 Effect of the monolayer/multilayer adsorption of the freshly-made gold seeds

On the basis of the results presented in section 3.3.6.3, QD/SiO_2/PVIS NPs covered with a monolayer of gold seeds (pH = 4.5) or a multilayer of gold seeds (pH = 3.5) can be formed from freshly-made gold seeds. These QD/SiO_2/PVIS/fresh Au_{seeds} NPs were used to study the effect of the gold seeds monolayer or multilayer adsorption on the formation of the gold nanoshells. Please note that the gold nanoshell growth from the fresh gold seeds took longer times compared to the aged gold seeds (fresh gold seeds are indeed less reactive, as already discussed in section 3.3.6.1).

QD/SiO_2 NPs with a monolayer of adsorbed gold seeds (Figure 3.14: fresh gold seeds; pH = 4.5; QD/SiO_2/PVIS NPs volume: 15 µL) or a multilayer of gold seeds (Figure 3.14: fresh gold seeds; pH = 3.5, QD/SiO_2/PVIS NPs volume: 15 µL) were used for the growth of gold nanoshells at the same QD/SiO_2 NPs concentration. 100 µL of QD/SiO_2 with monolayer or multilayer gold seeds were dispersed in 1.0 mL of Au plating solution, then 5 µL of CH_2O

(37 %) were added, stirred for 60 min and centrifuged (method 1 without the addition of PVP-K12). For each sample, the supernatant was separated and its absorption spectrum was measured to determine the amount of gold self-nucleation. Then the golden QDs nanoshells were washed with water once, redispersed in 1.0 mL of water and their extinction spectrum was measured.

As shown by the corresponding extinction spectra in Figure 3.24, the golden QDs obtained from QD/SiO_2/monolayer Au_{seeds} NPs incorporate a greater gold volume (extinction value at 350 nm) than those obtained from QD/SiO_2/multilayer Au_{seeds} NPs. This is consistent with the respective amount of gold self-nucleation observed in the two cases (plasmon resonance at ~ 520 nm). According to the results of the previous experiments, the gold nanoshells obtained when 1 mL of the gold plating solution is used for 100 µL of QD/SiO_2/Au_{seeds} NPs are not continuous (which is the case here). Consequently, as the golden QDs resulting from QD/SiO_2/monolayer Au_{seeds} NPs have a plasmonic resonance at a longer wavelength than those resulting from QD/SiO_2/multilayer Au_{seeds} NPs, this indicates that more continuous gold nanoshells are obtained in the case of QD/SiO_2/monolayer Au_{seeds} NPs.

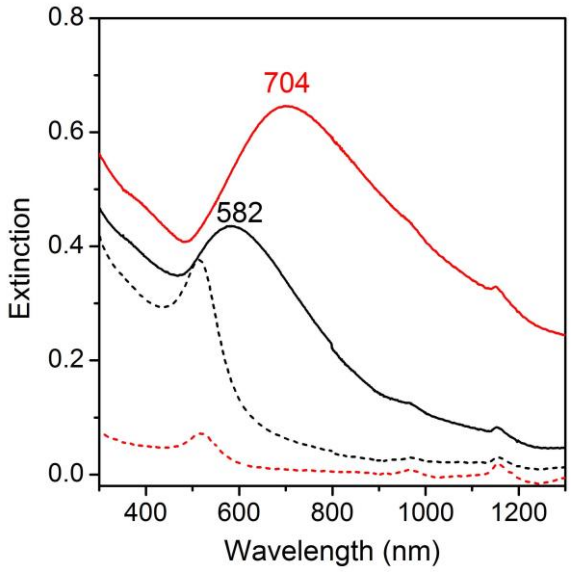

Figure 3.24. Effect of the monolayer/multilayer adsorption of the freshly-made gold seeds on the formation of the gold nanoshells. Extinction spectra without normalization of the QD/SiO_2/Au nanoshells (solid lines) and the corresponding supernatants (dashed lines) during the growth process from QD/SiO_2 NPs covered with a multilayer (black) or monolayer (red) of fresh gold seeds. The concentration of QD/SiO_2/Au NPs was the same in both cases.

The gold seeds adsorbed as a multilayer led to such an amount of self-nucleation of gold NPs because they were not strongly attached onto the silica surface (the multilayer adsorption results most likely from interactions *via* hydrogen bonds); as a consequence, a non negligible part of grown gold seeds could drop off during the growth process. Note that this self-nucleation becomes extremely important when the ratio between the quantity of gold plating solution and QD/SiO_2 NPs gets higher.

QD/SiO_2 NPs covered by gold seeds as a monolayer are consequently more suitable for the growth of gold shells than those covered by a multilayer of gold seeds.

To sum up, we optimized different synthesis conditions (such as the functionalization agent, the gold seeds adsorption conditions and the formation of gold nanoshells) to deposit continuous gold layers on QD/SiO_2 NPs with a radius of 50 nm. In the following sections, we will show that, under these optimized conditions (adsorption of aged gold seeds at pH = 4.5, with PVIS as the functionalizing agent, and a PVP-assisted gold growth using formaldehyde as the reducing agent), we can synthesize golden QDs with tailored gold and silica thicknesses.

3.4.6 Synthesis of golden QDs with tailored thicknesses of gold and silica

In this part, the method developed previously was applied to synthesize golden QDs NPs with well controlled dimensions.

3.4.6.1 Adjustment of the gold nanoshell thickness on QD/SiO_2 NPs with a fixed size

The gold nanoshell thickness can be tuned by changing the ratio between the quantity of gold ions and QD/SiO_2/Au_{seeds} NPs. To get thicker gold shells around QD/SiO_2 NPs, the amount of gold plating solution needs to be increased with respect to NPs concentration. However, as already mentioned, this can lead to important side self-nucleation of gold nanoparticles (even if PVP is used to control the reduction rate), and eventually, to inefficient growth of the gold layer. Non-negligible self-nucleation of gold nanoparticles was observed when more than 3 mL of gold plating solution were used for the growth of gold nanoshells from 100 µL of QD/SiO_2/Au_{seeds} NPs *(estimated concentration: 0.4 nM)*. This problem could

be solved by performing the synthesis of thicker gold nanoshells *via* a multi-step process, proceeding by successive additions of gold plating solution.

QD/SiO_2/PVIS/Au_{seeds} NPs dispersion (100 µL from the 1-mL water dispersion, estimated concentration: 0.4 nM) were diluted in 2.0 mL of gold plating solution, followed by the addition 80 µL of PVP-K12 (0.35 wt.% in water). 10.0 µL of CH_2O (37 wt.% in water) was added in one shot under stirring; 15 min later, the second addition of 2.0 mL of gold plating solution and 80 µL of PVP-K12 were performed. This was repeated for another time. The solution was stirred for 30 min and centrifuged. Golden QDs were washed with water and redispersed in water (2 mL).

This way, the ratio between the quantity of gold ions and the QD/SiO_2/Au_{seeds} NPs could be maintained below a certain value (typically, Au^{3+}/(QD/SiO_2/Au_{seeds} NPs) < 3.0×10^{11}) and the self-nucleation of gold nanoparticles could be avoided. As shown in Figure 3.25, gold nanoshells obtained *via* three successive additions of 2 mL of the gold plating solution have a plasmonic peak at 695 nm. This indicates that thicker gold nanoshells were obtained, compared to the golden QDs of Figure 3.21, P3: the plasmonic peak (695 nm) is indeed more blue-shifted in the former case than in the latter; and SEM characterization reveals that continuous gold nanoshells with a thickness of 30 nm have been grown efficiently.

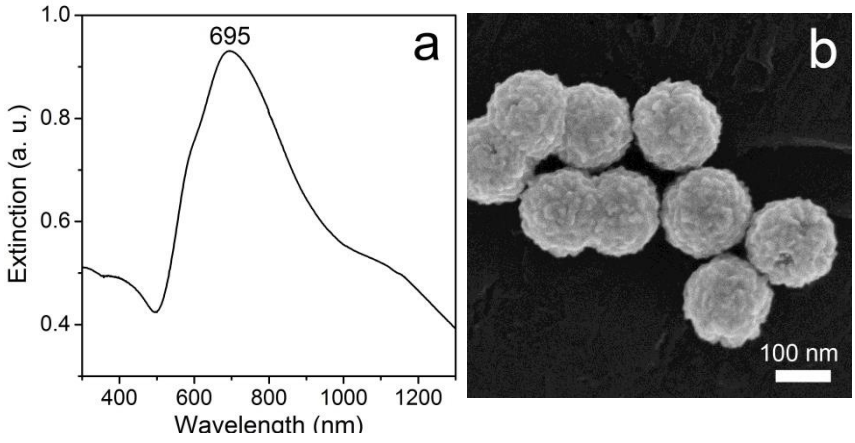

Figure 3.25 Extinction spectrum (a) and SEM image (b) of golden QDs with thicker gold nanoshells, obtained *via* a multi-step process.

With all the above optimized synthetic parameters, 15/35/T_2 QD/SiO_2/Au nanoshells with various gold thicknesses (T_2) could be synthesized successfully by tuning the ratio between the quantity of QD/SiO_2/Au_{seeds} NPs and the gold plating solution, as shown in Figure 3.26.

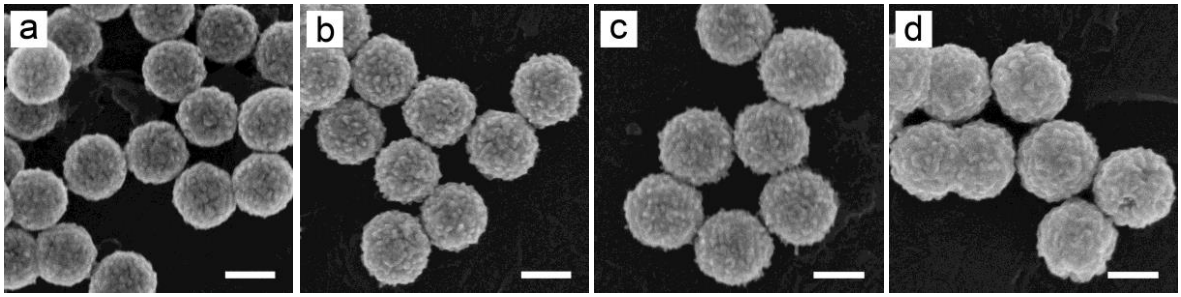

Figure 3.26. SEM images of 15/35/T_2 QD/SiO_2/Au nanoshells with various gold thicknesses T_2. a) 12 nm; b) 16 nm; c) 24 nm; d) 30 nm. Scale bars: 100 nm.

3.4.6.2 Gold nanoshell formation on QD/SiO_2 with various silica thicknesses

Figure 3.27 shows gold nanoshells of similar thicknesses grown on QD/SiO_2 NPs having different diameters. As the size of QD/SiO_2 decreased from 85 nm (Figure 3.27c) to 75 nm (Figure 3.27b), the quantity of dimeric or trimeric NPs resulting from aggregation increased. And we did not manage to synthesize individual golden QDs from 55-nm-in-diameter QD/SiO_2 NP. Korgel *et al.* found that silica NPs were highly prone to aggregate due to a low electrostatic double-layer potential.[29] Besides, this can also be explained by QD/SiO_2 beads that have already aggregated right after the encapsulation into silica, as proposed in the last chapter when the smaller QD/SiO_2 beads were used to try and regrow silica.

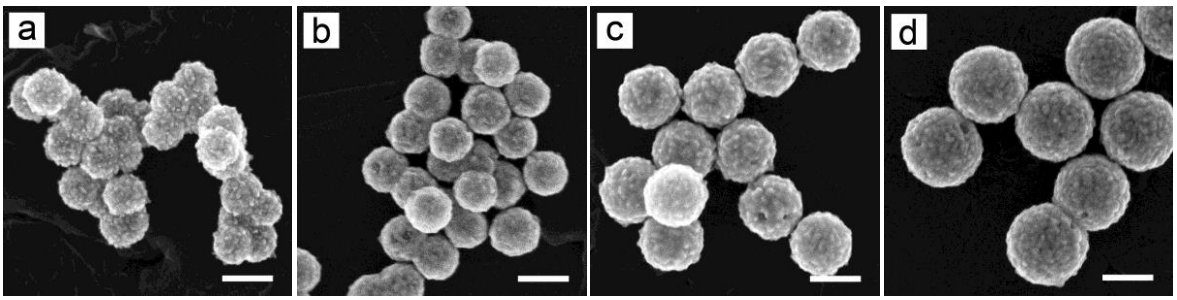

Figure 3.27. SEM images of R/T_1/T_2 QD/SiO_2/Au NPs with various silica thicknesses T_1 and similar gold thicknesses T_2; a) 6/21.5/14; b) 6/31.5/10; c) 6/37/15; d) 6/59/12. Scale bars: 100 nm.

3.5 Conclusion

In this chapter, colloidal single QD/SiO_2/Au core/shell/shell heterostructures were synthesized *via* a general method consisting in three steps: functionalization of QD/SiO_2 NPs by an adsorbing agent, adsorption of gold seeds and growth of the seeds to form a continuous shell. Several experimental parameters were explored to improve the synthesis. A dense coverage of gold seeds onto the surface of SiO_2 was obtained thanks to a polymer we have developed, namely PVIS. After comparison between different reducing processes, a reducing agent, CH_2O, was chosen and employed in a one-shot injection method. PVP was introduced to obtain a controlled and homogeneous growth of the gold seeds, leading also to a better dispersion of the gold nanoshells in water. All of these improvements enable a facile and efficient control of the deposition of the gold layer around silica, which greatly facilitates the adjustement of the coupling between the fluorescence of QDs and the surface plasmons of the gold nanoshells.

References

(1) Ma, X. D.; Tan, H.; Kipp, T.; Mews, A.: Fluorescence enhancement, blinking suppression, and gray states of individual semiconductor nanocrystals close to gold nanoparticles. *Nano Lett* **2010**, *10*, 4166-4174.

(2) Pompa, P. P.; Martiradonna, L.; Della Torre, A.; Della Sala, F.; Manna, L.; De Vittorio, M.; Calabi, F.; Cingolani, R.; Rinaldi, R.: Metal-enhanced fluorescence of colloidal nanocrystals with nanoscale control. *Nat Nanotechnol* **2006**, *1*, 126-130.

(3) Canneson, D.; Mallek-Zouari, I.; Buil, S.; Quelin, X.; Javaux, C.; Mahler, B.; Dubertret, B.; Hermier, J. P.: Strong Purcell effect observed in single thick-shell CdSe/CdS nanocrystals coupled to localized surface plasmons. *Physical Review B* **2011**, *84*, 245423.

(4) Kinkhabwala, A.; Yu, Z. F.; Fan, S. H.; Avlasevich, Y.; Mullen, K.; Moerner, W. E.: Large single-molecule fluorescence enhancements produced by a bowtie nanoantenna. *Nat Photonics* **2009**, *3*, 654-657.

(5) Yuan, H.; Khatua, S.; Zijlstra, P.; Yorulmaz, M.; Orrit, M.: Thousand-fold enhancement of single-molecule fluorescence near a single gold nanorod. *Angewandte Chemie International Edition* **2013**, *52*, 1217-1221.

(6) Ming, T.; Chen, H. J.; Jiang, R. B.; Li, Q.; Wang, J. F.: Plasmon-controlled fluorescence: beyond the intensity enhancement. *J Phys Chem Lett* **2012**, *3*, 191-202.

(7) Achermann, M.: Exciton-plasmon interactions in metal-semiconductor nanostructures. *J Phys Chem Lett* **2010**, *1*, 2837-2843.

(8) Zhang, J. A.; Fu, Y.; Lakowicz, J. R.: Emission behavior of fluorescently labeled silver nanoshell: enhanced self-quenching by metal nanostructure. *J Phys Chem C* **2007**, *111*, 1955-1961.

(9) Oldenburg, S. J.; Averitt, R. D.; Westcott, S. L.; Halas, N. J.: Nanoengineering of optical resonances. *Chemical Physics Letters* **1998**, *288*, 243-247.

(10) Prodan, E.; Radloff, C.; Halas, N. J.; Nordlander, P.: A hybridization model for the plasmon response of complex nanostructures. *Science* **2003**, *302*, 419-422.

(11) Jin, Y. D.; Gao, X. H.: Plasmonic fluorescent quantum dots. *Nat Nanotechnol* **2009**, *4*, 571-576.

(12) Ray, M.; Basu, T. S.; Bandyopadhyay, N. R.; Klie, R. F.; Ghosh, S.; Raja, S. O.; Dasgupta, A. K.: Highly lattice-mismatched semiconductor-metal hybrid nanostructures: gold nanoparticle encapsulated luminescent silicon quantum dots. *Nanoscale* **2014**, *6*, 2201-2210.

(13) Mokari, T.; Rothenberg, E.; Popov, I.; Costi, R.; Banin, U.: Selective growth of metal tips onto semiconductor quantum rods and tetrapods. *Science* **2004**, *304*, 1787-1790.

(14) Saunders, A. E.; Popov, I.; Banin, U.: Synthesis of hybrid CdS-Au colloidal nanostructures. *J Phys Chem B* **2006**, *110*, 25421-25429.

(15) Brinson, B. E.; Lassiter, J. B.; Levin, C. S.; Bardhan, R.; Mirin, N.; Halas, N. J.: Nanoshells made easy: improving Au layer growth on nanoparticle surfaces. *Langmuir* **2008**, *24*, 14166-14171.

(16) Westcott, S. L.; Oldenburg, S. J.; Lee, T. R.; Halas, N. J.: Formation and adsorption of clusters of gold nanoparticles onto functionalized silica nanoparticle surfaces. *Langmuir* **1998**, *14*, 5396-5401.

(17) Wang, H.; Brandl, D. W.; Nordlander, P.; Halas, N. J.: Plasmonic nanostructures: Artificial molecules. *Accounts of Chemical Research* **2007**, *40*, 53-62.

(18) Djalali, R.; Chen, Y.; Matsui, H.: Au nanowire fabrication from sequenced histidine-rich peptide. *J Am Chem Soc* **2002**, *124*, 13660-13661.

(19) Djalali, R.; Chen, Y. F.; Matsui, H.: Au nanocrystal growth on nanotubes controlled by conformations and charges of sequenced peptide templates. *J Am Chem Soc* **2003**, *125*, 5873-5879.

(20) Mouanda, B.: Grafting polyvinylimidazole onto silicon wafers via a copolymer of methacrylate epoxy and methacrylate-functional silane coupling agents. *Polymer* **1997**, *38*, 5301-5306.

(21) Duff, D. G.; Baiker, A.; Edwards, P. P.: A new hydrosol of gold clusters .1. formation and particle-size variation. *Langmuir* **1993**, *9*, 2301-2309.

(22) Jana, N. R.; Gearheart, L.; Murphy, C. J.: Seeding growth for size control of 5-40 nm diameter gold nanoparticles. *Langmuir* **2001**, *17*, 6782-6786.

(23) Link, S.; El-Sayed, M. A.: Spectral properties and relaxation dynamics of surface plasmon electronic oscillations in gold and silver nanodots and nanorods. *The Journal of Physical Chemistry B* **1999**, *103*, 8410-8426.

(24) Oldenberg, S. J.: Ph. D thesis. **1999**.

(25) Bardhan, R.; Grady, N. K.; Ali, T.; Halas, N. J.: Metallic nanoshells with semiconductor cores: optical characteristics modified by core medium properties. *Acs Nano* **2010**, *4*, 6169-6179.

(26) Graf, C.; van Blaaderen, A.: Metallodielectric colloidal core-shell particles for photonic applications. *Langmuir* **2002**, *18*, 524-534.

(27) Xia, Y. N.; Xiong, Y. J.; Lim, B.; Skrabalak, S. E.: Shape-controlled synthesis of metal nanocrystals: simple chemistry meets complex physics? *Angew Chem Int Edit* **2009**, *48*, 60-103.

(28) Kim, L. N.; Kim, E. G.; Kim, J.; Choi, S. E.; Park, W.; Kwon, S.: Fabrication and manipulation of gold 1D chain assemblies using magnetically controllable gold nanoparticles. *Bulletin of the Korean Chemical Society* **2012**, *33*, 3735-3739.

(29) Rasch, M. R.; Sokolov, K. V.; Korgel, B. A.: Limitations on the optical tunability of small diameter gold nanoshells. *Langmuir* **2009**, *25*, 11777-11785.

Chapter 4 Optical Properties of Golden QDs

4.1 Introduction

The fluorescence of QDs is much more stable than that of organic dyes,[1] but is still subject to two important limitations: i) under prolonged illumination or in presence of certain chemical moieties, the QDs' chemical composition degrades[2] and they eventually lose their fluorescent emission; and ii) at the single particle level, the QDs' fluorescence intensity fluctuates.[3] The first limitation is intrinsic to the QD. The nanocrystal is not chemically inert and some atoms or molecules may adsorb onto the QD surface, producing etching and charge carrier traps that can strongly alter the QD fluorescence emission.[4,5] In addition, chemical modification of the volume composition can result from the diffusion of ions present in the environment, as for example in the case of cation exchange.[6] The second limitation is mainly due to non-radiative Auger recombination.[7] For a neutral exciton, the bright state is dominated by the radiative recombination, which correlates long lifetime and high fluorescence intensity; when the exciton is charged, the recombination energy of the exciton is used to excite the remaining charge non–radiatively, and the latter will then relax intra-band without emitting photons; this process opens a fast, non-radiative channel, causing a short lifetime and low fluorescence intensity or even completely quenching.[8] It can be overcome if the Auger recombination is forbidden or if the Auger recombination happens in a time-scale longer than the radiative lifetime,[9,10] so that even if the QD is charged, the exciton will recombine radiatively, with the quantum yield up to 100%.[7]

The Golden QDs synthesized in the previous chapters are proposed to simultaneously circumvent these two limitations. In such a hybrid system, the gold nanoshell has two major roles. First, it acts as a barrier that greatly improves the QDs' photochemical robustness. Second, the metallic shell acts as a plasmon resonator that both increases the excitation field and the local density of states, resulting in much shorter fluorescence lifetime (Purcell effect).[11] Auger process become negligible compared to radiative recombination thanks to this Purcell effect.

As a matter of fact, the idea of coupling fluorescence emission and plasmon resonance is not new. Such hybrid systems have been studied for decades,[12] and it has been shown to

enhance by several orders of magnitude the fluorescence emission,[13-16] or to quench it almost completely.[17] The enhancement or quenching depends mostly on the control of the distance and the orientation of the fluorophore with respect to the metal surface, as well as on the topology of the metal surface. In the case of fluorescent nanocrystals, many studies have shown that QDs placed on/near metal films,[18-21] patterned metallic surfaces,[22-24] or at proximity of gold nanoparticles[25-28] have their fluorescence emission modified. But colloidal single QD/gold hybrids have rarely been synthesized, although these structures are very promising optically and can be handled very easily, since they remain dispersed in solution. One example of QD coated with a gold shell has been reported,[29] but no evidence of plasmon coupling between the gold shell and the QD was demonstrated.[13,30]

Here in this part, we investigated optical properties of single non-blinking plasmonic golden 15 nm-in-radius QDs heterostructure (synthesized in chapter 3). In addition, I will present a numerical simulation developed in collaboration with the group of **Jean-Jacques Greffet** at Laboratoire Charles Fabry, Institut d'Optique Graduate School, in order to model this QD/SiO_2/Au nanoshell system.[31]

4.2 Optical study of golden 15 nm-in-radius-QDs

With a fine tuning of the various parameters used during the synthesis, such as the molar ratio between the nanoparticles and the silica precursor or the gold(III) salt solution, the thicknesses of the silica and the gold layers – two important parameters of the golden QDs – can be tailored independently to various dimensions. For the golden QDs studied below, the thicknesses of the silica and the gold shells were tuned respectively to 35 nm and 18 nm (Figure 4.1), in order to maximize the coupling between QD emission and the resonance of the plasmon modes of the gold nanoshell. The corresponding extinction spectrum exhibits a strong and broad plasmonic resonance around 750 nm (Figure 4.2a).

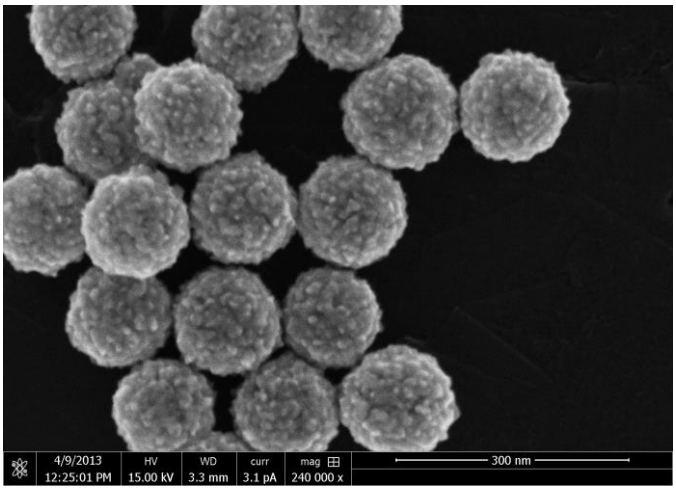

Figure 4.1 SEM image of the golden QDs (for a silica thickness of 35 nm and a gold thickness of 20 nm).

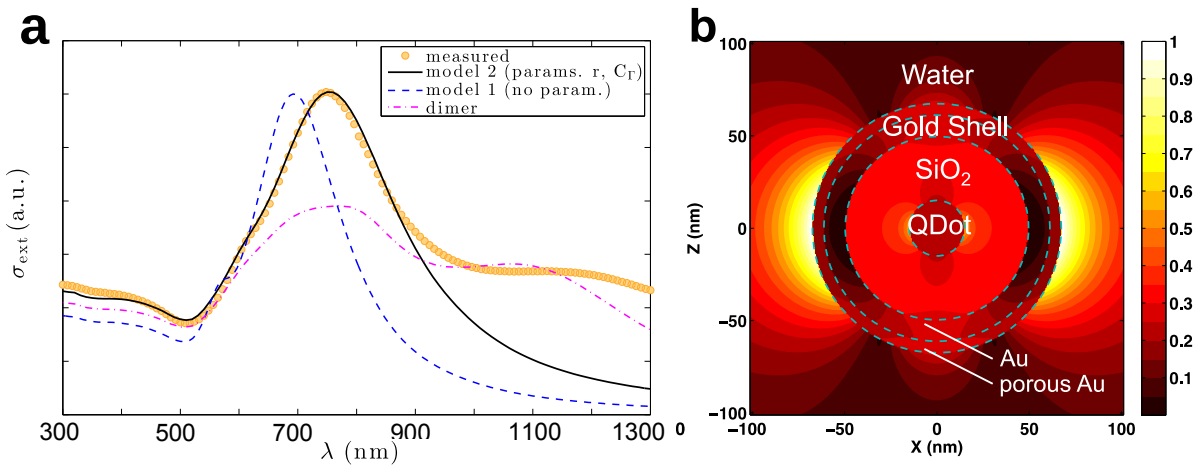

Figure 4.2 Simulations. a. Extinction spectrum of a solution of golden QDs and its fit with 2-parameter spherical model using Mie theory. We attribute the second resonance at λ = 1200 nm to the presence of dimers in solution (see the simulation part). **b.** Intensity distribution when the structure is illuminated at the wavelength of the main dipolar mode (λ = 750 nm).

To numerically compute the gold nanostructure and its extinction spectrum, a multilayer spherical model (Mie theory) has been used.[32] Using these above experimental parameters (a silica thickness of 35 nm and a gold nanoshell thickness of 18 nm) and a bulk dielectric function for the gold shell, a mismatch was observed between the experimental and theoretical resonance of the structure (Figure 4.2, Model 1). Since this model with smooth

interfaces and bulk optical properties for the gold layer could not fit the experimental extinction spectrum, it has been necessary to include the effect of gold roughness (revealed by the corresponding SEM image, Figure 4.1) and electron scattering in the shell by introducing two additional parameters (see the simulation section in the appendix). In order to simulate the gold roughness, the gold layer can be considered as consisting of two layers: an inner dense layer and an outer porous layer, as shown in Figure 4.2b. The gold roughness and electron scattering allow an excellent agreement with the experimental data around the plasmon resonance wavelength as seen in figure 4.2a (Model 2). The difference at high wavelength (~ 1,100 nm) in the spectrum can be attributed to the gold nanoshell dimer extinction (the model of the dimer in Figure 4.2a). Figure 4.2b shows the intensity distribution when the structure is illuminated at the wavelength of the main dipolar mode (λ = 750 nm). Once these parameters are adjusted by fitting the ensemble spectrum, we use them to predict the modification of the single particle lifetime and fluorescence intensity. In the following, we first discussed the mechanisms of the fluorescence emission for CdSe/CdS QDs and for golden QDs, followed by the investigation of the golden QDs system through both ensemble and single optical measurements, and also their photostability.

4.2.1 Mechanisms of the fluorescence emission for CdSe/CdS QDs and for golden QDs.

In a pulsed low-excitation regime (repetition rate R), the fluorescence intensity S (in photons per second) for a single QD can be written in the form (see simulation part in the appendix):

$$S = \frac{\Gamma_r}{\Gamma_r + \Gamma_{nr}} R \times f_{coll} \times \pi_{exc}$$

where f_{coll} is the collection efficiency and π_{exc} the probability for the QD to be in its excited state after the pulse. Γ_r is the radiative decay rate and Γ_{nr} the decay rate associated with intrinsic non-radiative channels (e.g. Auger recombination in the case of a charged QD). $1/(\Gamma_r + \Gamma_{nr}) = 1/\Gamma_{tot}$ is the measured fluorescence lifetime. In the presence of a plasmonic resonator, the fluorescence mechanism is modified, as depicted in Figure 4.3. First, the incident intensity at the center of the QD is enhanced by a factor K (denoting the excitation intensity increase),

then the emitter couples to the plasmon with an increased decay rate $F_P\Gamma_r$ (where F_P is the Purcell factor) due to the enhanced local density of states. The plasmon decays subsequently either by emitting a photon with a plasmon radiative efficiency η_p, or by Joule effect with the probability $1 - \eta_p$. In a pulsed low-excitation regime, the fluorescence signal in the presence of the nanoshell, denoted by S*, is thus given by:

$$S^* = \eta_p \frac{F_p \Gamma_r}{F_p \Gamma_r + \Gamma'_{nr}} R\, f_{coll}\, \pi_{exc}\, K$$

In a strong Purcell factor configuration ($F_P\Gamma_r >> \Gamma'_{nr}$), the intrinsic non-radiative channels can be bypassed and the nanoshell imposes its radiative efficiency:

$$S^* = \eta_p\, R\, f_{coll}\, \pi_{exc}\, K$$

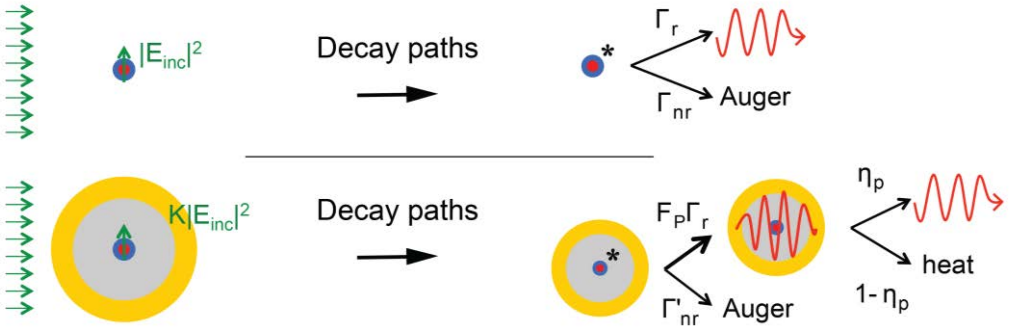

Figure 4.3. Mechanisms of the fluorescence emission for CdSe/CdS QDs (upper part) and for golden QDs (lower part).

4.2.2 Ensemble measurements

The optical measurements were performed in solution on an ensemble of nanoparticles. The PL lifetimes were measured in different buffers either in a cuvette with a fluorometer F900 (Edinburgh instrument) with a pulsed laser diode at 397 nm, or in a liquid droplet using a fluorescent microscope in a Microtime 200 setup (PicoQuant, with a Hanbury Brown and

Twiss setup (SPAD PDM; time resolution, 50 ps)) with a 405-nm pulsed laser diode. The fluorescence was collected with an air objective and sent into the confocal microscope. The signal was recorded using a HydraHarp 400 module in a time-tagged, time-resolved mode.

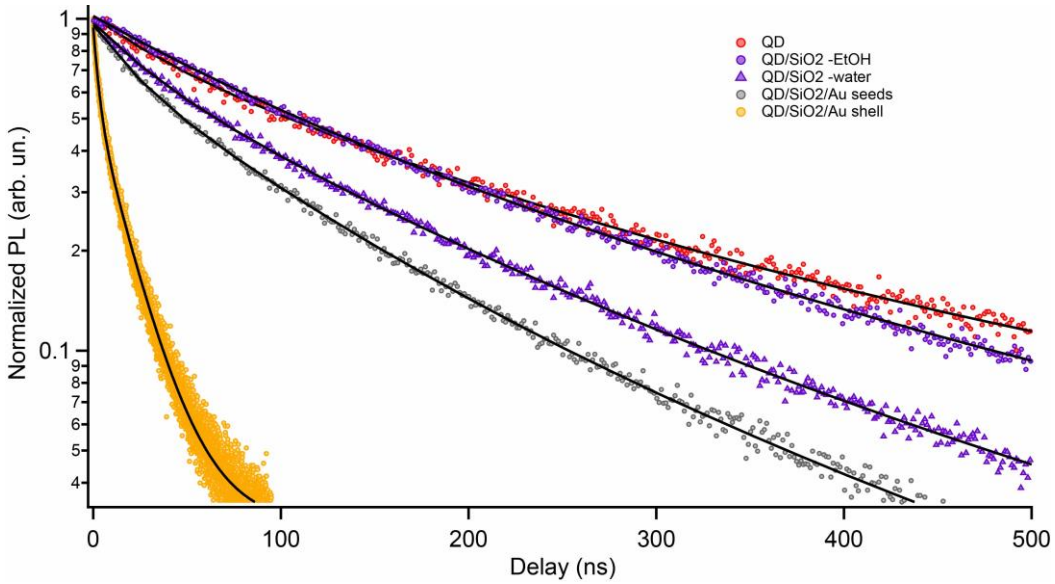

Figure 4.4. Evolution of the fluorescence lifetime of an ensemble of nanoparticles during golden QDs' synthesis.

The evolution of the QDs' fluorescence lifetime at each step that leads to golden QDs was first characterized by ensemble measurements (Figure 4.4 and Table 4.1). We show in this paragraph that we actually controlled the plasmonic coupling between a single QD and the gold nanoshell, and a final Purcell factor of ~ 6 was obtained. In the following table we summarize the experimental lifetime obtained for ensemble of QDs.

As already reported, thick-shell QD fluorescence lifetime is long ~ 160 ns, in good agreement with the quasi-type I band-alignment of the CdSe/CdS structure at room temperature.[33] The encapsulation of our thick-shell QDs in silica does not affect their fluorescence lifetime (from 165 to 160 ns). However, the following washing procedure leads to an irreversible shortening of the fluorescence lifetime to 123 ns. This value remains stable over time, even after the functionalization of the silica surface with PVIS.

Table 4.1. QD Fluorescence lifetimes τ, at different stages of the synthesis of golden QDs. The last two measurements correspond to a single particle on a glass slide. Numerical calculations of lifetime are added when available.

Nanoparticle		Experimental conditions	τ (ns)
	QD (CdSe/CdS)	as-synthesized, in hexane / cuvette	165
	QD/SiO_2	as-synthesized, in ethanol / cuvette	160
		after washing, in water / cuvette	123
	QD/SiO_2/PVIS	as-synthesized, in ethanol / cuvette	123
	$QD/SiO_2/Au_{seeds}$	as-synthesized, in water / cuvette	84
	Golden QD	as-synthesized, in water (n = 1.33) / droplet	20
		numerical simulation	20.7
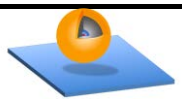	Single Golden QD	as-synthesized, on glass slide, dried	12
		numerical simulation	12.4
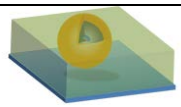	Single Golden QD	as-synthesized, on glass slide, covered with oil	28.3
		numerical simulation	27.8

When gold seeds are added onto the surface of the SiO_2 beads, the average PL lifetime decreases from 123 ns to 84 ns. This is attributed to the opening of new decay channels. Indeed, tiny gold nanoparticles are known to absorb efficiently and to have a negligible scattering cross section (see the simulation section in the appendix). As discussed in the simulation, this decay acceleration corresponds to the absorption by ~ 2700 gold seeds of 3 nm in diameter, which is consistent with the TEM images of $QD/SiO_2/Au_{seeds}$ (see Figure 3.8b in chapter 3). After the growth of the gold nanoshell, the PL lifetime goes down to 20 ns in water. Such a strong PL lifetime decrease could result from the diffusion in the silica bead of the gold(III) ions used during the nanoshell growth. In order to be sure that this lifetime decrease does not come from any new non-radiative channels opened during the gold ions deposition, a control experiment that $QD/SiO_2/Au_{seeds}$ hybrids being mixed gold(III) salt

solution without the reducing agent (CH_2O) was performed. This mixed solution has the same fluorescence emission than a solution of QD/SiO_2/Au_{seeds} hybrids only (Figure 4.5). We thus conclude from the data in Table 1 that the lifetime decay change from 123 ns (QD/SiO_2) to 20 ns (golden QDs) is due solely to the coupling of the gold nanoshell plasmons with the QD fluorescence. In order to confirm the electromagnetic origin of the spontaneous emission rate acceleration, we performed a numerical simulation. Using QD/SiO_2 in water as the reference, we found a Purcell factor of 6 for the golden QDs, corresponding to a value of 20.7 ns for the decay time, in excellent agreement with the experimental data. We further confirmed this electromagnetic origin of the increase in the decay rate by measuring the lifetime of a single golden QD in two different optical environments. The QD is first deposited on a glass substrate in air and then covered with oil. The lifetime we measured in air (resp. in oil) is 12 ns (resp. 28.3 ns), that is the value expected from the electromagnetic simulations including the effect of the glass substrate (see the simulation part) predict 12.4 ns (resp. 27.9 ns).

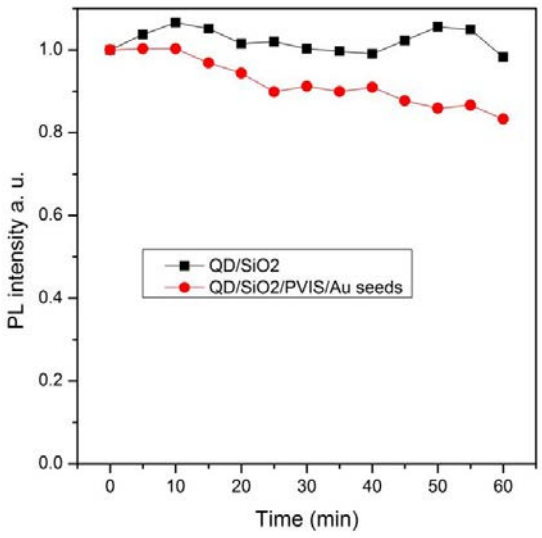

Figure 4.5. Photoluminescence evolution over time of QD/SiO_2 (black squares) and QD/SiO_2/Au_{seeds} hybrids (red circles) incubated with the gold(III) salt solution used for the synthesis (PL normalized at t = 0).

To summarize, the spontaneous emission acceleration we observe is well explained by the modification of the local density of states (Purcell effect) due to the plasmonic resonator. According to the synthetic process, 95 % of the separated golden QDs contain unique QD. In order to further explore the effect of plasmonic gold nanoshell on the QDs' fluorescence behavior (such as fluorescence trace and photostability), we now turn to the detailed analysis of the fluorescence intensity at the single nanoparticle level.

4.2.3 Single nanoparticle measurements

In order to ensure the optical study at single molecule level, all the studied golden QDs' solutions have been dispersed over home-made gridded glass coverslip. Hybrid nanocrystals are first observed on a confocal microscope (raster scan in Figure 4.6a) and analyzed individually. Afterwards, a study on a scanning electron microscope (SEM) allows us to clearly distinguish individual nanoparticles from aggregates (Figure 4.6b).

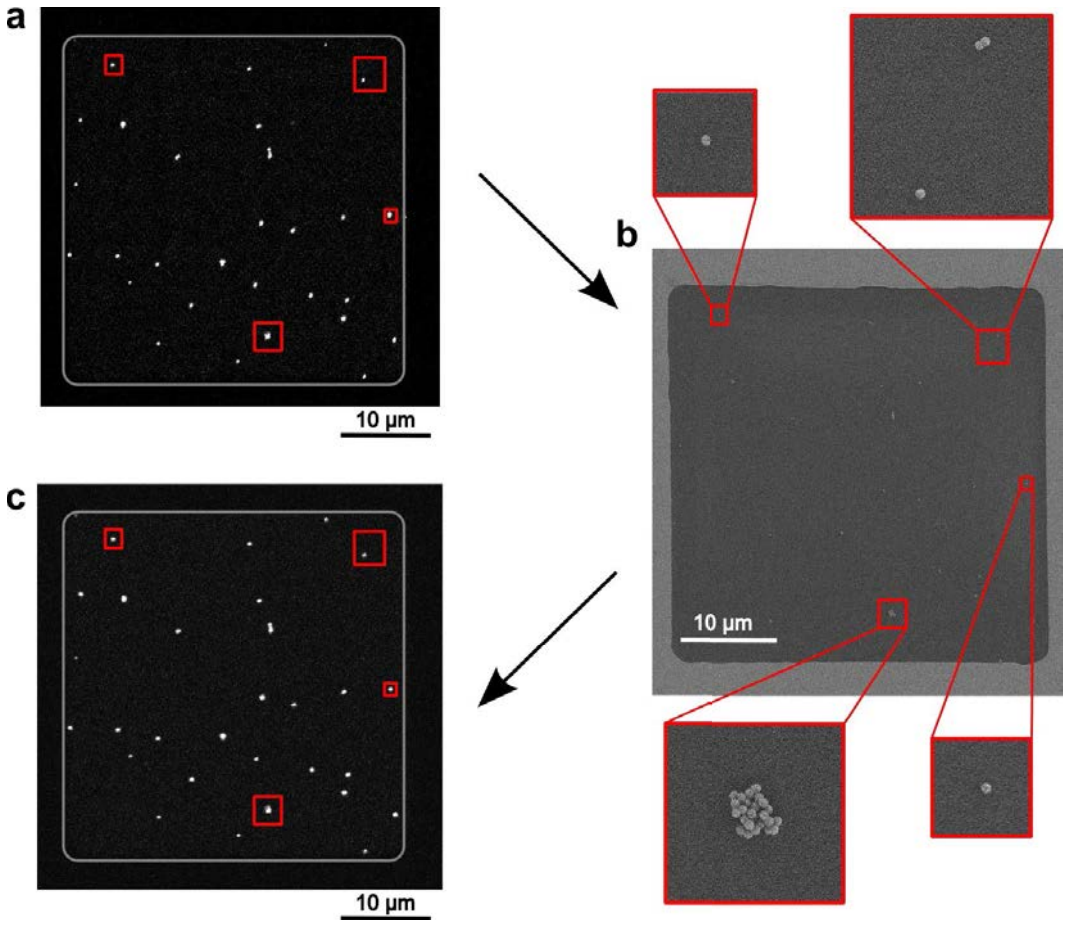

Figure 4.6. SEM/fluorescence correlation image for a typical sample of golden QDs. a. Fluorescence image of a square containing golden QDs spread on a TEM grid. **b.** SEM of the same region. **c.** Same as a. after SEM imaging.

Figure 4.7 shows the typical photoluminescence (PL) intensity and lifetime traces of single QD, QD/SiO_2/Au_{seeds} and golden QD nanoparticles evaporated from a diluted solution on a glass slide. The emission intensity of a single 15-nm-in-radius thick-shell QD (Figure 4.7a,

red trace) oscillates between two states that correspond to a grey state (charged) and a bright state (neutral QD), as already reported for this kind of nanoparticles.[7] The total fluorescence lifetimes can be extracted using a bi-exponential decay fit (Figure 4.7b, red trace): $1/\Gamma_{tot,N}$ = 160 ns for the neutral state (N) and $1/\Gamma_{tot,C}$ = 6 ns for the charged state (C). Using the same method as the one developed in Spinicelli *et al.*,[10] we extract from the experimental trace of a CdSe/CdS QDs (Figure 4.7a) the quantum yield of the QD in the charged state $S_C/S_N = \Gamma_{r,C}/\Gamma_{tot,C}$ = 0.32, and then the decay rates $\Gamma_{r,C} = (19\ ns)^{-1}$ and $\Gamma_{nr,C} = (9\ ns)^{-1}$ of the charged state. We attribute this non-radiative channel to Auger processes.

When the gold seeds coat the QD/SiO_2 nanoparticle, we observe a modification of the QD emission. A typical time trace of this hybrid structure (Figure 4.7a, grey trace) displays less intensity fluctuations, but the average intensity is lower than when no gold seeds are adsorbed. We also observe that the fluorescence lifetimes of these hybrid objects shorten. As we already discussed in the previous paragraph, this variation can be explained by the adsorption of the tiny gold nanoparticles. Since their effect is only efficient lights absorption, we suppose that they do not introduce any additional loss channels.

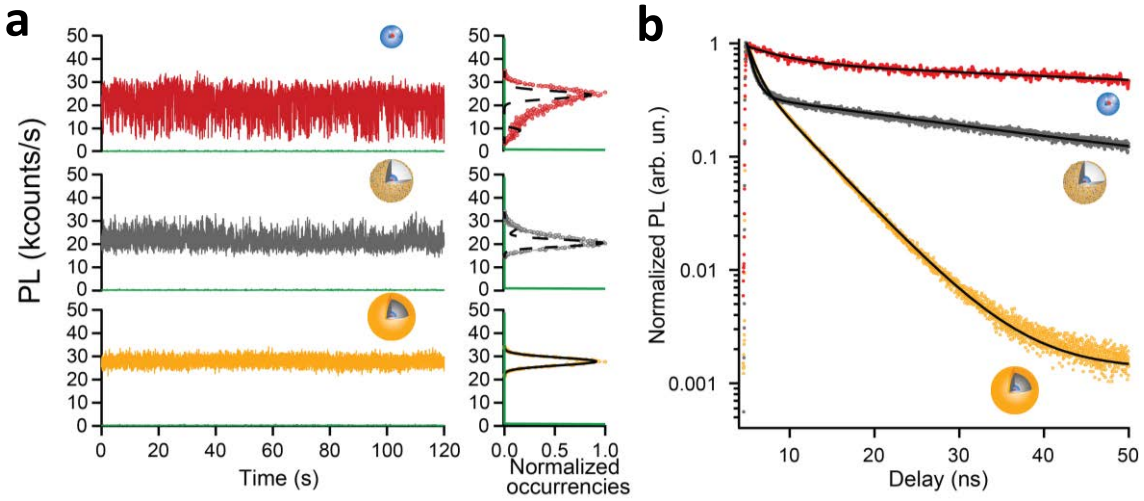

Figure 4.7. Single particle spectroscopy. a. Fluorescence intensity as a function of time (sampling time: 10 ms) for CdSe/CdS QDs (red trace), for QD/SiO_2/Au_{seeds} nanoparticles (grey trace) and for golden QDs (yellow trace); **b.** Corresponding fluorescence decay of the excitonic state for the three nanoparticles of figure 2b; excitation with a 405 nm diode laser, average intensity of few hundreds of pW, R = 10 MHz.

A different behavior is observed after the formation of the continuous gold shell, which acts as a resonator. The PL intensity shows no detectable fluctuation at the resolution of our setup (of the order of few ms for this kind of fluorescent emitters) as further confirmed by the fact

that the intensity distribution of nearly 85% of the golden QDs we studied (over ~ 25 nanoparticles observed) show a poissonian distribution (Figure 4.7a, yellow trace). This can be interpreted as follows; the neutral and charged states that we found in bare QDs now have comparable radiative efficiencies so that they do not appear any more as two distinguished emitting levels in the fluorescence signal. In other words, the emission intensities of the charged and neutral states were in a ratio of ~ 3 for the isolated QD and become almost equal in the presence of the plasmonic shell, resulting in a non-blinking fluorescent emitter. Due to the Purcell effect, Auger processes in the charged state are completely overcome by the radiative recombination. From the analysis of the lifetime for all the studied individual golden QDs, we obtained the lifetime for the bright state: ~12 ns, which is consistent with the one acquired from simulations (12.4 ns). Figure 4.7b shows a comparison of the typical decay time-traces for an individual QD, QD/SiO_2 and golden QDs.

Moreover, we can deduce the excitation intensity enhancement from PL measurements (Figure 4.7a). The PL intensity of the neutral state is slightly higher with the plasmonic shell (S_N*) than without (S_N). With an average on ~30 individual golden QDs, we find that S_N*/S_N = $\eta_p K$ = 1.12. The plasmon radiative efficiency is found to be η_p = 35% from numerical simulations using the parameters taken from the fit of ensemble measurements. We can thus deduce from the preceding measurement that the gold nanoshell enhances the incident intensity by a factor K = 3.2. Calculations performed at a wavelength λ_{exc} = 405 nm with a plane wave (instead of the Gaussian beam used in the experiment) yielded a value of K = 2.7.

4.2.4 Photostability

The poissonian trace shown in Figure 4.7a (yellow trace) is to the best of our knowledge the first perfectly stable trace of single QD obtained at room temperature. This behavior results from the enhanced optical density of states created by the gold nanoshell. However, the gold nanoshell has another role: it increases the photostability both versus time and versus the excitation power of the thick-shell CdSe/CdS QDs – which are already amongst the most robust QDs in terms of photostability. A diluted QDs or golden QDs ethanol solution were diluted and deposited by drop-casting on a glass substrate. The fluorescence intensity of QDs or golden QDs of an ensemble of single nanoparticles under continuous excitation (40mW) versus time was acquired by a charge-coupled device camera (Cascade 512B, Roper Scientific)

in an 8 mm×8 mm window. In Figure 4.8 we show the evolution of integrated PL intensity of several individual nanoparticles as a function of time under continuous UV excitation at high power (40 mW). While for bare CdSe/CdS nanocrystals we observe a dramatic fall of PL intensity after just 1 h, the signal of the golden QDs only decrease by 20% after the first few hours, and then remained stable for up to 16 h. The initial small loss of PL intensity can be explained by the presence of a small amount of particles with a non-perfectly continuous gold layer. In Figure 4.9 we show the fluorescence time trace of an Individual golden QD subjected to CW ultraviolet light (~ 1 mW) before and after 24 h of continuous excitation. We observe an average loss of intensity limited to 20% of the initial signal. A slight fluorescence fluctuation was observed in the trace, which probably because the multi-exciton emissions arising from the high excitation intensity. The increased photostability of the golden QDs is most probably due to the gold nanoshell that acts as a barrier against photo-oxidation.

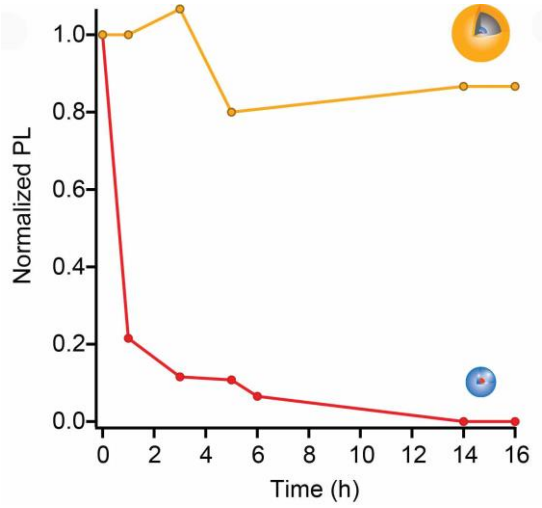

Figure 4.8. Normalized fluorescence intensity of an ensemble of single nanoparticles under continuous excitation (40mW), as a function of time. The golden QDs (yellow) are remarkably more stable over time than isolated QDs (red).

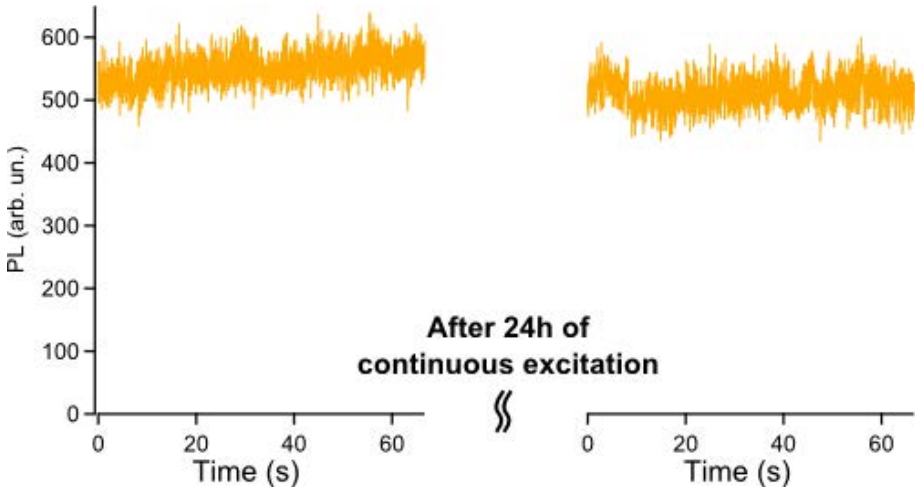

Figure 4.9. Fluorescence intensity of a typical single golden QD subjected to CW ultraviolet light (~1 mW) before and after 24 h of continuous excitation. In average, we observe an average loss of intensity limited to 20% of the initial signal.

In Figure 4.10, we compare the PL evolution versus the excitation power for bare and golden QDs. In the linear regime, i.e. less than 1 photon absorbed per pulse, the respective fluorescence intensities of both emitters have similar behavior ($S_N^*/S_N \sim 1$, as discussed previously; Figure 4.10b, inset). As soon as we further increase the excitation intensity, the multi-excitonic radiative recombination becomes not negligible and thus the PL evolution is no more linear. Moreover in the case of golden QDs, due to plasmonic coupling, the local density of states increases also for multi-excitons, so their radiative recombination is found to be much more efficient in golden QDs than in the bare ones.[21] Hence, the PL is significantly enhanced for golden QDs at similar excitation powers. This greater PL intensity in the non-linear regime comes with an increase in fluorescence stability. Indeed, golden QDs can withstand more than ten times the excitation power compared to CdSe/CdS QDs, once the PL has finally stabilized at a saturation plateau. This increased robustness of golden QDs is furthermore highlighted by SEM/fluorescence correlation experiments (see Figure 4.6), where we showed that their optical properties are not modified after electron beam excitation with an energy in the range of a few keV. A deeper study on single nanocrystals demonstrates that their optical properties (both average intensity and lifetime) have been perfectly preserved after the SEM study.

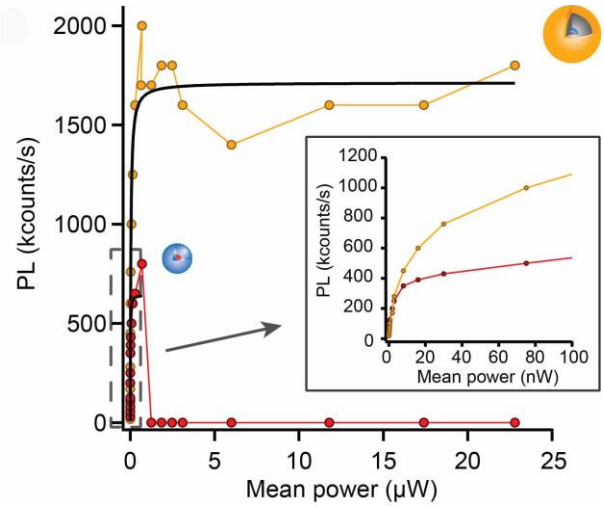

Figure 4.10. Evolution of fluorescence intensity of a single object as a function of excitation mean power in a pulsed regime (R = 10 MHz).

4.3 Conclusion

In this chapter we showed fluorescent quantum dots were coupled to the plasmon mode of gold nanoshells and displayed a 6-time shorter lifetime. The faster radiative emission rate becomes much faster than the one associated with the Auger recombination, which become very improbable. This results in non-blinking emitters. The photostability in time and in intensity of golden QDs was dramatically enhanced because of the separation of QDs from the external environment created by the continuous gold nanoshell and due to the radiative rate increase resulting from the plasmon coupling. This technique offers a general route to encapsulate the fluorophore in an electromagnetic cavity with the fluorescence being retained and has a great potential of applications in a variety of research fields. Golden QDs are indeed promising probes for biological media, since they offer biocompatibility, reduced toxicity (no or less release of toxic materials) and easy bio-functionalization using thiol-based ligands. They also demonstrated excellent photo- and electro-stability enabling technological applications such as electronic lithography.

References

(1) Resch-Genger, U.; Grabolle, M.; Cavaliere-Jaricot, S.; Nitschke, R.; Nann, T.: Quantum dots versus organic dyes as fluorescent labels. *Nat Methods* **2008**, *5*, 763-775.

(2) van Sark, W. G. J. H. M.; Frederix, P. L. T. M.; Van den Heuvel, D. J.; Gerritsen, H. C.; Bol, A. A.; van Lingen, J. N. J.; Donega, C. D.; Meijerink, A.: Photooxidation and photobleaching of single CdSe/ZnS quantum dots probed by room-temperature time-resolved spectroscopy. *J Phys Chem B* **2001**, *105*, 8281-8284.

(3) Kuno, M.; Fromm, D. P.; Hamann, H. F.; Gallagher, A.; Nesbitt, D. J.: Nonexponential "blinking" kinetics of single CdSe quantum dots: A universal power law behavior. *The Journal of Chemical Physics* **2000**, *112*, 3117-3120.

(4) Lim, S. J.; Kim, W.; Jung, S.; Seo, J.; Shin, S. K.: Anisotropic etching of semiconductor nanocrystals. *Chem Mater* **2011**, *23*, 5029-5036.

(5) Kalyuzhny, G.; Murray, R. W.: Ligand effects on optical properties of CdSe nanocrystals. *J Phys Chem B* **2005**, *109*, 7012-7021.

(6) Son, D. H.; Hughes, S. M.; Yin, Y. D.; Alivisatos, A. P.: Cation exchange reactions-in ionic nanocrystals. *Science* **2004**, *306*, 1009-1012.

(7) Javaux, C.; Mahler, B.; Dubertret, B.; Shabaev, A.; Rodina, A. V.; Efros, A. L.; Yakovlev, D. R.; Liu, F.; Bayer, M.; Camps, G.; Biadala, L.; Buil, S.; Quelin, X.; Hermier, J. P.: Thermal activation of non-radiative Auger recombination in charged colloidal nanocrystals. *Nat Nanotechnol* **2013**, *8*, 206-212.

(8) Galland, C.; Ghosh, Y.; Steinbruck, A.; Sykora, M.; Hollingsworth, J. A.; Klimov, V. I.; Htoon, H.: Two types of luminescence blinking revealed by spectroelectrochemistry of single quantum dots. *Nature* **2011**, *479*, 203-207.

(9) Cragg, G. E.; Efros, A. L.: Suppression of Auger processes in confined structures. *Nano Lett* **2010**, *10*, 313-317.

(10) Spinicelli, P.; Buil, S.; Quelin, X.; Mahler, B.; Dubertret, B.; Hermier, J. P.: Bright and grey states in CdSe-CdS nanocrystals exhibiting strongly reduced blinking. *Phys Rev Lett* **2009**, *102,* 136801.

(11) Pound, R. V.; Purcell, E. M.: Measurement of magnetic resonance absorption by nuclear moments in a solid. *Phys Rev* **1946**, *69*, 681-681.

(12) Gersten, J.; Nitzan, A.: Spectroscopic properties of molecules interacting with small dielectric particles. *J Chem Phys* **1981**, *75*, 1139-1152.

(13) Enderlein, J.: Theoretical study of single molecule fluorescence in a metallic nanocavity. *Appl Phys Lett* **2002**, *80*, 315-317.

(14) Kuhn, S.; Hakanson, U.; Rogobete, L.; Sandoghdar, V.: Enhancement of single-molecule fluorescence using a gold nanoparticle as an optical nanoantenna. *Phys Rev Lett* **2006**, *97*, 017402.

(15) Anger, P.; Bharadwaj, P.; Novotny, L.: Enhancement and quenching of single-molecule fluorescence. *Phys Rev Lett* **2006**, *96*, 113002.

(16) Yuan, H.; Khatua, S.; Zijlstra, P.; Yorulmaz, M.; Orrit, M.: Thousand-fold enhancement of single-molecule fluorescence near a single gold nanorod. *Angewandte Chemie International Edition* **2013**, *52*, 1217-1221.

(17) Dubertret, B.; Calame, M.; Libchaber, A. J.: Single-mismatch detection using gold-quenched fluorescent oligonucleotides. *Nat Biotechnol* **2001**, *19*, 365-370.

(18) Canneson, D.; Mallek-Zouari, I.; Buil, S.; Quelin, X.; Javaux, C.; Mahler, B.; Dubertret, B.; Hermier, J. P.: Strong Purcell effect observed in single thick-shell CdSe/CdS nanocrystals coupled to localized surface plasmons. *Physical Review B* **2011**, *84*, 245423.

(19) Shimizu, K. T.; Woo, W. K.; Fisher, B. R.; Eisler, H. J.; Bawendi, M. G.: Surface-enhanced emission from single semiconductor nanocrystals. *Phys Rev Lett* **2002**, *89*, 117401.

(20) Ito, Y.; Matsuda, K.; Kanemitsu, Y.: Mechanism of photoluminescence enhancement in single semiconductor nanocrystals on metal surfaces. *Physical Review B* **2007**, *75*, 033309.

(21) LeBlanc, S. J.; McClanahan, M. R.; Jones, M.; Moyer, P. J.: Enhancement of multiphoton emission from single CdSe quantum dots coupled to gold films. *Nano Lett* **2013**, *13*, 1662-1669.

(22) Pompa, P. P.; Martiradonna, L.; Della Torre, A.; Della Sala, F.; Manna, L.; De Vittorio, M.; Calabi, F.; Cingolani, R.; Rinaldi, R.: Metal-enhanced fluorescence of colloidal nanocrystals with nanoscale control. *Nat Nanotechnol* **2006**, *1*, 126-130.

(23) Song, J.-H.; Atay, T.; Shi, S.; Urabe, H.; Nurmikko, A. V.: Large enhancement of fluorescence efficiency from CdSe/ZnS quantum dots induced by resonant coupling to spatially controlled surface plasmons. *Nano Lett* **2005**, *5*, 1557-1561.

(24) Chan, Y. H.; Chen, J. X.; Wark, S. E.; Skiles, S. L.; Son, D. H.; Batteas, J. D.: Using patterned arrays of metal nanoparticles to probe plasmon enhanced luminescence of CdSe quantum dots. *Acs Nano* **2009**, *3*, 1735-1744.

(25) Liu, N. G.; Prall, B. S.; Klimov, V. I.: Hybrid gold/silica/nanocrystal-quantum-dot superstructures: Synthesis and analysis of semiconductor-metal interactions. *J Am Chem Soc* **2006**, *128*, 15362-15363.

(26) Ratchford, D.; Shafiei, F.; Kim, S.; Gray, S. K.; Li, X. Q.: Manipulating coupling between a single semiconductor quantum dot and single gold nanoparticle. *Nano Lett* **2011**, *11*, 1049-1054.

(27) Ma, X. D.; Fletcher, K.; Kipp, T.; Grzelczak, M. P.; Wang, Z.; Guerrero-Martinez, A.; Pastoriza-Santos, I.; Kornowski, A.; Liz-Marzan, L. M.; Mews, A.: Photoluminescence of individual Au/CdSe nanocrystal complexes with variable interparticle distances. *J Phys Chem Lett* **2011**, *2*, 2466-2471.

(28) Ma, X. D.; Tan, H.; Kipp, T.; Mews, A.: Fluorescence enhancement, blinking suppression, and gray states of individual semiconductor nanocrystals close to gold nanoparticles. *Nano Lett* **2010**, *10*, 4166-4174.

(29) Jin, Y. D.; Gao, X. H.: Plasmonic fluorescent quantum dots. *Nat Nanotechnol* **2009**, *4*, 571-576.

(30) Prodan, E.; Radloff, C.; Halas, N. J.; Nordlander, P.: A hybridization model for the plasmon response of complex nanostructures. *Science* **2003**, *302*, 419-422.

(31) Habert, B.; Greffet, J. J.: Ph. D. Thesis. *Université Paris-Sud 11* **2014**.

(32) Mie, G.: Contributions to the optics of turbid media, particularly of colloidal metal solutions. *Annalen der Physik* **1908**, *330*, 377-345.

(33) Mahler, B.; Spinicelli, P.; Buil, S.; Quelin, X.; Hermier, J. P.; Dubertret, B.: Towards non-blinking colloidal quantum dots. *Nat Mater* **2008**, *7*, 659-664.

Chapter 5 Self-assembled Colloidal Superparticles

5.1 Introduction

Colloidal semiconductor quantum dots (QDs) attract great attention due to their exceptional optical properties including high photostability and narrow emission in wide spectral range.[1] However, their emission intensity strongly depends on their charging state and their local environment.[2,3] This dependence leads to blinking at single particle level or even complete fluorescence quenching, and limits the applications of QDs when used as fluorescent particles.[4] Blinking and related intensity fluctuations have been reduced using core/shell QDs with a thick shell,[5,6] a composition gradient between the core and the shell,[7,8] or coupling to gold surface plasmons.[9]

A simple way to overcome this drawback is to assemble multiple QDs into higher-ordered colloidal architectures (superparticles, SPs). Besides, the fluorescence intensity of these SPs can be extremely bright, which is extraordinary important when they are used as imaging markers. Moreover, multi-functional SPs can also be fabricated by assembling QDs with different emission colors or other nanoparticles, such as plasmonic and/or magnetic nanocrystals, and may have great potentials in a variety of applications including catalysis, optoelectronics and biological labeling.[10-14] To date, SPs with well-controlled size and shape have been fabricated by micro-emulsion-droplet-template method and controlled induction of solvophobic interactions method.[15-17] The formation of SPs was driven by the solvophobic interactions between the original hydrophobic ligands on the surface of component building blocks. The surfactant (such as cetyltrimethylammonium bromide, CTAB) or polymer molecules (like poly(N-vinylpyrrolidone), PVP) absorb on the surface of SPs and make them be dispersed in polar solvents.[15,17] However, these SPs will decompose after long time storage or in the presence of organic solvents, due to the weak interaction inside the SPs themselves.[18] The stability of SPs needs to be enhanced.

In this chapter, we applied the micro-emulsion-droplet-template method to synthesize relatively monodispersed SPs from hydrophobic QDs with different emission colors and sizes. The size of SPs could be well tuned in a wide range. Magnetic SPs could also be obtained by

mixing QDs and magnetic nanocrystals. A silica layer was deposited on SPs, which extremely enhances the stability of SPs. This was also followed by the growth of a gold nanoshell on SPs/SiO_2 NPs through the method we previously developed. The schematic representation of the synthesis is shown in Figure 5.1. The improved optical properties of these SPs/SiO_2 and golden SPs including high fluorescence intensity, non-blinking, high stability and/or plasmon-coupled fluorescence, make them highly suitable in a variety of applications from biosensing and targeting to nanophotonics engineering.

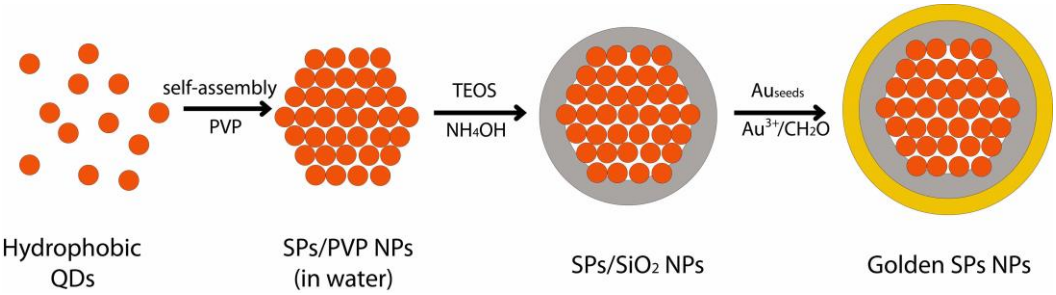

Figure 5.1. Schematic Representation of the steps in the synthesis of golden SPs NPs. First, SPs are synthesized through a micro-emulsion-droplet-template method. PVP molecules adsorb on SPs for the subsequent silica deposition via Stöber method. Golden SPs NPs are obtained through the method we previously developed. PVP: poly(N-vinylpyrrolidone); TEOS: tetraethyl orthosilicate.

5.2 Synthesis of SPs

5.2.1 Self-assembly of hydrophobic nanocrystals: the mechanism

We applied a micro-emulsion-droplet-template method developed by Li *et al.* with slight modifications.[15] The basic synthesis mechanism of the self-assembled colloidal SPs is presented in Scheme 5.1. The oil phase solution which contained pre-synthesized well-dispersed nanocrystals was added to the aqueous solution containing the surfactant. Stable oil/water (O/W) micro-emulsions droplets were obtained through an emulsification process under vigorous stirring. The alkane chain of the surfactant points toward the interior of the droplet whereas the polar end of the surfactant makes the droplet disperse in water. Subsequently, the oil phase was evaporated completely by heating at the temperature which did not damage the O/W micelle stability. In this process, the interparticle distance decreased

and eventually SPs with a supercrystalline structure were formed. These 3D colloidal spheres were separated and redispersed in water.

In our synthesis, we applied chloroform as the organic phase and DTAB as the surfactant. First, we started the synthesis of colloidal SPs with CdSe/CdS/ZnS QDs (PL-610 nm) as follows.

Scheme 5.1. Schematic representation of the synthesis mechanism of self-assembled colloidal superparticles by the micro-emulsion-droplet-template method. Reprinted from Ref [15].

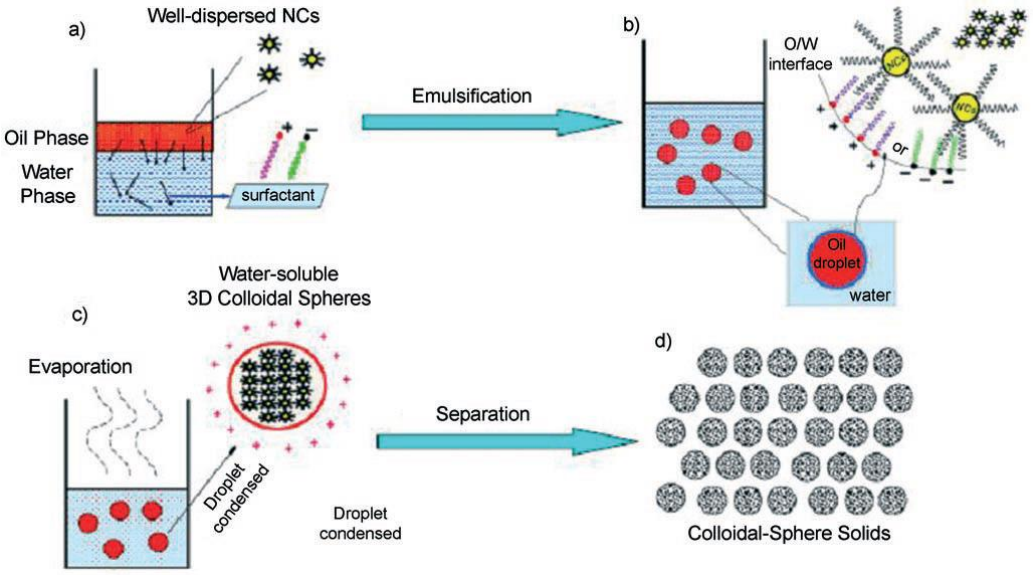

5.2.2 Synthesis of colloidal SPs via self-assembly of QDs.

14 mg of QDs (CdSe/CdS/ZnS, PL-610 nm, dispersed in hexane) were precipitated with ethanol and redispersed in 1.0 mL of $CHCl_3$, and then this solution was added to 1.5 mL of water which contained 60 mg of dodecyltrimethylammonium bromide (DTAB). This solution was mixed through vortex (30 s), stirred for 30 min at the speed of RPM (rounds per minute) 2000 (the mixing manner). All of the $CHCl_3$ were removed by heating this solution at 80 ^oC for 15 min. The volume of this micelle solution was around 1.0 mL.

The QD micelles solution was centrifuged (RPM 5000, 10-15 min). The supernatant was removed and the solid was redispersed in 1.0 mL of water. Then this aqueous solution was injected to ethylene glycol (EG) with PVP (molecular weight: 55,000; 2 mM) (the injection solution) and stirred for 30 min. The SPs were precipitated, washed with ethanol for 3 times and redispersed in 7.0 mL of ethanol.

Typical TEM images of SPs reveal that 3D assembled colloidal SPs display a relatively mono-dispersed size in the range of 70 - 90 nm and hexagonal shape, in which the minimum surface energy can be accomplished (Figure 5.2). Super-crystalline can also be distinguished. However, these colloidal SPs don't have good dispersion in water and seem to aggregate according to the TEM images. Afterward, SPs aqueous solution was injected to ethylene glycol solution with PVP. The high solubility of the surfactant DTAB in ethylene glycol will cause the loss of DTAB and thereby weaken the van der Walls interactions between SPs and DTAB. The polymer molecules PVP will replace the surfactant and adsorb on the surface of SPs.17 Corresponding TEM images of SPs/PVP are presented in Figure 5.3. The SPs/PVP NPs maintain the original shape and are well separated with each other. The adsorption of PVP greatly improves the stability. However, SPs/PVP NPs still disassemble when they are dispersed in water or ethanol for weeks even stored at 4 oC, indicating the desorption of PVP molecules.

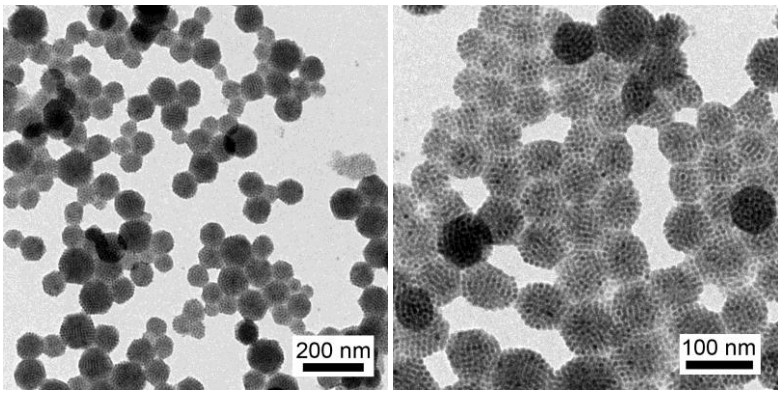

Figure 5.2. Typical TEM images of SPs NPs from CdSe/CdS/ZnS QDs.

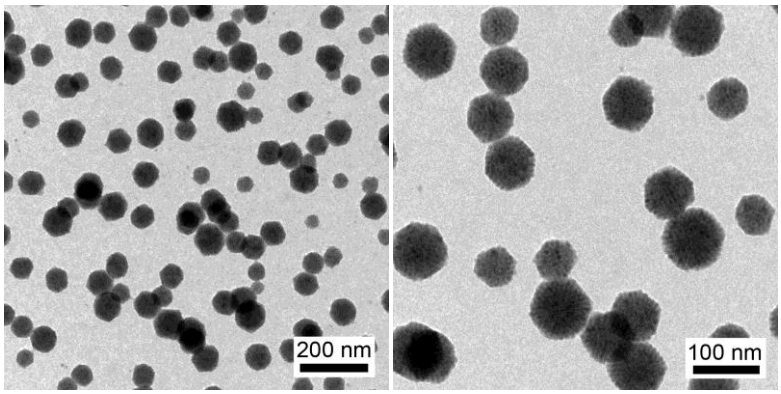

Figure 5.3. Typical TEM images of SPs/PVP NPs from CdSe/CdS/ZnS QDs.

5.2.3 Adjustment of the size of SPs

The size of the colloidal SPs can be tuned by the regulation of the emulsification process, such as the nanocrystal quantity, the surfactant concentration, the oil-to-water ratio and the way of mixing the oil phase and the water phase. Here, we show the size adjustment by changing the surfactant amount and the way the aqueous and organic solutions are mixed.

The size adjustment of SPs by changing the surfactant quantity. *Different DTAB amounts (40, 20 and 12 mg) were applied to tune the size of the resulting SPs in a similar procedure in the section 5.2.2.*

The size adjustment of SPs by changing the way the aqueous and organic solutions are mixed. *14 mg of QDs-610 nm, 1.0 mL of $CHCl_3$, 12 mg of DTAB and 1.5 mL of water were used in this protocol. The two solutions were mixed through vortex (30 s), followed by a strong probe-immersed sonication for 120 seconds. Then the same procedure was applied as the section 5.2.2.*

First we show that the SPs size is adjusted by changing the ratio between the quantity of the nanocrystals and the surfactant. In our synthesis, we tuned this ratio by fixing the quantity of QDs (14 mg) and changing the amount of the surfactant. As shown in figure 5.4, the SPs is around 100 - 130 nm when 40 mg of DTAB were used. When the amount of DTAB is further decreased to 20 mg and 12 mg, the diameter of SPs increased to 160 - 300 nm and 250 - 400 nm respectively. It should be noted that there were always some SPs with smaller size, which can be easily removed by a size-sorting procedure. The mechanism of the size adjustment of

the SPs can be understood that smaller SPs expose more surfaces to the aqueous phase than those of larger SPs and therefor more surfactants are required in the former case.

The mixing way also has a strong influence on the size of SPs. When the micelle solution was sonicated for 2 minutes instead of stirring, the size of the obtained SPs is around 45 - 70 nm, as shown in Figure 5.5, which is much smaller than SPs synthesized under the same condition but stirring is employed (Figure 5.4c).

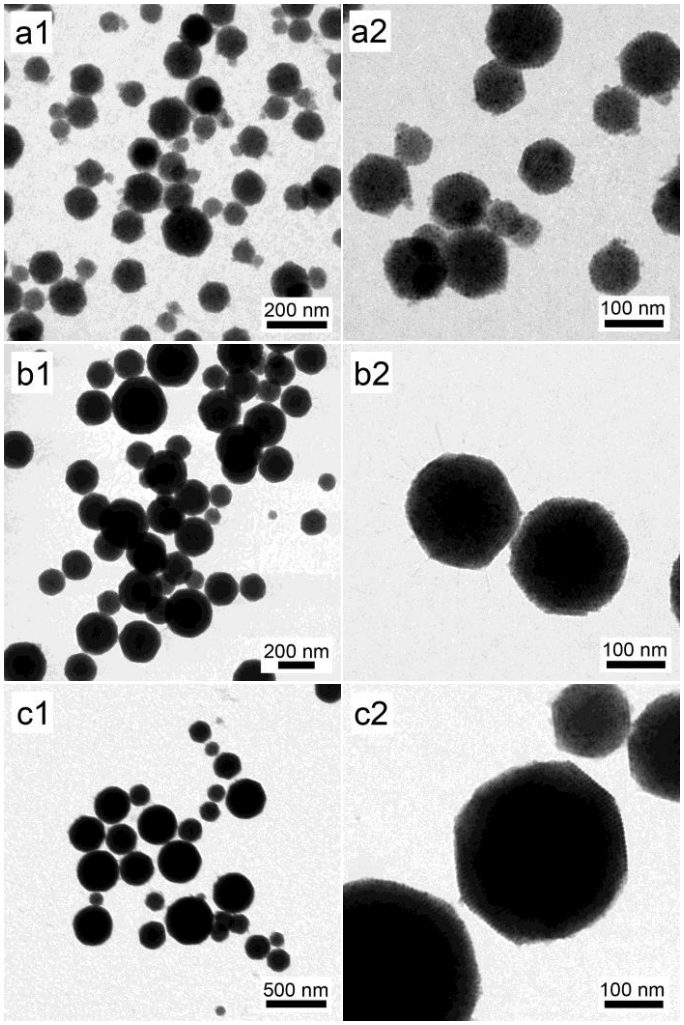

Figure 5.4. TEM images of SPs NPs with adjustment of sizes by changing the amount of DTAB: a) 40 mg; b) 20 mg; c) 12 mg.

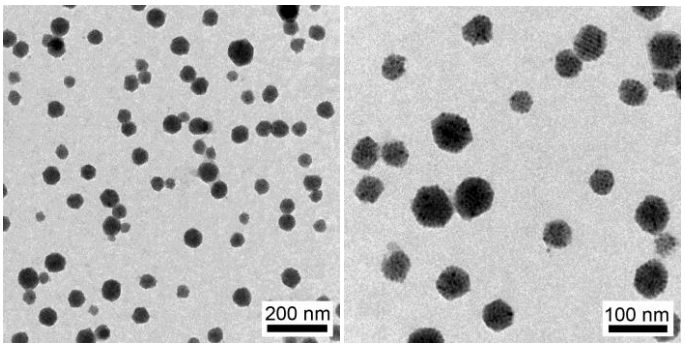

Figure 5.5. Typical TEM images of SPs/PVP NPs synthesized through strong-sonication-assisted mixing.

5.3 The incorporation of SPs in silica

The adsorption of PVP not only improves the dispersion of SPs in polar solvent (such as water and ethanol), but also acts as the nucleation site for the silica deposition, due to the sufficiently high affinity of PVP-passivated SPs surface to silica.[19] Thereby, a silica layer can be deposited on SPs/PVP NPs directly *via* the Stöber method.[20]

Silica deposition on SPs/PVP NPs. *SPs/PVP NPs ethanol solution (5 mL from the 7-mL ethanol dispersion) was added in 10 mL of ethanol which contained 660 μL of NH_4OH (29% in water) with a final volume concentration of 4.2%, followed by the dropwise injection of 1.0 mL of TEOS/ethanol (v/v = 1:9) in 2 hours. The solution was stirred overnight. SPs/SiO_2 NPs were washed with ethanol for 2 times and redispersed in 5.0 mL of ethanol.*

5.3.1 The effect of injection solvent on the silica shell growth

We find that the injection solvent has an important effect on the morphology of the silica. SPs aqueous solution were injected into three solvents (water, ethanol and ethylene glycol) at the same concentration of PVP (MW = 55,000). Then the silica shell deposition was performed. According to the TEM images of SPs (Figure 5.6a, 5.7a and 5.8a), more aggregated SPs can be observed when water or ethanol is used respect to SPs synthesized with

ethylene glycol. The aggregation becomes more serious when silica is deposited on those SPs as shown in Figure 5.6b, 5.7b, compared to SPs/SiO_2 NPs in Figure 5.8b.

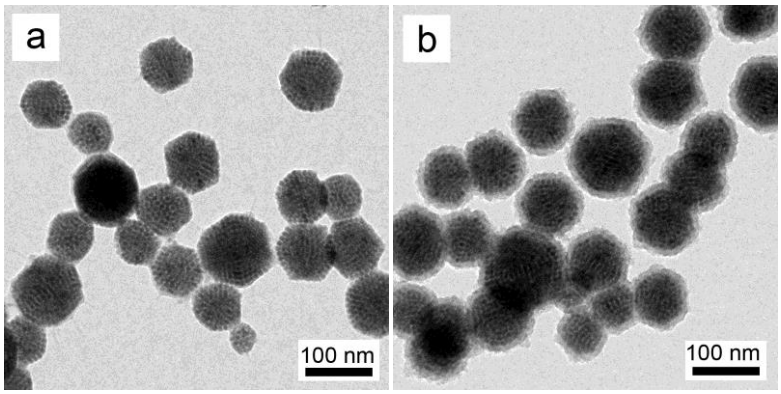

Figure 5.6. Typical TEM images of SPs/PVP NPs (a) obtained by injecting SPs into PVP/H_2O and corresponding SPs/SiO_2 NPs (b).

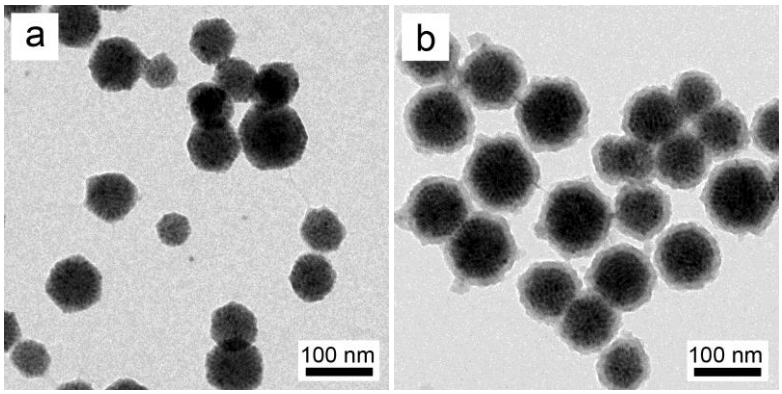

Figure 5.7. Typical TEM images of SPs/PVP NPs (a) obtained by injecting SPs into PVP/ethanol and corresponding SPs/SiO_2 NPs (b).

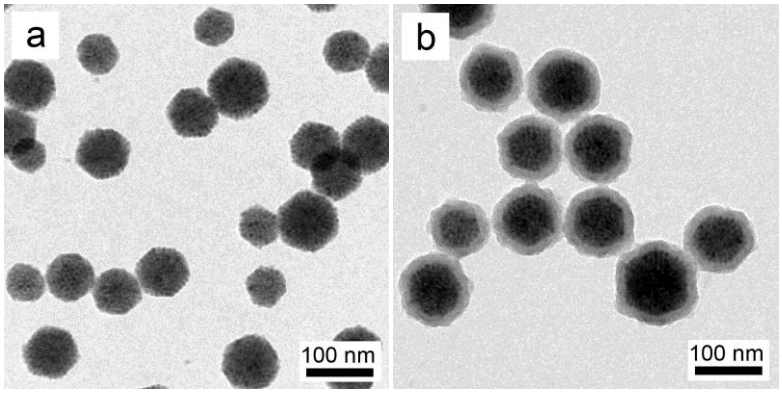

Figure 5.8. Typical TEM images of SPs/PVP NPs (a) obtained by injecting SPs into PVP/EG and corresponding SPs/SiO_2 NPs (b).

5.3.2 The effect of PVP molecular weight on the silica shell growth

The molecular weight of PVP was also tested for the growth of silica. It is difficult to distinguish the difference of SPs/PVP from the TEM images when PVP with small molecular weight (PVP-K12, the average molecular weight is about 10, 000 g/mol) (Figure 5.9a) or large molecular weight (PVP, the average molecular weight is about 55, 000 g/mol) were used (Figure 5.8a). However, the aggregation appears after the deposition of silica on SPs with PVP-K12 as stabilizing agent as illustrated in Figure 5.9b. Apparently, PVP with small molecular weight cannot sufficiently stabilize SPs during the growth of silica, possibly because the PVP cannot sufficiently shield the large van der Waals forces between the SPs.[19]

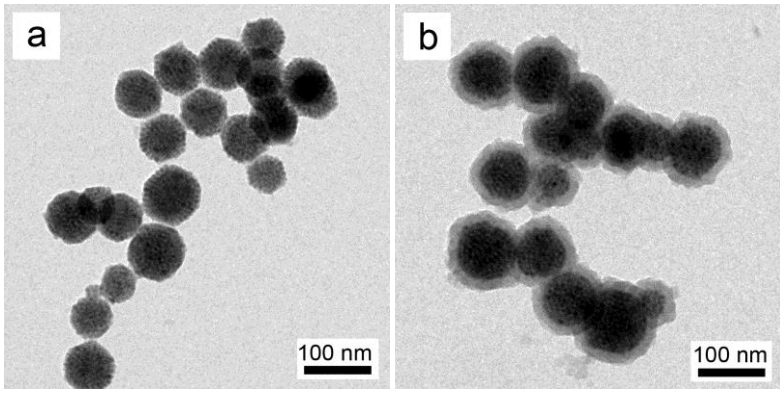

Figure 5.9. Typical TEM images of SPs/PVP NPs (a) obtained by injecting SPs into PVP-K12/EG and corresponding SPs/SiO_2 NPs (b).

5.3.3 Growth of thick silica shell on SPs/SiO_2

Thicker silica shell can be obtained by using these SPs/SiO_2 NPs as nucleation seeds in isopropanol through a fast silica growth process.

SPs/SiO_2 NPs (1 mL from the 5-mL ethanol dispersion) were precipitated and redispersed in 14 mL of isopropanol, followed by the addition of 0.24 mL of NH_4OH (29% in water), and then 30 μL of TEOS were added under stirring. The obtained NPs were collected in 2 hours. The SPs/SiO_2 NPs were washed with ethanol for 3 times and redispersed in 2.0 mL of ethanol.

As shown in Figure 5.10, the silica thickness increased to about 100 nm and the surface is very smooth.

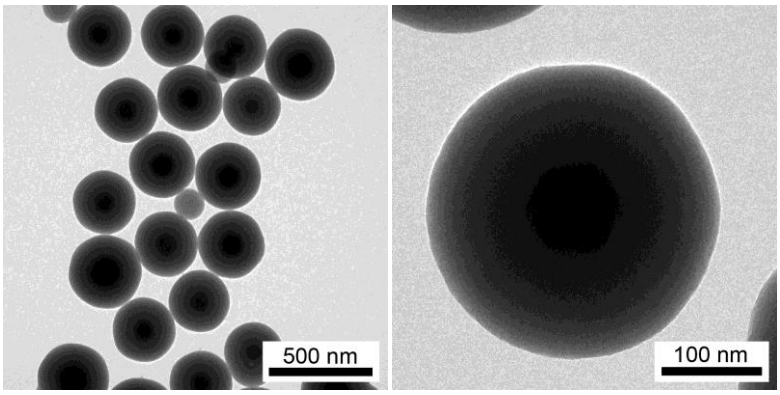

Figure 5.10. Typical TEM images of SPs/SiO_2 NPs through the regrowth of silica.

5.4 Synthesis of SPs and SPs/SiO_2 from different types of nanocrystals

Here we show a generalized method for preparing colloidal spheres from hydrophobic nanocrystals building blocks. In particular, QDs with different emission colors and sizes can act as the building blocks. Through this approach, multicolored SPs can be obtained by mixing QDs with different emission colors through this approach. Moreover, multi-functional SPs with both magnetism and fluorescence can also be synthesized by using QDs and magnetic nanocrystals.

Synthesis of SPs/PVP and SPs/SiO_2 NPs from various hydrophobic nanocrystals. *A variety of hydrophobic QDs and magnetic nanocrystals bellows were used to synthesize SPs in the previous synthetic route. 1) 14 mg of QDs (CdSe/CdS/ZnS, PL-550 nm); 2) 14 mg of QDs (CdSe/CdS/ZnS, PL-650 nm); 3) 5.95 mg of QDs (PL-550 nm), 3.64 mg of QDs (PL-610 nm), and 4.52 mg of QDs (PL-650 nm): QDs with three different colors were mixed with equal fluorescence intensity; 4) 14 mg of QDs (PL-670 nm, 30 nm in diameter, in this case, 30 and 15 mg of DTAB were used.) 5) 13 mg of QDs (CdSe/CdS/ZnS, PL-610 nm) and 1 mg of Fe_3O_4 (8 nm) 6) 11 mg of QDs (CdSe/CdS/ZnS, PL-610 nm) and 3 mg of Fe_3O_4 (8 nm); 7) 14 mg of CdSe nanoplatelets (PL-510 nm); 8) 14 mg of CdSe/CdS core/crown nanoplatelets. The*

quantity of DTAB was 60 mg if not specified. The obtained SPs/PVP NPs were washed with ethanol, followed by the silica deposition.

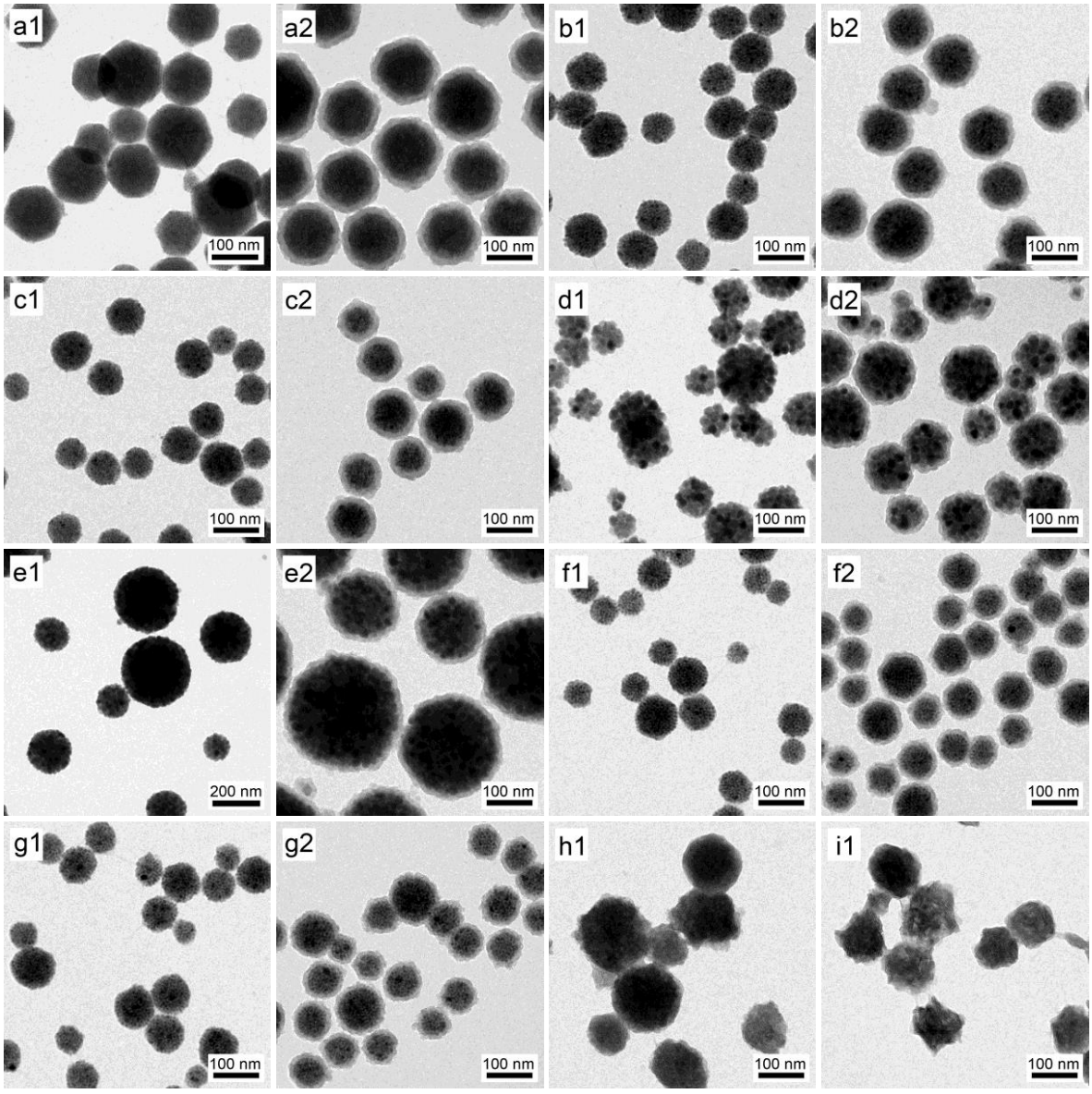

Figure 5.11. Typical TEM images of SPs (**1**) and corresponding SPs/SiO_2 (**2**) from different types of hydrophobic nanocrystals: a) QDs-550 nm, D: ~ 8 nm; b) QDs-650 nm, D: ~ 12 nm; c) mixed QDs, 550/610/650 nm; d) QDs-670 nm, D: ~ 30 nm, DTAB: 30 mg; e) QDs-670 nm, D: ~ 30 nm, DTAB: 15 mg; f) QDs-610 nm: 13 mg, Fe_3O_4 (D: ~ 8 nm): 1 mg; g) QDs-610 nm: 11 mg, Fe_3O_4 (D: ~ 8 nm): 3 mg; h) CdSe nanoplatelets; i) CdSe/CdS core/crown nanoplatelets.

Figure 5.11 shows the SPs synthesis with different types of nanocrystals and also the followed silica shell growth. All of the obtained SPs display nearly spherical shape, regardless of the morphology of the building blocks. The (QDs and Fe_3O_4)/SiO_2 SPs preserve both magnetic and fluorescent features, as presented in figure 5.12. Specifically, SPs synthesized from CdSe nanoplaelets (figure 5.11 h1) and CdSe/CdS core/crown (figure 5.11 i1) did not have visible fluorescence any more. This fluorescence quenching happened when the nanoplatelets chloroform solution was mixed with the aqueous surfactant solution. The fluorescence of nanoplatelets structures is more sensible to the external environments than that of QDs and can be completely quenched by the introduction of water.[21,22]

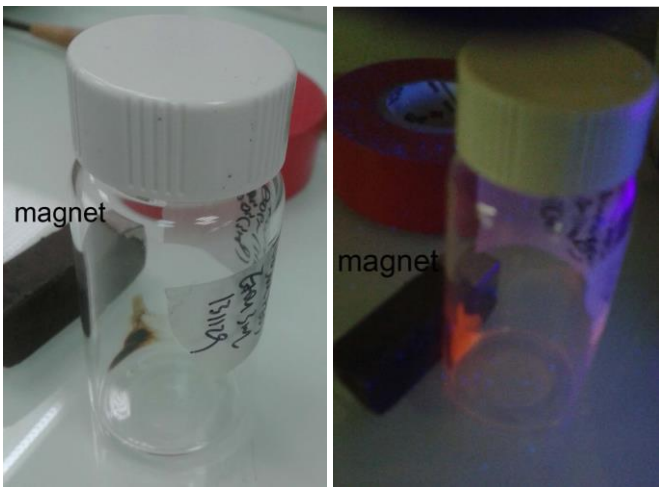

Figure 5.12. Pictures of (QDs and Fe_3O_4)/SiO_2 SPs (Figure 5.10 g2) with a magnet under visible light (left) and under UV light (Right). A fluorescence signal clearly appears under UV light excitation.

5.5 Synthesis of SPs/SiO_2/Au nanoshells (golden SPs)

The SPs/SiO_2 can be further covered by a gold nanoshell through the previously developed approach. First, SPs/SiO_2 were functionalized by a polymer, PVIS, followed by the adsorption of tiny gold seeds which acted as the nucleation sites for the growth of gold.

1) Functionalization of SPs/SiO_2 NPs with PVIS. *SPs/SiO_2 NPs (2.0 mL from the previous 5-mL ethanol dispersion) were dispersed in 7.0 mL of ethanol which contained 1 mg of PVIS.*

This solution was heated at 80 ^{o}C for 1 hour. SPs/SiO_2/PVIS NPs were washed with ethanol for three times and redispersed in 2.0 mL of ethanol.

2) Synthesis of gold-seed-decorated SPs/SiO_2 NPs. *SPs/SiO_2/PVIS NPs (150 µL from the previous 2-mL ethanol dispersion) were added in 3.0 mL of two-week-aged Au seeds solution and stirred for 1 hour. Free Au seeds were removed by washing with water for three times. SPs/SiO_2/PVIS/Au_{seeds} were redispersed in 300 µL of water.*

3) Growth of Au nanoshells on SPs/SiO_2/Au seeds NPs. *SPs/SiO_2/Au_{seeds} NPs (150 µL from the previous 300-µL ethanol dispersion) were added to 1.0 or 2.0 mL of gold plating solution; and then 50 or 100 µL of PVP (mw: 3,500, 0.35 wt%) was added and stirred for 2 min, followed by the addition of 5.0 or 10.0 µL of CH_2O respectively. The solution was stirred for 1 hour. Golden SPs were washed one time with water and redispersed in 2.0 mL of water.*

As shown in Figure 5.13, the coverage of adsorbed Au seeds was dense and uniform. Continuous gold nanoshells were fabricated by reducing more gold ions. The plasmonic peak corresponding to the thickness of gold nanoshells can be tuned by changing the amount of gold ions. When 1.0 mL of Au plating solution was used for 100 µL of SPs/SiO_2/Au_{seeds} NPs, the golden SPs displays a plasmonic adsorption at ~ 850 nm (Figure 5.14 Left); the gold layer was continuous and had a thickness of around 20 nm (Figure 5.14a). Increasing the volume of gold plating solution to 2.0 mL, the plasmonic peak shifted to red and located at ~ 800 nm, corresponding to a gold layer thickness of 26 nm (Figure 5.14b).

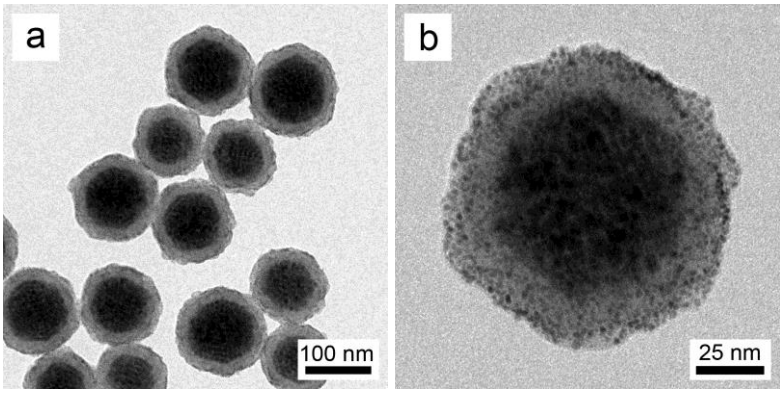

Figure 5.13. Typical TEM images of SPs/SiO_2/Au_{seeds} NPs

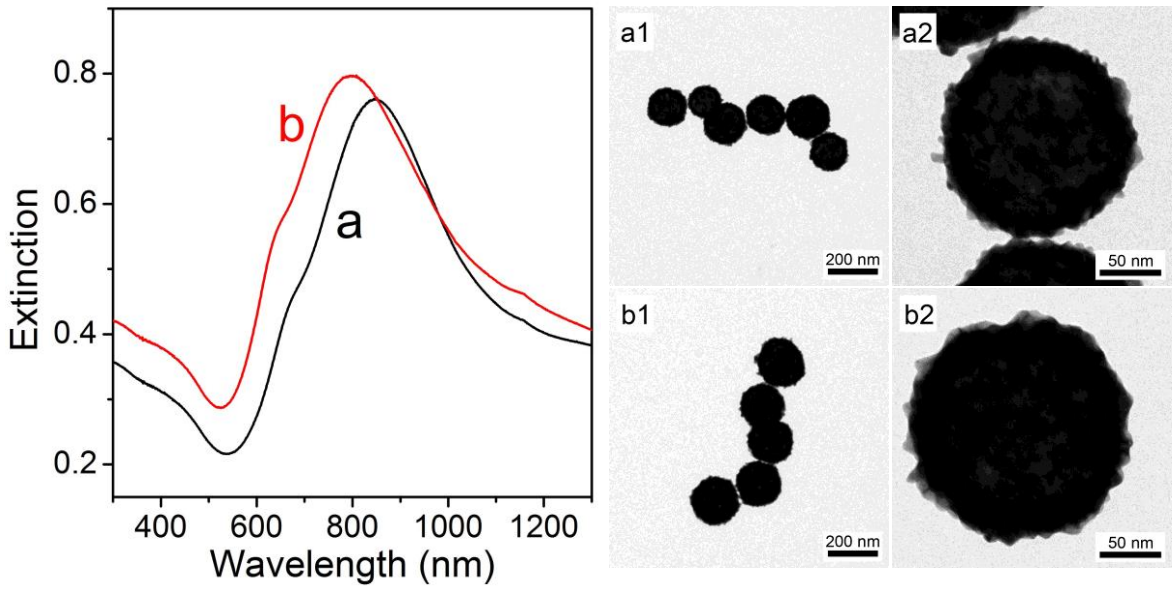

Figure 5.14. Left: Extinction spectra of golden SPs synthesized with a) 1.0 mL; b) 2.0 mL of gold plating solution. **Right**: corresponding TEM images of golden SPs at different resolutions.

5.6 Conclusion

In this chapter, based on the micro-emulsion-droplet-template, a versatile bottom-up self-assembly approach is developed to assemble hydrophobic QDs to colloidal spherical superparticles, followed by the deposition of a silica layer. The multiple QDs make the SPs display non-blinking fluorescence and high brightness, which are extremely suitable for imaging applications. The surrounded silica layer prevents the decomposition of SPs and thereby enhances the SPs stability when stored for a long time or in the presence of organic solvents. Moreover, through this approach, QDs with different emission colors or other types of nanocrystals can be assembled in one single colloidal sphere, which can possess multiple properties, such as fluorescence and magnetism. The SPs/SiO_2 can also be covered by a gold nanoshell, which can accelerate the radiative decay rate *via* the plasmon-fluorescence coupling, and also further raise the SPs' photostability and improve the biocompatibility.

References

(1) Michalet, X.; Pinaud, F. F.; Bentolila, L. A.; Tsay, J. M.; Doose, S.; Li, J. J.; Sundaresan, G.; Wu, A. M.; Gambhir, S. S.; Weiss, S.: Quantum dots for live cells, in *vivo* imaging, and diagnostics. *Science* **2005**, *307*, 538-544.

(2) Spinicelli, P.; Buil, S.; Quelin, X.; Mahler, B.; Dubertret, B.; Hermier, J. P.: Bright and grey states in CdSe-CdS nanocrystals exhibiting strongly reduced blinking. *Phys Rev Lett* **2009**, *102*, 136801.

(3) Wuister, S. F.; Donega, C. D.; Meijerink, A.: Influence of thiol capping on the exciton luminescence and decay kinetics of CdTe and CdSe quantum. *J Phys Chem B* **2004**, *108*, 17393-17397.

(4) Nirmal, M.; Dabbousi, B. O.; Bawendi, M. G.; Macklin, J. J.; Trautman, J. K.; Harris, T. D.; Brus, L. E.: Fluorescence intermittency in single cadmium selenide nanocrystals. *Nature* **1996**, *383*, 802-804.

(5) Mahler, B.; Spinicelli, P.; Buil, S.; Quelin, X.; Hermier, J. P.; Dubertret, B.: Towards non-blinking colloidal quantum dots. *Nat Mater* **2008**, *7*, 659-664.

(6) Chen, Y.; Vela, J.; Htoon, H.; Casson, J. L.; Werder, D. J.; Bussian, D. A.; Klimov, V. I.; Hollingsworth, J. A.: "Giant" multishell CdSe nanocrystal quantum dots with suppressed blinking. *J Am Chem Soc* **2008**, *130*, 5026-5027.

(7) Wang, X. Y.; Ren, X. F.; Kahen, K.; Hahn, M. A.; Rajeswaran, M.; Maccagnano-Zacher, S.; Silcox, J.; Cragg, G. E.; Efros, A. L.; Krauss, T. D.: Non-blinking semiconductor nanocrystals. *Nature* **2009**, *459*, 686-689.

(8) Park, Y. S.; Bae, W. K.; Padilha, L. A.; Pietryga, J. M.; Klimov, V. I.: Effect of the core/shell interface on Auger recombination evaluated by single-quantum-dot spectroscopy. *Nano Lett* **2014**, *14*, 396-402.

(9) Canneson, D.; Mallek-Zouari, I.; Buil, S.; Quelin, X.; Javaux, C.; Mahler, B.; Dubertret, B.; Hermier, J. P.: Strong purcell effect observed in single thick-shell CdSe/CdS nanocrystals coupled to localized surface plasmons. *Physical Review B* **2011**, *84*, 245423.

(10) Zhong, Y.; Wang, Z. X.; Zhang, R. F.; Bai, F.; Wu, H. M.; Haddad, R.; Fan, H. Y.: Interfacial self-assembly driven formation of hierarchically structured nanocrystals with photocatalytic activity. *Acs Nano* **2014**, *8*, 827-833.

(11) Wang, T.; Zhuang, J. Q.; Lynch, J.; Chen, O.; Wang, Z. L.; Wang, X. R.; LaMontagne, D.; Wu, H. M.; Wang, Z. W.; Cao, Y. C.: Self-assembled colloidal superparticles from nanorods. *Science* **2012**, *338*, 358-363.

(12) Huang, S.; Bai, M.; Wang, L. Y.: General and facile surface functionalization of hydrophobic nanocrystals with poly(amino acid) for cell luminescence imaging. *Sci Rep-Uk* **2013**, *3*, 2023.

(13) Lee, S. H.; Yu, S. H.; Lee, J. E.; Jin, A. H.; Lee, D. J.; Lee, N.; Jo, H.; Shin, K.; Ahn, T. Y.; Kim, Y. W.; Choe, H.; Sung, Y. E.; Hyeon, T.: Self-assembled Fe_3O_4 nanoparticle clusters as high-Performance anodes for lithium ion batteries *via* geometric confinement. *Nano Lett* **2013**, *13*, 4249-4256.

(14) Han, J. S.; Zhang, X.; Zhou, Y. B.; Ning, Y.; Wu, J. E.; Liang, S.; Sun, H. C.; Zhang, H.; Yang, B.: Fabrication of CdTe nanoparticles-based superparticles for an improved detection of Cu^{2+} and Ag^{+}. *Journal of Materials Chemistry* **2012**, *22*, 2679-2686.

(15) Bai, F.; Wang, D. S.; Huo, Z. Y.; Chen, W.; Liu, L. P.; Liang, X.; Chen, C.; Wang, X.; Peng, Q.; Li, Y. D.: A versatile bottom-up assembly approach to colloidal spheres from nanocrystals. *Angew Chem Int Edit* **2007**, *46*, 6650-6653.

(16) Zhuang, J. Q.; Wu, H. M.; Yang, Y. A.; Cao, Y. C.: Supercrystalline colloidal particles from artificial atoms. *J Am Chem Soc* **2007**, *129*, 14166-14167.

(17) Zhuang, J. Q.; Wu, H. M.; Yang, Y. G.; Cao, Y. C.: Controlling colloidal superparticle growth through solvophobic interactions. *Angew Chem Int Edit* **2008**, *47*, 2208-2212.

(18) Wu, J.; Zhang, X.; Yao, T. J.; Li, J.; Zhang, H.; Yang, B.: Improvement of the stability of colloidal gold superparticles by polypyrrole modification. *Langmuir* **2010**, *26*, 8751-8755.

(19) Graf, C.; Vossen, D. L. J.; Imhof, A.; van Blaaderen, A.: A general method to coat colloidal particles with silica. *Langmuir* **2003**, *19*, 6693-6700.

(20) Stober, W.; Fink, A.; Bohn, E.: Controlled growth of monodisperse silica spheres in micron size range. *J Colloid Interf Sci* **1968**, *26*, 62-69.

(21) Mahler, B.; Nadal, B.; Bouet, C.; Patriarche, G.; Dubertret, B.: Core/shell colloidal semiconductor nanoplatelets. *J Am Chem Soc* **2012**, *134*, 18591-18598.

(22) Tessier, M. D.; Spinicelli, P.; Dupont, D.; Patriarche, G.; Ithurria, S.; Dubertret, B.: Efficient exciton concentrators built from colloidal core/crown CdSe/CdS semiconductor nanoplatelets. *Nano Lett* **2013**, *14*, 207-213.

General Conclusion and Perspectives

General conclusion

During this three-year research work, we have synthesized QD/SiO_2/Au core/shell/shell hybrid nanostructures (golden QDs) and studied the coupling between QD exciton and metallic plasmons. The work has started with the colloidal synthesis of CdSe/CdS core/shell QDs. It continued with their incorporation into silica and the subsequent coverage by a gold nanoshell to form the desired golden QDs. Then, these hybrid nanostructures were thoroughly characterized optically. Finally, we concluded with the self-assembly of QDs and/or other hydrophobic nanocrystals into colloidal superparticles (SPs).

First, we synthesized CdSe nanocrystals with two different radii: ~ 3 and 6 nm; then, a CdS shell was deposited *via* a continuous injection of the shell precursors into the CdSe core solution. This method, developed in our lab, produced CdSe/CdS core/thick shell QDs with final radii of 6 and 15 nm respectively. These hydrophobic QDs were individually encapsulated in silica beads *via* a reverse microemulsion method. The silica thickness – the first important parameter of the golden QDs – could be precisely tuned in the 10-60 nm range by changing the amount of the silica precursor TEOS in the emulsion solution.

In the second section, we presented the synthesis of golden QDs *via* a multi-step process. We explored several experimental parameters to improve the synthesis. A polymer, PVIS, was developed to functionalize the previously synthesized QD/SiO_2 NPs and adsorb aged gold seeds so that they cover up to ~ 80% of the silica surface. For the gold nanoshells formation process, a one-shot injection method using CH_2O as the reducing agent was chosen; thanks to the introduction of PVP, a controlled and homogeneous growth of the gold seeds could be obtained, resulting in continuous and monodispersed gold nanoshells with improved dispersion in water. With a fine tuning of the molar ratio between the QD/SiO_2 NPs and the gold(III) salt solution, the thicknesses of the gold layer – the second important parameter of the golden QDs – could be tailored to various dimensions.

Next, we studied the optical properties of golden QDs (QDs radius: 15 nm) with the thicknesses of the silica and the gold shells tuned respectively to 35 nm and 20 nm. Both

ensemble and single optical measurements were performed. The fluorescent QDs were coupled to the plasmon mode of gold nanoshells and displayed a 6-time shorter lifetime. When the QDs are in the charged state, the accelerated radiative recombination can completely overcome the Auger processes, resulting in radiative efficiencies that are similar to those measured when the QDs are in the neutral state. Hence, a fluorescence intensity trace with no detectable fluctuation over time was observed. The gold nanoshell acts also as a shield that protects the QD fluorescence and enhances its resistance to high-power photoexcitation or high-energy electron beams. This novel kind of hybrid object is, to the best of our knowledge, the first example of colloidal material that brings together a QD and a metal nanoshell in a resonant manner.

In the last section, we managed to assemble hydrophobic QDs into colloidal superparticles (SPs) *via* a micro-emulsion-droplet-templated method. The SPs size could be tuned by changing the surfactant quantity and the way the aqueous and organic solutions were mixed. These SPs were highly fluorescent and non-blinking. Multi-functional SPs could also be obtained by assembling fluorescent and magnetic nanocrystals. The SPs dispersion in water was improved by the adsorption of a polymer (PVP), which also provided nucleation sites for the subsequent SiO_2 growth. The SiO_2 shell conferred to the SPs a long-term stability. The coverage of SP/SiO_2 NPs by gold was also demonstrated.

Perspectives

The QDs fluorescence is quenched (especially for small QDs) when QD/SiO_2 NPs are washed with water because the water molecules can diffuse through the porous SiO_2 layer and reach the QDs surface. The protocol of the silica growth needs to be improved to maintain the QDs fluorescence. For instance, a more dense silica layer can be used to prevent the water diffusion; besides, QDs with a cross-linked polymer shell (*ACS Nano,* ***6****, 3346*) show extremely stable fluorescence and can be a choice for the synthesis of golden QDs without degraded fluorescence. In order to obtain a stronger Purcell effect using golden QDs, the distance between gold and QDs (the thickness of silica in our case) needs to be decreased. However, we observed an important aggregation during the gold seeds growth process when QD/SiO_2 NPs were small. Experimental conditions need to be optimized to synthesize well separated smaller golden QDs. The Purcell effect on the fluorescence of small QDs

(compared to the giant core/thick shell CdSe/CdS QDs) would also be interesting to study. Thanks to the continuous gold nanoshell which acts as a shield from the external environment, the golden QDs can be excited by the laser with much more higher power, which is necessary to give rise to the multi-exciton. The multi-exciton can be coupled with metallic plasmons more efficiently than mono-exciton and shows great potential to improve the efficiency of the third-generation solar cells. Furthermore, the SPs could make up some of these shortcomings, as well as blinking and low fluorescence intensity when single QDs are used as bioimaging markers, and would be very promising nanostructures in diverse practical applications.

Appendices

A1-Simulation part: numerical model

By Benjamin Habert, Francois Marquier, Jean-Jacques Greffet

1 Calculation of extinction spectrum

We use a multilayer spherical system to describe numerically the QD/SiO_2/Au Shell nanostructure. We use SEM images to measure the diameters of the quantum-dot and silica bead as well as the total thickness of the gold shell (H_{Shell} = 18 nm). Using these measured parameters and a bulk dielectric function for the gold shell, we observe a mismatch between the experimental and theoretical resonance of the structure (see model 1 in Figure 1, dashed blue line). We consequently implement a more accurate numerical model (see model 2 in Figure 1, solid black line). The consecutive layers of this model are: quantum-dot (n = 2.8, D_{QD} = 30 nm), silica core (n=1.47[1], D_{core} = 99 nm), continuous gold layer ($\varepsilon_{Au}(\omega, C_\Gamma)$, thickness $r \times H_{Shell}$), porous gold layer ($\frac{1}{2}(\varepsilon_{Au}(\omega, C_\Gamma) + \varepsilon_{ext})$, thickness = $(1-r) \times H_{Shell}$). The model has two free parameters: C_Γ and r. C_Γ takes into account the surface scattering of electrons in the gold shell and introduces homogenous broadening of the plasmonic resonance.[2,3] Using this parameter, the dielectric function for gold is the sum of an interband contribution and a modified Drude model dielectric function:

$$\varepsilon_{Au}(\omega, C_\Gamma) = \varepsilon_{inter}(\omega) + \left(1 - \frac{{\omega_p}^2}{\omega^2 + i\Gamma_{bulk} C_\Gamma}\right)$$

Where $\varepsilon_{inter}(\omega)$ and the Drude model parameters (ω_p, Γ_{bulk}) are extracted from experimental data (Christy 1972).[4] To account for its roughness, the gold shell is divided in two layers of different composition. The first one (thickness $r \times H_{Shell}$) is a continuous gold layer whereas the second one (thickness $(1-r) \times H_{Shell}$) is considered a mixture of gold and water (surrounding medium). The dielectric function for this layer is thus $\frac{1}{2}(\varepsilon_{Au}(\omega, C_\Gamma) + \varepsilon_{ext})$.

Mie theory calculations were used to compute the extinction spectrum of the multilayer system. A fit against an experimental extinction spectrum allowed us to extract the value of the two parameters: $C_\Gamma = 0.54$ and $r = 0.65$ (see Figure 1). We use these adjusted parameters in the calculation of Purcell factor. The experimental extinction spectrum shows a second resonance around λ = 1200 nm that we attribute to the presence of dimers in the solution.

We checked that this model could reproduce accurately the extinction spectra measured for several core/shell systems (D_{core} ranging from 86 to 125 nm, H_{Shell} from 13 to 30 nm). We also checked that the width of the plasmonic resonance could not be attributed to inhomogeneous broadening caused by size polydispersity.

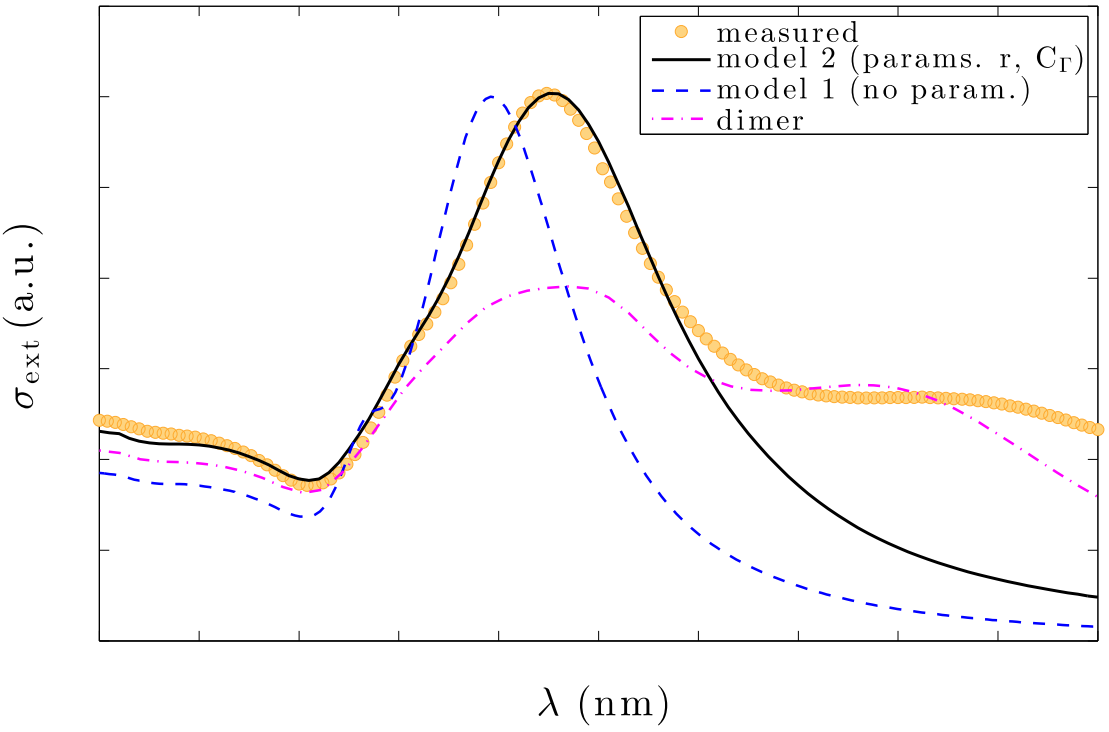

Figure 1. Measured (gold dots) and calculated extinction spectra for the QD/SiO2/Au Shell structure. For the dashed blue line we used the bulk dielectric function of gold and obtain a mismatch for the position and width of the resonance. Black line is the two-parameter model used in the article where surface scattering of electrons and shell roughness is taken into account. The calculated extinction spectrum for a dimer (magenta) shows a second resonance around 1100nm.

2 Purcell Factor for a nanoshell on a glass slab

We use a classical electromagnetic simulation to compute how the multilayer spherical structure can modify the lifetime τ of the quantum-dot. In such a simulation, the two-level

system is represented by a point dipole placed at the center of the multilayered spherical system and the power P emitted by this dipole is calculated (including losses in the metal). We use the equivalence $F_{Purcell} = \tau_0/\tau = P/P_0$ to deduce from the calculation the modification of lifetime. In the previous equation the subscript 0 corresponds to the reference: quantum-dot without the core/shell structure.

Using Mie theory, it is straightforward to compute the power emitted by the dipole in the multilayer spherical system in a homogeneous environment. However, the lifetime measurements were performed in a fluorescence microscopy setup: the emitter is deposited on a glass slab. Accounting for the interface is important as it modifies significantly the local density of states. We used the method described in references to account for the interface.[5,6] The basic idea of the method is to replace the nanoshell by an ensemble of effective dipolar scatterers located on a sphere of radius 3 nm. The polarizability of these dipoles is adjusted in order to reproduce the field scattered by the nanoshell in a homogeneous environment. The advantage of the technique is that the influence of the interface on dipoles can then be included easily. In our case, we found that 20 dipolar scatterers were enough to compute accurately the emitted power.

3 Influence of gold seeds on QD lifetime

The decay rate of the QD/SiO_2 system in water is $\Gamma_0 = 1/123$ ns^{-1}. When gold nanoparticles (seeds) are deposited on the silica surface, the decay rates increases to $\Gamma^* = 1/84$ ns^{-1}. This can be interpreted by the presence of a non-radiative decay channel characterized by the rate $\Gamma_{NR} = \Gamma^* - \Gamma_0 = 1/265$ ns^{-1}. We will show here that this additional decay rate can be attributed to the light absorption by the nanoparticles, thus proving that the QD is not chemically altered during this step.

Let us consider a dipole emitter (λ = 670 nm) at the center of the QD/SiO_2 structure. We first compute the power radiated by this dipole P_{rad}. We now consider a gold nanoparticle (radius r_{seed} = 1.5nm) deposited on the silica bead and we compute the electric field $\mathbf{E}_0$ at its position. The power absorbed by this nanoparticle is given by:

$$P_{abs} = -\frac{1}{2}\omega \,\mathrm{Re}\left\{\mathrm{p}.E_0^*\right\}$$

Where the dipole moment induced in the nanoparticle is given by its polarisability α:

$$p = \varepsilon_0 \varepsilon_{ext} \alpha E_0$$

$$\alpha = 4\pi r_{seed}^3 \frac{\varepsilon_{Au} - \varepsilon_{ext}}{\varepsilon_{Au} + 2\varepsilon_{ext}}$$

Where $\varepsilon_{ext} = 1.77$ and $\varepsilon_{Au} = -13.3 + 4.4i$ are the dielectric functions of the surrounding medium (water) and the gold nanoparticle (we use the same dielectric functions as in section *1*). The power scattered by this small nanoparticle is negligible:[7]

$$\frac{\sigma_{scatt}}{\sigma_{abs}} \propto \frac{\mathrm{k}^4 \mathrm{r}_{\mathrm{seed}}^6}{\mathrm{k}\, \mathrm{r}_{\mathrm{seed}}^3} \approx 10^{-6}$$

We can now compare the power absorbed by the gold nanoparticle to the total power radiated by the source dipole:

$$\frac{P_{abs}}{P_{rad}} = 1.7 \times 10^{-4}$$

We now estimate the amount N of gold nanoparticles required to explain the experimental modification of decay rate:

$$\frac{N\, P_{abs}}{P_{rad}} = \frac{\Gamma_{NR}}{\Gamma_0} = 0.46$$

This yields N ≈ 2700 nanoparticles, which would cover 62% of the silica surface and represent a volume of 3.8×10^{-5} μm^3 of gold. This is consistent with what is observed using SEM imaging of the QD/SiO_2/Au seeds structures. The shortening of fluorescence lifetime from 123 ns to 84 ns can consequently be attributed to the absorption of light by the gold nanoparticles.

4 Fluorescence signal in a pulsed excitation regime

We derive in this section a model for the fluorescence signal under a pulsed excitation. This will be applied to the low-excitation regime.

Considering an ensemble of N_{tot} emitters, we first derive the number of emitters in the excited state as a function of time $N_e(t)$. We consider periodic pulses with a repetition rate R of small duration δt that excite emitters in the ground state with a probability π. Let $N_e(0^-)$ be the number of excited emitters before the pulse; the number of excited emitters after the pulse is thus:

$$N_e(0^+) = N_e(0^-) + \pi \times (N_{tot} - N_e(0^-))$$

This population decays with a rate Γ and the number of excited emitters at the end of a cycle is:

$$N_e(t = 1/R) = N_e(0^+)\, e^{-\Gamma/R}$$

Because the excitation is periodic, we have $N_e(t = 1/R) = N_e(0^-)$. We consequently derive the number of excited emitters as a function of time:

$$N_e(t) = N_e(0^+) e^{-\Gamma t},$$

$$N_e(0^+) = N_{tot} \frac{\pi}{1 - (1-\pi) e^{-\frac{\Gamma}{R}}}$$

We can now use the population to derive the emitted intensity. The radiative decay rate of the emitter is Γ_r and the collection efficiency of the system is f_{coll}. During an excitation cycle, the mean intensity collected (photons.s-1) is:

$$I = R \int_{0+}^{1/R} \Gamma_r \; f_{coll} \; N_e(t) dt,$$

which yields:

$$I = \frac{\Gamma_r}{\Gamma} R \, f_{coll} \, N_{tot} \frac{\pi}{1 - (1-\pi) e^{-\frac{\Gamma}{R}}} \left(1 - e^{-\frac{\Gamma}{R}} \right) \qquad (1)$$

We can further extend the relevance of this model by providing the excitation probability as a function of pump irradiance ϕ_{inc} and absorption cross-section σ_{abs}. During the excitation (duration δt), the population equation is:

$$\frac{dN_e}{dt} = \frac{\sigma_{abs}\,\phi_{inc}}{h\,\omega_{inc}}\left(N_{tot} - N_e(t)\right) - \Gamma_{tot} N_e(t).$$

We solve this equation for $N_e(0) = 0$. The transition probability π for an emitter initially in its ground state can then be cast in the form:

$$\pi(\phi_{inc}) = \frac{N_e(\delta t)}{N_{tot}} = \frac{1}{1 + \dfrac{\Gamma\, h\,\omega_{inc}}{\sigma_{abs}\,\phi_{inc}}}\left(1 - e^{-\frac{\delta t\,\sigma_{abs}}{h\,\omega_{inc}}\phi_{inc}}\, e^{-\Gamma \delta t}\right)$$

This expression can be simplified when the duration of the pulse is short compared to the lifetime of the emitter $(\delta t << 1)$, which is often verified during measurements. The probability becomes:

$$\pi(\phi_{inc}) = (1 - e^{-\phi_{inc}/\phi_0}),\ with\ \phi_0 = \frac{h\,\omega_{inc}}{\delta t\,\sigma_{abs}} \qquad (2)$$

Equations (1) and (2) give us a model for the fluorescence collected in a pulsed excitation regime, regardless of the relative magnitude of the repetition rate *R* and decay rate Γ. In the case of a low-excitation regime ($\phi_{inc}/\phi_0 << 1$, and consequently $\pi << 1$), we get:

$$I = \frac{\Gamma_r}{\Gamma} R\, f_{coll}\, N_{tot}\, \pi$$

which corresponds to the formula used in the article for a single emitter. (Note that we obtain the same expression in the case of a small repetition rate $\left(\frac{\Gamma}{R} >> 1\right)$, regardless of the pump

irradiance). As explained in the article, we can take into account the presence of the gold shell by modifying the values of Γ and Γ_r. The gold shell also changes the excitation probability π; in the low-excitation regime, the probability is simply multiplied by a constant $K = \sigma_{abs}^{shell} / \sigma_{abs}^{QD}$ as π is proportional to the absorption cross-section of the emitter. Although it is not the case for this structure, an antenna can also modify the emission pattern and thus increase the collection rate f_{coll}.

References

(1) Khlebtsov, B. N.; Khanadeev, V. A.; Khlebtsov, N. G.: Determination of the Size, Concentration, and Refractive Index of Silica Nanoparticles from Turbidity Spectra. *Langmuir* **2008**, *24*, 8964-8970.

(2) Averitt, R. D.; Westcott, S. L.; Halas, N. J.: Linear optical properties of gold nanoshells. *J. Opt. Soc. Am. B* **1999**, *16*, 1824-1832.

(3) Westcott, S. L.; Jackson, J. B.; Radloff, C.; Halas, N. J.: Relative contributions to the plasmon line shape of metal nanoshells. *Physical Review B* **2002**, *66*, 155431.

(4) Johnson, P. B.; Christy, R. W.: Optical Constants of the Noble Metals. *Physical Review B* **1972**, *6*, 4370-4379.

(5) Castanié, E.; Vincent, R.; Pierrat, R.; Carminati, R.: Dressed polarizability and absorption of a dipole nano-antenna in an arbitrary environment. *AIP Conference Proceedings* **2012**, *1475*, 116-118.

(6) Stout, B.; Auger, J. C.; Devilez, A.: Recursive T matrix algorithm for resonant multiple scattering: applications to localized plasmon excitations. *J. Opt. Soc. Am. A* **2008**, *25*, 2549-2557.

(7) Bohren, C. F.; Huffman, D. R.: Absorption and scattering of light by small particles. *John Wiley & Sons* **2008**.

A2-List of abbreviations

Ag	Silver
AIBN	Azobisisobutyronitrile
APTES	3-aminopropyl)triethoxysilane
APTMS	3-aminopropyl)trimethoxysilane
Au	Gold
CdS	Cadmium sulfide
CdSe	Cadmium selenide
CdTe	Cadmium telluride
CH_2O	Formaldehyde
CTAB	Cetyltrimethylammonium bromide,
DTAB	Dodecyltrimethylammonium bromide
EG	Ethylene glycol
Fe_3O_4	Iron(II, III) oxide
ESPCI	Ecole Supérieure de Physique et de Chimie Industrielles
FWHM	Full width at half maximum
Golden QDs	QD/SiO_2/Au nanoshell
Igepal CO-520	Polyoxyethylene (5) nonylphenylether
LPEM	Laboratoire de Physique et d'Etude des Matériaux
NH_2OH•HCl	Hydroxylammonium chloride
NH_4OH	Ammonium hydroxide
PL	Photoluminescence
PLE	Photoluminescence excitation
PSPR	Propagating surface plasmon resonance
PVP	Poly(N-vinylpyrrolidone)
LSPR	Localized surface plasmon resonance
NPs	Nanoparticles
PVIS	Poly(1-vinylimidazole-*co*-vinyltrimethoxysilane)

QDs	Quantum dots
QY	Quantum yield
RPM	Rounds per minute
SEM	Scanning electron microscopy
SILAR	Successive ion layer adsorption reaction
SiO_2	Silica
SPR	Surface plasmon resonance
SPs	Superparticles
TEM	Transmission electron microscopy
TEOS	Tetraethyl orthosilicate
THPC	Tetrakis(hydroxymethyl)phosphonium chloride
Triton X-100	Poly(ethylene glycol) p-(1,1,3,3-tetramethylbutyl)-phenyl ether
ZnO	Zinc oxide
ZnS	Zinc sulfide

Abstract

Due to the surface plasmons in metallic nanostructures and the exceptional optical and electrical properties of colloidal semiconductor quantum dots (QDs), QD/metal hybrid nanostructures have attracted much attention over the past decade because of their diverse potential applications. However, colloidal single QD/gold hybrids have rarely been synthesized, although these structures are very promising optically and can be handled very easily, since they remain dispersed in solution.

In this work, we managed to develop for the first time a generalized synthetic route to synthesize a QD/SiO_2/Au core/shell/shell hybrid structure (golden QDs). First, hydrophobic QDs were individually encapsulated in silica beads *via* a reverse microemulsion method. The obtained QD/SiO_2 nanoparticles were then coated with a continuous gold nanoshell using a solution deposition process. The thicknesses of the silica and the gold layers – two important parameters of the golden QDs – could be tailored independently to various dimensions. We showed that single golden thick-shell CdSe/CdS QDs provided a system with a stable and poissonian emission at room temperature and a high photostability. This novel hybrid golden QD structure behaved as a plasmonic resonator with a strong (~ 6) Purcell factor, in very good agreement with simulations.

We also present the self-assembly of hydrophobic QDs into colloidal superparticles (SPs). With a fine choice of QDs, SPs could indeed possess outstanding properties including non-blinking fluorescence, high fluorescence intensity and multi-color emission. Multi-functional SPs could also be obtained by mixing fluorescent or magnetic nanocrystals. The subsequent growth of a silica shell on the SPs allowed an enhancement of their stability and we demonstrated this silica shell could itself be covered by a gold nanoshell to further improve the SPs photostability and biocompatibility.

Keywords

Nanomaterials; semiconductor nanocrystals; quantum dots; fluorescence; silica; gold nanoshell; plasmon resonance; optical coupling; Purcell effect; core/shell structures; self-assembly.

Résumé

Grâce aux plasmons de surface des nanoparticules métalliques et aux propriétés optiques et électroniques exceptionnelles des quantum dots (QDs), les nanostructures hybrides QD/métal ont suscité beaucoup d'intérêt depuis une dizaine d'années en raison de leurs nombreuses applications potentielles. Cependant, les hybrides QD/or colloïdaux n'ont été que rarement obtenus bien que ces structures soient particulièrement prometteuses du point de vue optique et qu'elles puissent être manipulées très facilement, car dispersées en solution.

Dans cette étude, nous avons réussi à mettre au point pour la première fois une méthode de synthèse généralisée permettant d'obtenir des structures hybrides cœur/coque/coque QD/SiO_2/Au (autrement appelés QDs dorés). Tout d'abord, les QDs hydrophobes ont été encapsulés individuellement dans des billes de silice par une méthode d'émulsion inverse. Les nanoparticules QDs/SiO_2 ainsi obtenues ont ensuite été recouvertes d'une nanocoque continue d'or *via* un processus de dépôt en solution. Les épaisseurs de la silice et de la couche d'or – deux paramètres importants pour les QDs dorés – peuvent être ajustées indépendamment afin d'obtenir les dimensions souhaitées. Nous avons montré que les QDs dorés individuels à base de QDs CdSe/CdS à coque épaisse possèdent une émission stable et poissonienne à température ambiante et sont très photostables. Cette nouvelle structure de QDs dorés se comporte comme un résonateur plasmonique avec un facteur de Purcell élevé (~6), en très bon accord avec les simulations.

Nous présentons également des auto-assemblages de QDs hydrophobes en superparticules (SPs). Un choix judicieux de QDs donne aux SPs des propriétés exceptionnelles telles qu'une émission de fluorescence intense, non-clignotante et multicolore. Des SPs multifonctionnelles peuvent aussi être obtenues en associant des nanocristaux magnétiques et fluorescents. La croissance d'une coque de silice sur les SPs a permis d'augmenter leur stabilité et nous avons démontré que cette couche de silice pouvait elle-même être recouverte d'une nanocoque d'or pour améliorer la photostabilité et la biocompatibilité de ces SPs.

Mots-clés

Nanomatériaux ; nanocristaux semiconducteurs ; quantums dots ; fluorescence ; silice ; nanocoque d'or ; résonance plasmon ; couplage optique ; effet Purcell ; structure cœur/coque ; auto-assemblage.